The Dissertation Committee for Oscar Mauricio Vargas Hernandez Certifies that this is the approved version of the following dissertation:

Patterns and Processes in the Evolution of the High Andean genus *Diplostephium* (Asteraceae, Astereae)

Committee:

Beryl B. Simpson, Supervisor

David Cannatella

Robert K. Jansen

James D. Mauseth

Kenneth R. Young

Patterns and Processes in the Evolution of the High Andean genus *Diplostephium* (Asteraceae, Astereae)

by

Oscar Mauricio Vargas Hernandez, B.S., M.S.

Dissertation

Presented to the Faculty of the Graduate School of

The University of Texas at Austin

in Partial Fulfillment

of the Requirements

for the Degree of

Doctor of Philosophy

The University of Texas at Austin

August 2016

Dedication

To Amanda, Romano, and Iván.

Acknowledgements

First, I want to thank my Ph.D. supervisor Beryl Simpson, who supported, inspired, and improved my work in my attempt to become a botanist. My committee members David Cannatella, Robert Jansen, James Mauseth, and Ken Young provided substantial advice and knowledge for the development and execution of my project.

Fernando Alzate, Santiago Díaz Piedrahita, Santiago Madriñán, Victor Quipuscoa, Katya Romoleroux, and Roberto Sánchez helped with field and herbarium logistics; in some cases they also accompanied me to hunt plant specimens. I had several conversions with all of them in which they spared their botanical knowledge.

Edgardo Ortiz and Teofil Nakov listened to my rants about plant phylogenetics and always provided useful feedback.

In addition to discuss, proofread, and help with the design of many illustrations printed in this document, Sarah Sussman, my partner and best friend, also supported me as a human being. Sarah's fascination for nature, art, and culture has always been a source for inspiration and encouragement.

Alejandro Berrio is family, he and I enjoyed and endured together the joys and troubles of being a foreigner in Austin while pursuing a doctorate.

I lived happily in Austin thanks to the company of several folks that I attempt to list here: Laura Abondano, Matt Ashworth, Moises Bernal, Mariska Brady, Catalina Cuellar, Amalia Diaz, Ignacio Gallardo, Monica Guerra, Deise Goncalves, Carlos Guarnizo, Rafael Guerrero, Tinisha Hankock, Debra Hansen, Maria José La Rota, Vanessa Rivera, Nathan Leclear, Sean Maguire, Juan Diego Palacio, Alejandro Puyana, Sofia Rodriguez, Patricia Salerno, Rebecca Tarvin, Lina Maria Valencia, Mariana Vasconcellos, and Mao-Lun Wen.

The Garden Club of America, the C. L. Lundell Chair of Systematic Botany, the Linda Escobar Award, Lorraine Stengl, the Plant Biology Program and Plant Resources Center at U.T. Austin, the National U.S. Herbarium at the Smithsonian Institution, and Sigma Xi financed this dissertation.

Patterns and Processes in the Evolution of the High Andean genus *Diplostephium* (Asteraceae, Astereae)

Oscar Mauricio Vargas Hernandez, Ph.D.

The University of Texas at Austin, 2016

Supervisor: Beryl B. Simpson

With a complex topography and a recent orogeny (5–20 my), the Andes Cordillera is a hotspot for plant biodiversity and an ideal region to study recent plant speciation events. This dissertation aims to understand the patterns and processes of plant evolution in the Andes throughout the study of a high Andean genus of plants. *Diplostephium* (*sensu* Cuatrecasas) comprises 111 species of shrubs and small trees that have been considered a main component of the high Andean flora. In the first chapter, I study the phylogenetic patterns of *Diplostephium* and its allied genera from three DNA sources: the chloroplast genome, the mitochondrial genome, and the nuclear ribosomal region. The phylogenies obtained revealed that most species of traditional *Diplostephium* belong to two non-sister clades and that introgressive hybridization played an important role in the evolutionary history its species and their allies. In the second chapter, I reinstate the genus *Piofontia* and transfer several species into it based on the phylogenic results and morphological characters. In the third chapter, I infer the biogeographic history and speciation rates of *Diplostephium* and *Piofontia,* and I evaluate the relative role of geographic isolation and ecological divergence in *Piofontia* by employing an original framework of sister-taxa comparisons that incorporates geographic distributions and leaf areas as an indicator of ecological divergence. My results show that speciation

rates in *Diplostephium* and *Piofontia* were significantly affected by mountain uplift and Pleistocene climate, and that geographic isolation appears to be the main cause of speciation in the Northern Andes. In the fourth chapter, I compare anatomical characteristics of stems and leaves from 11 species of *Diplostephium* and *Piofontia* that dwell in different Andean habitats. The stem and leaf anatomies of the species I studied, suggest that the páramo and the humid puna present similar physiological challenges to plants that result in similar morpho-anatomical features associated with physiological dry and semi-dry environments. Cloud forest species, on the other hand, have stem and leaf anatomies that reflect mesic conditions caused by a downslope colonization event in *Piofontia*.

Table of Contents

List of Tables

List of Figures

Chapter 1: Conflicting phylogenomic signals reveal a pattern of reticulate evolution in a recent high-Andean diversification (Asteraceae: Astereae: *Diplostephium*)

INTRODUCTION

Rapid diversifications usually occur in landscapes like archipelagos and mountain ranges that provide disjunct terranes suitable for speciation via isolation and ecological divergence (Givnish, 1997). The Andes Cordillera is one of these landscapes in which numerous plant groups have undergone rapid diversifications after its recent rise (Madriñán *et al*., 2013; Luebert & Weigend, 2014; Hughes & Atchinson, 2015). Phylogenies of Andean taxa based on Sanger sequencing often suffer from lack of resolution and support, especially in crown clades where rapid evolution occurred (e.g. Rauscher, 2002; Emshwiller, 2002; Sánchez-Baracaldo, 2004; Bell & Donoghue, 2005; Hughes & Eastwood, 2006; Zapata, 2013; Nürk *et al*., 2013). Advances in high-throughput sequencing have created new opportunities for overcoming the difficulties of working with recently diversified taxa (Bock *et al*., 2014; Ma *et al*., 2014; Mort *et al*., 2015). The amount of data obtained by next-generation sequencing is usually one or two orders of magnitude higher than that obtained by Sanger sequencing. Genome skimming, or shallow shotgun sequencing, is a next-generation sequencing approach in which whole genomic DNA is sequenced in order to recover bioinformatically useful phylogenetic high-copy DNA regions (Straub *et al*., 2012); this technique provides information about markers with different inheritance patterns and can be employed with non-model organisms and museum specimens (Straub *et al*., 2012). The biparentally inherited (Volkov *et al*., 2007) complete nuclear ribosomal DNA has proved to be a useful marker for inferring species-level phylogenies (Linder *et al*., 2000; Straub *et al*., 2012; Bock *et al*., 2014). The mostly non-recombinant and uniparentally inherited (Birky, 1995; Jansen

& Ruhlman, 2012) chloroplast DNA has been used to reconstruct the phylogeny of Asteraceae at the tribal, generic, and species level (Kim *et al*., 2005, Panero & Funk, 2008, Bock *et al*., 2014; Panero *et al*., 2014). Finally, the mostly non-recombinant uniparentally inherited (Birky, 1995) mitochondrial DNA has been employed mainly to infer the evolutionary history of angiosperms at the family and order level (Qiu *et al*., 2010; Sun *et al*., 2015) but more recently it has been used to study phylogenetic patterns among species (Bock *et al*., 2014). The comparison among the histories of these uniparentally and biparentally inherited markers has the potential to elucidate patterns of hybridization and introgression (Rieseberg & Soltis, 1991; Hardig *et al*., 2000; Bock *et al*., 2014; Sun *et al*., 2015).

Diplostephium is a main component of the tropical high Andean flora. The genus appears to have undergone a recent diversification leading to its numerous species (Vargas, 2011), high morphological diversity (Cuatrecasas, 1969), and low molecular divergence (Vargas & Madriñán, 2012). *Diplostephium* traditionally comprises 111 species (Vargas, 2011) characterized by a woody habit (ranging from decumbent subshrubs 10 cm tall to trees 10 m tall), abaxially-lanate alternate leaves, radiate capitula, functionally male disk florets, white to purple ray floret corollas, and a double pappus (Blake, 1928; Cuatrecasas, 1969; Vargas & Madriñán, 2006). *Diplostephium* inhabits the high altitudes of the Talamanca Cordillera, the Northern Andes, and the Central Andes in tropical Central and South America. Most species of the genus (ca. 60) inhabit the páramo, a Northern Andean ecosystem known for its high degree of plant diversity (Luteyn, 1999), island-like geographical coverage (Luteyn, 1999), and numerous recent plant diversifications (Madriñán *et al*., 2013; Luebert & Weigend, 2014). In addition to the páramo, *Diplostephium* species inhabit the Central Andean puna and the upper limit of the high Andean forest.

Diplostephium belongs to Astereae, where it has traditionally been classified as part of the *Chiliotrichum* group, a subset of the subtribe Hinterhuberinae (Nesom, 1994; Nesom & Robinson, 2007). Molecular phylogenies have shown that Hinterhuberinae and its subdivisions are polyphyletic (Noyes & Rieseberg, 1999; Sancho & Karaman-Castro, 2008; Brouillet *et al*., 2009; Karaman-Castro & Urbatsch, 2009; Sancho *et al*., 2010; Vargas & Madriñán, 2012). Furthermore, a molecular phylogenetic analysis of Astereae (Brouillet *et al*., 2009) showed that all its traditional subtribes are polyphyletic and need to be recircumscribed. South American Hinterhuberinae species are nested in two groups (Brouillet *et al*., 2009): the "Paleo South American Clade" placed at an early diverging position in Astereae, and the "South American lineages" comprising a grade in a more derived position in the tree. This grade contains genera from the subtribes Baccharidinae, Grangeinae, Hinterhuberinae, Podocominae, and Lagenophorinae. *Diplostephium* belongs to the "South American lineages" grade but its ambiguous position in the published phylogenies (Noyes & Rieseberg, 1999; Brouillet *et al*., 2009; Karaman-Castro & Urbatsch, 2009; Vargas & Madriñán, 2012) has obscured its place among its closest relatives. Vargas & Madriñán (2012) tried to evaluate the monophyly of the genus by constructing a phylogeny of *Diplostephium* using the internal transcribed spacers of the nuclear ribosomal DNA (ITS) of 27 (24%) species of the genus. Their sampling was focused on the Colombian *Diplostephium* and included only three Ecuadorian and two Peruvian species. The aims of Vargas & Madriñán (2012) were thwarted by the low resolution and support of the ITS phylogeny. Vargas & Madriñán (2012) also tested the chloroplast regions *psbA-trnH, rpoB,* and *rpoC1* as phylogenetic markers and concluded that they lacked significant interspecific variation to warrant their use. The low molecular variation found by Vargas & Madriñán (2012) in *Diplostephium* highlighted the problems

of inferring the phylogeny of a rapid diversification with limited taxon sampling and Sanger sequencing.

In this study, we focused on uncovering the phylogenetic patterns of *Diplostephium* and its allied genera in the "South American lineages" using high-throughput sequencing. The aims of this study were twofold: to compare the phylogenetic signal of the nuclear ribosomal, chloroplast, and mitochondrial DNA; and to elucidate the species tree of *Diplostephium* and its closely related genera.

MATERIALS AND METHODS

Taxon Sampling

We focused our sampling on the genus *Diplostephium* and its allied genera. A total of 91 samples were sequenced. The ingroup contained 74 samples of *Diplostephium* (69 species, c. 62% of the total number of species) and 14 samples from 13 allied genera in Astereae (Table 1.1). We chose ingroup and outgroup genera based on their phylogenetic positions in Astereae inferred by Brouillet *et al*. (2009). The majority of the samples (63) were collected in the field where leaf tissue was dried using silica gel. Vouchers from those specimens were deposited in ANDES, HUSA, QCA, and TEX. The remaining samples were taken from herbarium specimens deposited in ANDES, F, FMB, HUA, HUSA, TEX, US, and USM (Table 1.1).

Data Collection

We performed total genomic DNA extractions with the DNeasy Plant Mini Kit (Qiagen, CA, USA) following the manufacturer's protocol. To increase the yield of DNA from herbarium material, we added 50 μL of proteinase K (Qiagen; activity >600 mAU/ml) to the lysis solution and incubated it overnight at 45ºC after the initial 10 min incubation. Standard genomic DNA Illumina paired-end libraries with an average of c.

400 bp length fragment size were prepared at the Genomic Sequencing and Analysis Facility at The University of Texas at Austin and then sequenced by an Illumina HiSeq 2500. The sequencing targeted 10 million paired-end reads (101 bp length) per sample. We inspected the quality of the reads with the program FASTQC v.0.10.1 (Andrews, 2010). We filtered the raw data with the program "process_shortreads" of the software package STACKS v.1.20 (Catchen *et al*., 2011). The command discarded any reads with uncalled bases or average low quality scores (<10/40 Phred score) and trimmed the last 10 bp of the reads when their average quality was low.

We employed a two-step strategy to create three subsets of reads per sample: nuclear ribosomal, chloroplast, and mitochondrial. By including only the necessary subset of genomic data to perform its assemblage, we aimed to reduce noise and increase the accuracy and computational efficiency in our downstream analyses. Our first step consisted in performing a *de novo* assembly in each sample using all the genomic data. The software RAY v.2.3.1 (Boisvert *et al*., 2012) performed the assembly using three different k-mer values visually selected from the report graph provided by KMERGENIE (Chikhi & Medvedev, 2014). The contigs resulting from the RAY assemblage were parsed with the "-search" function of RAY using *Helianthus annuus* L. nuclear ribosomal, chloroplast, and mitochondrial reference sequences (GenBank accessions HM638217.1, NC_007977.1, and KF815390.1, respectively); this step provided a subset of RAY contigs for each genomic region. The second step consisted in separating the whole genomic reads into nuclear ribosomal, chloroplast, and mitochondrial subsets by mapping all of each samples' reads against the RAY contig produced after the first step. For example, whole genome reads of *Diplostephium haenkei* were mapped against their own RAY chloroplast contigs to obtain a chloroplast subset of reads. BOWTIE v.2.2.3. (Langmead & Salzberg, 2012) performed the mapping. We then analyzed with different

pipelines the three subsets of reads obtained per sample to obtain the corresponding sequence alignments (Fig. 1.1).

Assembly of the Matrices

Due to the intraindividual polymorphic nature of the nuclear ribosomal DNA, we assembled this genomic region in two steps. First, we created a *de novo* draft assembly with the nuclear ribosomal reads subset in each sample using SPAdes v.3.5.0 (Bankevich *et al*., 2012). Then, we back-mapped the nuclear ribosomal reads to their draft assembly in GENEIOUS v.7.1.4 (Biomatters, 2014). This strategy involved creating a map for each sample from which we calculated three consensus sequences per sample using three different threshold percentages (50%, 75%, and 90%, Fig. 1.1). By doing this, we were able to account for the different levels of intraindividual polymorphisms found in the nuclear ribosomal tandem repeats and evaluate their effects on phylogenetic estimation. The 50% consensus called a nucleotide in a polymorphic position only if the nucleotide were present in more than 50% of the reads containing that position. Therefore, the 50% consensus sequence set had fewer ambiguities than the 75% and 90% consensus sequences. All the 273 nuclear ribosomal sequences (three per sample) were aligned in MAFFT v.7.017 (Katoh *et al*., 2002) into a master alignment. We corrected the master alignment by hand using GENEIOUS. Finally, we extracted from the master alignment three matrices corresponding to the three percentage thresholds (nr50, nr75, and nr90). Each matrix obtained was analyzed individually.

A *de novo* assembly for each sample's chloroplast reads subset was performed with SPAdes. First, we annotated the chloroplast genome of *Diplostephium haenkei* using DOGMA (Wyman *et al*., 2004). Then, we corrected the DOGMA annotation by hand using the chloroplast genome of *Guizotia abyssinica* (L.f.) Cass. (GenBank accession

EU549769.1) in GENEIOUS. We used the chloroplast of *D. haenkei* to merge and annotate the chloroplast-SPAdes contigs of the remaining 90 samples using GENEIOUS (Fig. 1.1). We employed MAFFT to create the chloroplast genome alignment that was later corrected by hand in GENEIOUS. For the phylogenetic analysis, we only included one IR in our alignment and manually removed three unalignable regions comprising a total of c. 2,300 characters.

Due to the high degree of rearrangements and the discontinuity found in the mitochondrial assemblies performed with SPAdes, it was not feasible to make a direct alignment of our mitochondrial genomes. Instead, we assembled the *de novo* mitochondrial genome of *Diplostephium hartwegii,* and then we used this genome as a reference for assembly by mapping the remaining 90 samples. We chose *D. hartwegii* as a reference based on the continuity and the high coverage of the mitochondrial contig obtained by RAY for this sample. We expected all the mitochondrial assemblies with the exception of *D. hartwegii* to have missing data at the boundaries of DNA blocks where rearrangements occurred relative to *D. hartwegii*. With this strategy we intended to obtain a gapped mitochondrial genome assembly for each sample in which the order of the mitochondrial blocks matched the one of *D. hartwegii* making their alignment feasible. We employed SPAdes and MITOFYv.1.3.1 (Alverson *et al*., 2010) to assemble and annotate the mitochondrial genome of *D. hartwegii*. Before mapping, we filtered the mitochondrial reads of each sample because we detected a small proportion of chloroplast reads mixed in. The intraindividual presence of chloroplast reads in the mitochondrial subset is explained by the similarity of some tRNAs and the transfer of DNA between these two genomes (Alverson *et al*., 2011). To filter out the chloroplast reads from the mitochondrial reads subsets, we mapped every sample's mitochondrial reads subset against its *de novo* chloroplast genome assembled in this study (e.g. the mitochondrial

reads of *D. colombianum* were mapped to the chloroplast genome of *D. colombianum*). The reads not mapped to the chloroplast genome were mapped to the mitochondrial reference (*D. hartwegii*) to create a consensus sequence per sample (Fig. 1.1). MAFFT performed the alignment of the 91 mitochondrial sequences. We visually inspected the matrix in GENEIOUS, regions difficult to align or with significant amounts of missing data were excluded from the matrix. We also removed the mitochondrial rRNA genes *rrn5*, *rrnL*, and *rrnS* from the alignment because we found bacterial DNA matching some hyperconserved regions of these genes. We suspect that the source of bacterial DNA in our dataset came from bacteria living on the leaf surfaces of our plant samples.

Phylogenetic Analyses

We performed independent phylogenetic analyses for each dataset using Bayesian Inference (BI) and Maximum Likelihood (ML). We evaluated a non-partitioned (M0) vs. a partitioned model (M1). The M1 of the chloroplast and mitochondrial matrices contained a coding and a non-coding partition. The M1 of the nuclear ribosomal DNA dataset contained three partitions: rRNA, transcribed spacers (the external transcribed spacer [ETS], the ITS) and the non-transcribed spacer (NTS). We compared M0 and M1 for each dataset by calculating the stepping stone marginal likelihood (Xie *et al*., 2011) of both model schemes with MrBayes v.3.2.2 (Ronquist & Huelsenbeck, 2003) on the CIPRES Science Gateway Server (Miller *et al*., 2010) using 10 million generations, 2 runs, 4 chains per run, and assuming a GTR+Γ model of evolution. The stepping stone marginal likelihood values were compared using Bayes factors (Fan *et al*., 2011).

To calculate the model of evolution of the partitions we employed a mixed strategy. First, we inferred the use +Γ and +I parameters in our partitions using the corrected Akaike information criterion (AICc) (Hurvich & Tsai, 1989) employed in

jModelTest v.2.1.7 (Guindon & Gascuel, 2003; Darriba *et al*., 2012). Then, we calculated the substitution parameters among nucleotides with reversible jump Markov Chain Monte Carlo simulations (Huelsenbeck *et al*., 2004) using MrBayes with 10 million generations, 2 runs, 4 chains per run, and the +Γ and/or +I parameters if suggested by the AICc. A final MrBayes analyses with 10 million generations, 2 runs, and 4 chains per run was performed for each dataset using the best partition model along with the model of evolution inferred. We performed the ML analyses with RAxML v.8.1.11 (Stamatakis, 2014) in the CIPRES portal using the partitioned schemes favored, 100 rapid bootstrap replicates, and the GTR+Γ model of evolution (as recommended by RAxML manual Stamatakis, 2015). FigTree v.1.4.2 (Rambaut, 2014) allowed us to inspect, compare, and export the trees obtained to image editors. For all the Bayesian analysis we used a burnin fraction of 0.25. We employed TRACER v.1.6.0 (Rambaut *et al*., 2014) to confirm the convergence of parallel MCMC runs (ESS >100).

Analyses of the Nuclear Ribosomal Ambiguities

To evaluate if nuclear ribosomal ambiguities could provide information about hybridization, we counted the number of ambiguities in each sample in the 90% nuclear ribosomal matrix (nr90). Then, we mapped the number of ambiguities onto the chronogram, and tested them against a Brownian model of evolution on the Bayesian tree. If ambiguities are correlated with recent hybridization, their pattern of evolution on the species tree should deviate from a Brownian model of evolution. We calculated Blomberg *et al*.'s (2003) K and Pagel's (1999) lambda (λ) by employing the "phylosig" function incorporated in the R package PHYTOOLS (Revell, 2012) using 1,000 simulations. Both statistics evaluate whether traits at the tips are more similar or more different than expected in relation to a Brownian motion model of evolution. We mapped

with MESQUITE v.3.04 (Maddison & Maddison, 2015) the number of ambiguities onto the phylogram using a parsimony model.

Congruence Assessment and Visualization

We visually inspected the congruence of the topologies obtained by different phylogenetic analyses with the multidimensional scaling of tree space using the Robinson–Foulds distance implemented in TreeSetViz v3.0 (Amenta & Klingner, 2002). The first comparison was made among the results obtained by the BI and ML analysis of the three nuclear ribosomal datasets (nr50, nr75, and nr90). The second comparison contrasted the trees resulted from the BI and ML analyses of the nuclear ribosomal 90%, chloroplast, and mitochondrial datasets. From the BI analyses, we sampled the maximum credibility tree and 50 random Bayesian topologies from each dataset after a 0.25 burn-in. From the ML analyses, we sampled the best tree obtained and 50 random bootstrap replicates from each ML subset analysis. A hierarchical likelihood-ratio congruence test among the nuclear ribosomal 90%, chloroplast, and mitochondrial datasets was performed with CONCATERPILLAR v.1.8a (Leigh *et al*., 2008) coupled with RAxML v.7.2.8. (Stamatakis, 2006).

To visualize reticulate evolution we inferred a phylogenetic network from the nuclear ribosomal 90% and chloroplast Bayesian topologies using SplitsTree4 v.4.13.1 (Huson & Bryant, 2006). We excluded the mitochondrial tree in order to make a conservative inference about reticulation. Assuming that the chloroplast and mitochondrial genomes are both inherited maternally, the chloroplast topology should more accurately represent the history of these two genomes since it has a stronger phylogenetic signal (see results). Previous studies of the mitochondrial genome have

reported high indices of genomic rearrangements and low mutation rates (Palmer & Herbon, 1998; Alverson *et al*., 2010; Rice *et al*., 2013; Z. Wu *et al*., 2015).

RESULTS

Characteristics of the Datasets

The shortest nuclear ribosomal cistron sequence belongs to *Laennecia sophiifolia* with 8,132 bp whereas the longest belongs to *Llerasia caucana* with 10,929 bp. While the nr50 matrix contains only 25 ambiguities, the nr75 and the nr90 present 3,201 and 5,012 ambiguities, respectively. The nuclear ribosomal matrices comprise 13,362 characters of which 1,203–1,425 (9.00–10.66%, depending on the consensus threshold), are PICs excluding the outgroup (Table 1.2). When compared with the chloroplast and mitochondrial matrices, the nuclear ribosomal DNA contained the highest proportion of PICs relative to its length. The shortest chloroplast genome belongs to *Soliva sessilis* with 150,784 bp and the longest belongs to *Baccharis genistelloides* with 153,239 bp. The chloroplast genome of *Diplostephium haenkei* contains 85 genes plus 36 tRNAs and 8 rRNAs (Fig. 1.2). No significant rearrangements or gene losses were found across the sampled species relative to *Guizotia abyssinica* with the exception of the loss of the *rps*19 gene for *Baccharis genistelloides* and *trnT-GGU* for *B. genistelloides*, *B. tricuneata*, and *Llerasia caucana*. Fifty-six of the 91 genomes present gaps, codified as missing data, in their assemblies due to the low coverage of reads obtained in regions with a high number of repeats. The length of the chloroplast matrix is 135,440 characters of which 2,169 (1.69%) are PICs excluding the outgroup (Table 1.2). In comparison with the nuclear ribosomal and mitochondrial datasets, the chloroplast matrix contains the higher number of PICs. The *de novo* mitochondrial genome of *Diplostephium hartwegii* has a total length of 277,718 bp, containing 56 genes plus 3 chloroplast-like tRNAs (Fig. 1.3). The

final mitochondrial matrix has a length of 209,392. The mitochondrial matrix contains 1,730 (0.83%) PICs excluding the outgroup (Table 1.2). The mitochondrial matrix contained the lowest proportion of PICs relative to its size in comparison with the nuclear ribosomal and chloroplast matrices.

Consensus sequences were deposited in GenBank (Table 1.1). Subsets of reads and aligned matrices are available at Dryad on-line repository.

Phylogenetic Analysis

In all cases, the Bayes factors favor a partitioned matrix analysis over a non-partitioned one (Tables 1.3, 1.4). Overall, the phylogenetic topologies obtained are well resolved with highly supported nodes (Figs. 1.4–1.13). The two topologies obtained by BI and ML for each of the matrices analyzed (e.g. the BI-chloroplast tree compared to the ML-chloroplast tree) are consistent excluding clades with low support [bootstrap support (BS) <50%, Bayesian posterior probability (BPP) <0.5].

Nuclear Ribosomal Topologies and Ambiguities

The BI and ML backbones of the nr50, nr75, and nr90 trees are all highly congruent with the exception being the position of *Diplostephium meyenii,* which has low support on all of the trees. All the nuclear topologies place *Diplostephium* species in three clades, A, B, and C excepting the BI-nr50, ML-nr50, and ML-nr75 trees (Figs. 1.4–1.9) that place *D. meyenii* as a sister to *Floscaldasia hypsophila* (instead of part of clade C). Despite the general agreement among the nuclear ribosomal topologies, there are some incongruences located towards the tip of the trees inside clades A and C (Fig. 1.4–1.9). For example, *Diplostephium schultzii,* a species represented by two samples, is polyphyletic in the BI-nr50 and ML-nr50 topologies (Figs. 1.5, 1.7), whereas it is

monophyletic in the BI-nr75, BI-nr90, ML-nr75 and ML-nr90 topologies (Figs. 1.4, 1.6, 1.8, 1.9).

The visualization of the Robinson-Foulds tree distances of each of six nuclear ribosomal tree subsets (BI-nr50, BI-nr75, BI-nr90, ML-nr50, ML-nr75, and ML-nr90) shows four clusters of topologies (Fig. 1.14a). None of the four clouds are formed exclusively by all the trees of one subset. The best ML-nr75 tree falls inside one of the two BI-nr75 tree-clouds; similarly, the best ML-nr90 tree is positioned between the BI-nr90 topologies. The largest cloud contains trees from the BI-nr50, ML-nr50, ML-nr75, and ML-nr90 subsets. This visualization emphasizes that even though there is a general backbone agreement between all six tree subsets, there are some differences towards the tips of the topologies among these trees. These differences are virtually all due to different positions of taxa inside clades A and C (Fig 1.4–1.9). Because the nr50, nr75, and nr90 backbones are congruent and the details about the interspecific relationships inside clades A and C are outside of the scope of this paper, we selected the nr90 dataset to make comparisons with the chloroplast and mitochondrial datasets. The nr90 matrix captures a considerable amount of the intraindividual polymorphisms, informative to MrBayes and RAxML (Ronquist *et al*., 2011; Stamatakis, 2015), without incorporating sequencing errors.

For the remaining part of the paper we will therefore refer to the nuclear ribosomal 90% dataset simply as "nuclear ribosomal."

The average number of ambiguities from our 91 samples is 55.1, with *Exostigma notobellidiastrum, Laennecia sophiifolia,* and *Laestadia muscicola* having no ambiguities and *Diplostephium heterophyllum* having the maximum of 198 (Table 1.5). Clade A has an average of 84.5 ambiguities while Clade C has 36.5. Visual inspection of the ambiguities mapped on the nuclear ribosomal phylogram (Fig. 1.15) shows that their

distribution seems to depart from a random model of evolution; this is confirmed by Blomberg's K=0.061 and Pagel's λ=0.781, both departing from a Brownian model with P=0.001 and P<0.001 respectively.

Incongruence Among the Genomic Datasets

To avoid confusion in our results and discussion, we only use the BI topologies when comparing the nuclear ribosomal, chloroplast, and mitochondrial datasets since the BI and ML backbone topologies from the same matrices are almost identical.

Incongruence is significant between the topologies obtained from the nuclear ribosomal, chloroplast, and mitochondrial genomic regions (Figs. 1.4, 1.10, 1.12). In addition to recovering contrasting generic relationships, these topologies also represent different clades of *Diplostephium* species. While the nuclear ribosomal topology recovers three clades of *Diplostephium* species (clades A, B, and C), the chloroplast and mitochondrial trees recover eight and nine *Diplostephium* clades, respectively (Figs. 1.4, 1.10, 1.12). The topological incongruence is also obvious in the visualization of the Robinson-Foulds tree distances (Fig. 1.14b), which depicts three independent clouds of topologies corresponding to the nuclear ribosomal, chloroplast, and mitochondrial tree subsets. The three clouds of genomic datasets do not overlap, with the chloroplast and mitochondrial clouds positioned more closely together relative to the nuclear ribosomal trees. The hierarchical likelihood-ratio test performed by CONCATERPILLAR rejected the concatenation of the most congruent dataset combination, chloroplast plus mitochondrial DNA ($p<0.0001$). The phylogenetic network (Fig. 1.16) shows that most *Diplostephium* species comprise two main groups, A and C. While group A does not show reticulation with other genera, group C reticulates with allied genera (e.g.,

Aztecaster, Baccharis, Paratrephia) and group B. Interspecific reticulation is also present inside *Diplostephium* groups A and C.

DISCUSSION

Nuclear Ribosomal Cistron Datasets

The comparison between the three nuclear ribosomal trees calculated from different consensus thresholds (50%, 75%, and 90%) shows a general agreement among their backbone structures. However, there are topological differences towards the tree tips inside clades A and C, produced by the different numbers of ambiguities in the three datasets (Table 1.2). It is expected that nodes close to the tips of the trees are more sensitive to the presence of polymorphisms at informative sites since fewer characters (due to the recency of the taxa they represent) support these nodes. Therefore, our results suggest that nuclear ribosomal polymorphisms mostly affect the phylogenetic position of recently diverged taxa located in derived nodes in the tree and have little impact on the nodes comprising the backbone of our phylogeny. We suggest that researchers should be conservative and use elevated consensus thresholds (c. 90%) when calculating sequences from nuclear ribosomal data, so that intraindividual polymorphisms are captured and included in the analysis.

Our results show that the number and distribution of ambiguities over the nuclear ribosomal phylogeny does not follow a Brownian model of evolution. Since the nuclear ribosomal cistron is inherited biparentally, it is expected that taxa that underwent recent hybridization would exhibit a high number of ambiguities in their nuclear ribosomal sequences. The two species with the most ambiguities *Diplostephium heterophyllum* (198) and *D.* sp. nov. CAJ (173) have conflicting and derived positions among the nuclear ribosomal, chloroplast, and mitochondrial phylogenies indicating that these taxa

have experienced recent hybridization (Fig. 1.15). Contrastingly, *Parastrephia quadrangularis,* which we suspect experienced ancestral hybridization because of its long branch (see detailed discussion below), only has 19 ambiguities, suggesting that concerted evolution might have homogenized its nuclear ribosomal intraindividual variability. The mapping (Fig. 1.15) shows that clade A, with a mean of 84.5 ambiguities, has more ambiguities on average than clade C, which has a mean of 36.5 ambiguities. We hypothesize that the higher average number of ambiguities found in clade A in relation to clade C, is a consequence of higher levels of recent hybridization in clade A. The short branches of most species of clade A indicate a recent origin and therefore a high probability of hybridization among its species. Our observations align with the results of West *et al*. (2014) on *Saccharomyces cerevisiae* Hansen, in which the high number of nuclear ribosomal ambiguities matches strains having mosaic genomes as the result of recent hybridization.

Incongruence and Reticulate Evolution

Even though hybridization is difficult to distinguish from incomplete lineage sorting (Joly *et al*., 2009), the backbone topological incongruence found between the three genomic regions provides compelling evidence for a complex process of reticulate evolution due to ancient and recent introgression. However, the low divergence found in the mitochondrial matrix and the partial similarity between the mitochondrial and chloroplast trees lead us to believe that the incongruence between these two regions are mainly due to the low rate of mutation found in the mitochondrial DNA; an alternative hypothesis is a decoupling of the chloroplast and mitochondrial DNA inheritance.

Parastrephia and *Diplostephium* group B illustrate examples of intergeneric hybridization in our dataset. *Parastrephia quadrangularis* has an ambiguous and poorly

supported position in the nuclear ribosomal analyses. While in the IB-nr90 analysis, *P. quadrangularis* is sister to the clade comprised by *Floscaldasia* and *Diplostephium* clade C (Fig. 1.4), in the rest of the nuclear ribosomal topologies it is related to *Baccharis*, *Heterothalamus*, and *Diplostephium* clade B (Figs. 1.5–1.9). In the chloroplast and mitochondrial phylogenies, *P. quadrangularis* is nested with high support in a major clade containing group C *Diplostephium* species (Figs. 1.10–1.3). The contradicting positions in the phylogenies along with its long branch in the nuclear ribosomal topology (Fig. 1.15) suggest that *P. quadrangularis* has experienced ancient hybridization. We suspect that the nuclear ribosomal cistron of *P. quadrangularis* is hybrid, probably having segments of a *Diplostephium* clade C ancestor and a *Baccharis-Heterothalamus* species ancestor. On the other hand, the well-supported phylogenetic position of *P. quadrangularis* in the chloroplast and mitochondrial phylogenies suggests that the chloroplast and mitochondrial genomes of *P. quadrangularis* are not hybrid, instead, they were inherited from a *Diplostephium* group C ancestor via hybridization or introgression. These observations are supported by the recombinant and biparental inheritance of the nuclear ribosomal cistron (Hughes & Petersen, 2001; Volkov *et al*., 2007; Ambrose & Crease, 2011) and the mostly non-recombinant and uniparental inheritance of the chloroplast and mitochondrial genomes (Birky, 1995; Jansen & Ruhlman, 2012). Likewise, group B species, *Diplostephium cinereum* and *D*. sp. nov. CAJ2, are closely associated with *Baccharis* and *Heterothalamus* in the nuclear ribosomal topologies (Fig. 1.4) but are nested, positioned near *P. quadrangularis,* in a clade comprised of group C *Diplostephium* species in the chloroplast and mitochondrial topologies (Figs. 1.10, 1.12). We hypothesize that *Diplostephium* clade B is the result of a hybridization event between a *Parastrephia* ancestor and a *Diplostephium* clade C ancestor. This hypothesis is supported by morphological evidence in the case of *Diplostephium* sp. nov. CAJ2, which

has scale-like leaves similar to *P. quadrangularis* but heterogamous capitula with ray flowers that characterize *Diplostephium* species (Fig. 1.16).

Interspecific reticulation is also evident in our dataset. For example, *Diplostephium tenuifolium* is nested in clade A1 in the nuclear ribosomal topology (Fig. 1.4), but it is sister to *D. rosmarinifolium* in the chloroplast and mitochondrial trees, far from other clade A1 species (Figs. 1.10, 1.12). *Diplostephium rosmarinifolium* is widely distributed throughout Colombia, overlapping in range with *D. tenuifolium,* which is restricted to the department of Boyaca in Colombia. Because *D. tenuifolium* presents morphological characteristics of the group A1 (tree shapes of up to 10 m tall, big leaves, and capitulescences with numerous small heads) and does not seem to have a hybrid morphology, we hypothesize that that *D. tenuifolium* recently acquired the chloroplast and mitochondrial genome of *D. rosmarinifolium* via introgression (Fig. 1.16).

Our evidence demonstrates that reticulation has played an ongoing role in the recent diversification of the "South American lineages" within Astereae. The phylogenetic network (Fig. 1.16) shows a complex pattern of reticulate evolution among *Diplostephium* species and between *Diplostephium* clade C and the ancestors of ten other genera. We speculate that intergeneric reticulation occurred early in the divergence of these genera, and, that interspecific hybridization inside *Diplostephium* clades A and C is a current process, as illustrated by the *D. tenuifolium* example and the high number of nuclear ribosomal ambiguities present in numerous *Diplostephium* species. In order to further investigate the processes of hybridization and introgression in the "South American lineages" it would be necessary to employ a technique that surveys the entire nuclear genome. Next-generation sequencing methods like hybrid enrichment (Albert *et al*., 2007, Gnirke *et al*., 2009) and RAD-seq (Peterson *et al*., 2012) could be used to obtain several loci from the nuclear genome. A coalescent analysis of independent

nuclear loci would allow for the inference of a species tree (Heled & Drummond, 2010; Liu *et al*., 2010; Mirarab & Warnow, 2015) and the detection of introgressive nuclear DNA in reticulate evolution scenarios (Pease & Hahn, 2015).

Gene Trees, Species Trees, and Networks

Phylogenetic networks can illustrate processes like hybridization and horizontal gene transfer that cannot be represented by dichotomous trees (Doolittle, 1999; Huson & Bryant, 2006; Rieppel, 2010). Since networks do not have a hierarchical structure, they conflict with traditional taxonomic classification (Doolittle, 1999; Rieppel, 2010) and are not commonly used by systematists as the basis for classification. Instead, systematists try to identify hybrid taxa (e.g., Rieseberg, 1995; Sun *et al*., 2015) and use multiple loci to remove or account for horizontal gene transfer in order to infer a dichotomous species tree (Doolittle, 1999; Davidson *et al*., 2015). The latter statement is especially true for eukaryotes. Therefore, while a network better represents the genetic transfer among lineages, a dichotomous branching tree illustrates hierarchically the speciation history of such lineages.

Numerous authors have proposed that horizontal gene transfer via introgression could cause deviation of the chloroplast and mitochondrial phylogenies from the species tree (Rieseberg & Soltis, 1991; Moore, 1995; Hardig *et al*., 2000; Sun *et al*., 2015). Because chloroplast and mitochondrial inheritance is mostly uniparental and there is generally no recombination following fertilization (Birky, 1995; Jansen & Ruhlman, 2012), an event of chloroplast and mitochondrial capture would completely replace the original chloroplast and mitochondrial DNA of a lineage by an alien one (Rieseberg & Soltis, 1991). This event would erase the inheritance history of the original chloroplast and mitochondrial genomes confounding their history relative to the species tree. Our

dataset confirms the above statements and made us conclude that the gene trees obtained from the chloroplast and mitochondrial DNA are unequivocally different from the species tree. The nuclear ribosomal topology is more congruent with the morphological taxonomy and biogeography of our sampling than the chloroplast and mitochondrial trees. We believe that the nuclear ribosomal region is better at capturing signal to infer the species tree than the chloroplast and mitochondrial DNA because the nuclear ribosomal cistron is biparentally inherited (Volkov *et al*., 2007) and it recombines (Hughes & Petersen, 2001; Ambrose & Crease, 2011) with its copies located on multiple chromosomes (Phillips *et al*., 1971; Álvares & Wendel, 2003). Coalescent methods employed in software packages like ASTRAL (Mirarab & Warnow, 2015), MP-EST (Liu *et al*., 2010), and *BEAST (Heled & Drummond, 2010) are designed to calculate a species tree from multiple loci incorporating models that account for incomplete lineage sorting but not horizontal gene transfer. However, certain levels of horizontal gene transfer can be accounted for when numerous loci are analyzed (>50) with ASTRAL (Davidson *et al*., 2015). Since our dataset shows compelling evidence of horizontal gene transfer and is practicably composed by three markers these methods are not applicable to our dataset.

The nuclear ribosomal topology places most *Diplostephium* (*sensu* Cuatrecasas 1969) species into clades A and C. Clade B has two *Diplostephium* species and is likely a partial descendant of clade C after a hybridization event (Figs. 1.4, 1.16). Clade A is primarily Northern Andean while clade C is primarily Central Andean (Fig. 1.16). Because the type of the genus, *D. ericoides*, is a member of clade C (*Diplostephium* s.s.), clade A must be circumscribed as a different taxon (Vargas, in prep.).

CONCLUSIONS

We urge plant systematists to avoid concatenating data with different inheritance patterns (e.g. chloroplast and nuclear markers) without testing for congruence, and to use caution when using chloroplast and mitochondrial phylogenies as the basis for taxonomic classification taking into consideration that their history could be biased by hybridization and introgression. Topological deviation from the species tree present in chloroplast and mitochondrial markers could potentially affect time calibrations, historical biogeographic reconstructions, and comparative phylogenetic analyses. The evidence presented in our study builds on numerous reports (e.g., Sessa *et al*., 2012; Sun *et al*., 2015; Sochor *et al*., 2015; J. Wu *et al*., 2015) that emphasize a central role of reticulation in plant evolution.

TABLES

Table 1.1 List of specimens with their voucher and GenBank (GB) accession numbers.

Species	Collection	Herbarium	Nuclear ribosomal	Chloroplast	Mitochondrial
Archibaccharis asperifolia (Benth.) S.F.Blake	Trujillo-1192	TEX	KX063950	KX063859	
Aztecaster matudae (Rzed.) G.L.Nesom	Hinton-29102	TEX	KX063978	KX063935	
Baccharis genistelloides (Lam.) Pers.	Vargas-358	HUSA	KX063991	KX063864	
Baccharis tricuneata (L.f.) Pers.	Vargas-356	HUSA	KX063954	KX063888	
Blakiella bartsiifolia (S.F.Blake) Cuatrec.	Cuatrecasas-28129	TEX	KX063989	KX063886	
Diplostephium alveolatum Cuatrec.	Vargas-205	ANDES	KX063979	KX063856	
Diplostephium antioquense Cuatrec.	Vargas-533	ANDES	KX064025	KX063898	
Diplostephium apiculatum S.F.Blake	Vargas-332	ANDES	KX063986	KX063943	
Diplostephium azureum Cuatrec.	Vargas-389	HUSA	KX063947	KX063907	
Diplostephium barclayanum Cuatrec.	Vargas-477	QCA, TEX	KX064022	KX063865	
Diplostephium cajamarquillense Cuatrec.	Sagastegui-17024	F	KX063963	KX063894	
Diplostephium callilepis S.F.Blake	Vargas-376	HUSA	KX063983	KX063870	
Diplostephium camargoanum Cuatrec.	Vargas-319	ANDES	KX064016	KX063933	
Diplostephium cayambense Cuatrec.	Vargas-234	ANDES	KX064019	KX063912	
Diplostephium cinerascens Cuatrec.	Vargas-446	ANDES	KX063975	KX063862	
Diplostephium cinereum Cuatrec.	Caceres-1494	HUSA	KX063999	KX063889	
Diplostephium colombianum (Cuatrec.) Cuatrec.	Vargas-299	ANDES	KX063996	KX063876	
Diplostephium coriaceum Cuatrec.	Barclay-6691	US	KX063969	KX063937	
Diplostephium costaricense S.F.Blake	Martinez-33	TEX	KX063987	KX063901	
Diplostephium crypteriophyllum Cuatrec.	Vargas-467	QCA, TEX	KX063966	KX063905	
Diplostephium empetrifolium S.F.Blake	Vargas-469	QCA, TEX	KX063970	KX063925	
Diplostephium ericoides (Lam.) Cabrera	Vargas-489	QCA, TEX	KX064026	KX063892	

Table 1.1. (Continued)

Diplostephium eriophorum Wedd.	Vargas-505	ANDES	KX063985	KX063896	
Diplostephium espinosae Cuatrec.	Vargas-464	QCA, TEX	KX063992	KX063903	
Diplostephium floribundum (Benth.) Wedd.	Vargas-499	ANDES	KX064010	KX063872	
Diplostephium foliosissimum S.F.Blake	Sagastegui-16804	F	KX064035	KX063909	
Diplostephium frontinense Cuatrec.	Vargas-524	ANDES	KX063973	KX063927	
Diplostephium glandulosum Hieron.	Vargas-247	ANDES	KX063993	KX063866	
Diplostephium glutinosum S.F.Blake	Vargas-339	ANDES	KX063958	KX063897	
Diplostephium gnidioides S.F.Blake	Vargas-430	HUSA	KX063960	KX063887	
Diplostephium goodspeedii Cuatrec.	Vargas-373	HUSA	KX064021	KX063940	
Diplostephium gynoxyoides Cuatrec.	Vargas-395	HUSA	KX064023	KX063877	
Diplostephium haenkei (DC.) Wedd.	Vargas-372	HUSA	KX063971	KX063893	
Diplostephium hartwegii Hieron.	Vargas-456	QCA, TEX	KX064007	KX063880	KX063855
Diplostephium heterophyllum Cuatrec.	Vargas-162	ANDES	KX064036	KX063931	
Diplostephium hippophae S.F.Blake	Vargas-393	HUSA	KX063997	KX063944	
Diplostephium huertasii Cuatrec.	Vargas-518	ANDES	KX063967	KX063915	
Diplostephium inesianum Cuatrec.	Barclay-6546	US	KX063961	KX063930	
Diplostephium jaramilloi Cuatrec.	Prieto-1118	FMB	KX064018	KX063928	
Diplostephium jelskii Hieron.	Cano-14716	USM	KX064013	KX063860	
Diplostephium jenesanum S.Díaz & Morales-P.	Vargas-509	ANDES	KX064033	KX063934	
Diplostephium juajibioyi Cuatrec.	Vargas-50	ANDES	KX063968	KX063913	
Diplostephium juniperinum Cuatrec.	Vargas-480	QCA, TEX	KX063988	KX063883	
Diplostephium lacunosum Cuatrec.	Vargas-260	ANDES	KX063965	KX063900	
Diplostephium lechleri (Sch.Bip.) Wedd.	Vargas-381	HUSA	KX063952	KX063868	
Diplostephium meyenii (Sch.Bip. ex Wedd.) S.F.Blake	Vargas-351	HUSA	KX064005	KX063919	
Diplostephium mutiscuanum Cuatrec.	Vargas-346	ANDES	KX064020	KX063929	
Diplostephium oblanceolatum S.F.Blake	Vargas-465	QCA, TEX	KX064028	KX063941	

Table 1.1. (Continued)

Diplostephium oblongifolium Cuatrec.	Vargas-344	ANDES	KX063984	KX063906
Diplostephium obtusum S.F.Blake	Dorr-9246	US	KX064029	KX063920
Diplostephium ochraceum (Kunth) Nees	Vargas-161	ANDES	KX063959	KX063945
Diplostephium oxapampanum Cuatrec.	Vargas-408	HUSA	KX063976	KX063884
Diplostephium phylicoides (Kunth) Wedd.	Vargas-301	ANDES	KX064024	KX063895
Diplostephium pulchrum S.F.Blake [OXA]	Ortiz-722	HUSA	KX063980	KX063857
Diplostephium pulchrum S.F.Blake [PAS]	Vargas-404	HUSA	KX063956	KX063942
Diplostephium revolutum S.F.Blake	Vargas-321	ANDES	KX064002	KX063878
Diplostephium rhododendroides Hieron.	Vargas-233	ANDES	KX063981	KX063885
Diplostephium rhomboidale Cuatrec. [COL]	Vargas-340	ANDES	KX064032	KX063890
Diplostephium rhomboidale Cuatrec. [ECU]	Vargas-492	QCA, TEX	KX063972	KX063874
Diplostephium romeroi Cuatrec.	Barclay-6775	US	KX063948	KX063911
Diplostephium rosmarinifolium (Benth.) Wedd.	Vargas-304	ANDES	KX063995	KX063939
Diplostephium rupestre (Kunth) Wedd.	Vargas-504	ANDES	KX063977	KX063882
Diplostephium sagasteguii Cuatrec.	Sagastegui-16951	F	KX064017	KX063932
Diplostephium schultzii Wedd. [CAL]	Vargas-500	ANDES	KX064037	KX063936
Diplostephium schultzii Wedd. [CUN]	Vargas-164	ANDES	KX063962	KX063926
Diplostephium serratifolium Cuatrec.	Sagastegui-16159a	F	KX063990	KX063924
Diplostephium sp. nov. [ANT]	Alzate-3284	HUA	KX064015	KX063918
Diplostephium sp. nov. [CAJ]	Sanchez-11193	F	KX063982	KX063858
Diplostephium sp. nov. [CAJ2]	Sagastegui-15758	F	KX064006	KX063904
Diplostephium sp. nov. [JUN]	Vargas-427	HUSA	KX064012	KX063938
Diplostephium sp. nov. [JUN2]	Vargas-414	HUSA	KX064003	KX063946
Diplostephium sp. nov. [JUN3]	Vargas-419	HUSA	KX063955	KX063902
Diplostephium sp. nov. [JUN4]	Vargas-415	HUSA	KX063998	KX063871
Diplostephium sp. nov. [OXA]	Ortiz-815	HUSA	KX064009	KX063867
Diplostephium spinulosum Wedd.	Vargas-445	ANDES	KX064031	KX063917

Table 1.1. (Continued)

Diplostephium tachirense V.M.Badillo	Vargas-336	ANDES	KX064004	KX063922
Diplostephium tenuifolium Cuatrec.	Vargas-520	ANDES	KX064027	KX063875
Diplostephium venezuelense Cuatrec.	Norrbom-89V33	US	KX063951	KX063914
Diplostephium violaceum Cuatrec.	Vargas-501	ANDES	KX064000	KX063891
Exostigma notobellidiastrum (Griseb.) Sancho	Tressens-6388	TEX	KX064014	KX063881
Floscaldasia hypsophila Cuatrec.	Cleef-10912	ANDES	KX063957	KX063916
Heterothalamus alienus (Spreng.) Kuntze	Bartlett-20909	TEX	KX063964	KX063869
Hinterhubera ericoides Wedd.	Stergios-20385	TEX	KX063974	KX063910
Laennecia sophiifolia (Kunth) G.L.Nesom	Reina-2010-805	TEX	KX064011	KX063899
Laestadia muscicola Sch.Bip. ex Wedd.	Paco-31	TEX	KX063953	KX063873
Lagenophora cuchumatanica Beaman & De Jong	De Jong-694	TEX	KX064034	KX063879
Llerasia caucana (S.F.Blake) Cuatrec.	Vargas-444	ANDES	KX064001	KX063908
Oritrophium peruvianum (Lam.) Cuatrec.	Vargas-448	ANDES	KX063949	KX063861
Parastrephia quadrangularis (Meyen) Cabrera	Vargas-440	HUSA	KX064008	KX063923
Soliva sessilis Ruiz & Pav.	Sagastegui-17106	F	KX064030	KX063863
Westoniella kohkemperi Cuatrec.	Pruskii-3925	TEX	KX063994	KX063921

Table 1.2. Descriptive statistics of the matrices obtained. PICs: parsimony informative sites (calculated excluding outgroups). TS: transcribed spacers (including ETS, ITS1, and ITS2). NTS: non-transcribed spacer. nr: nuclear ribosomal.

Dataset	Sites	Missing data %	Ambiguities	PICs	Coding PICs (%)	Non-coding PICs (%, TS+NTS% if applicable)
nr50	13,362	0.00%	25 (0.003%)	1,425 (10.66%)	114(8.00%)	1,311 (34.32+57.68%)
nr75	13,362	0.00%	3201 (0.384%)	1,273 (9.53%)	93(7.31%)	1,180 (34.01+58.68%)
nr90	13,362	0.00%	5012 (0.602%)	1,203 (9.00%)	86(7.15%)	1,117 (33.83+59.02%)
chloroplast	135,440	0.02%	103 (0.022%)	2,169 (1.60%)	709 (32.69%)	1,460 (67.31%)
mitochondrial	209,392	1.50%	0	1,124 (0.54%)	40(3.56%)	1,084 (96.44%)

Table 1.3 Bayesian factor comparison between the two partition models calculated with MrBayes in each dataset. M0: unpartitioned model. M1: partitioned model. nr: nuclear ribosomal matrix. cp: chloroplast matrix. mt: mitochondrial matrix.

Region	Harmonic mean marginal ln*L*		Bayes Factor	Stepping-stone marginal ln*L*		Bayes Factor
	M0	M1	M0 – M1	M0	M1	M0 – M1
nr50	-72698.76	-68046.52	-4652.24	-73447.88	-68805.2	-4642.68
nr75	-67156.72	-62591.73	-4564.99	-67934.08	-63360.31	-4573.77
nr90	-65102.02	-60592.81	-4509.21	-65858.43	-61379.04	-4479.39
cp	-293607.91	-290782.09	-2825.82	-294399.45	-291582.59	-2816.86
mt	-410381.23	-408912.98	-1468.25	-411267.49	-409841.04	-1426.45

Table 1.4 Models of evolution inferred by jModelTest and MrBayes on the partitions used. The final MrBayes analysis used the nucleotide substitution model inferred by MrBayes plus the +Γ and +I parameters in suggested by jModeltest. nr: nuclear ribosomal matrix. cp: chloroplast matrix. mt: mitochondrial matrix.

Dataset	Partition	AICc model	-lnL	AICc score	MrBayes model	Posterior Probability
nr75	coding	GTR+I+Γ	10236.83329	20867.81749	122345	0.285
	transcribed spacers	GTR+I+Γ	17071.14411	34554.87915	123451	0.336
	non-coding (NTS)	012232+Γ+F	34224.70918	68836.35287	121121	0.375
cp	coding	012313+I+Γ+F	140860.8997	282098.7494	123145	0.672
	non-coding	012310+I+Γ+F	149090.4473	298558.0724	123342	0.289
mt	coding	001102+I+Γ+F	47170.9926	94718.24837	122211	0.188
	non-coding	TPM1uf+I+Γ	360919.2953	722212.9854	123321	0.821

Table 1.5. Number of ambiguities (IUPAC symbols M, R, W, S, Y, K, V, H, D, and B) calculated from the nuclear ribosomal 90% threshold consensus.

Species	Number of ambiguities
Archibaccharis asperifolia	20
Aztecaster matudae	72
Baccharis genistelloides	24
Baccharis tricuneata	13
Blakiella bartsiifolia	6
Diplostephium alveolatum	89
Diplostephium antioquense	84
Diplostephium apiculatum	80
Diplostephium azureum	5
Diplostephium barclayanum	10
Diplostephium cajamarquillens	6
Diplostephium callilepis	28
Diplostephium camargoanum	133
Diplostephium cayambense	83
Diplostephium cinerascens	64
Diplostephium cinereum	20
Diplostephium colombianum	118
Diplostephium coriaceum	107
Diplostephium costaricense	79
Diplostephium crypteriophyllu	14
Diplostephium empetrifolium	19
Diplostephium ericoides	18
Diplostephium eriophorum	3
Diplostephium espinosae	5
Diplostephium floribundum	86
Diplostephium foliosissimum	37
Diplostephium frontinense	129
Diplostephium glandulosum	2
Diplostephium glutinosum	121
Diplostephium gnidioides	37
Diplostephium goodspeedii	49
Diplostephium gynoxyoides	121
Diplostephium haenkei	37
Diplostephium hartwegii	15
Diplostephium heterophyllum	198

Table 1.5. (Continued)

Diplostephium hippophae	21
Diplostephium huertasii	4
Diplostephium inesianum	104
Diplostephium jaramilloi	97
Diplostephium jelskii	8
Diplostephium jenesanum	80
Diplostephium juajibioyi	101
Diplostephium juniperinum	20
Diplostephium lacunosum	76
Diplostephium lechleri	46
Diplostephium meyenii	8
Diplostephium mutiscuanum	57
Diplostephium oblanceolatum	43
Diplostephium oblongifolium	46
Diplostephium obtusum	67
Diplostephium ochraceum	95
Diplostephium oxapampanum	34
Diplostephium phylicoides	81
Diplostephium pulchrum OXA	59
Diplostephium pulchrum PAS	42
Diplostephium revolutum	93
Diplostephium rhododendroides	120
Diplostephium rhomboidale COL	115
Diplostephium rhomboidale ECU	97
Diplostephium romeroi	12
Diplostephium rosmarinifolium	120
Diplostephium rupestre	14
Diplostephium sagasteguii	11
Diplostephium schultzii CAL	33
Diplostephium schultzii CUN	113
Diplostephium serratifolium	23
Diplostephium sp. nov. ANT	104
Diplostephium sp. nov. CAJ	173
Diplostephium sp. nov. CAJ2	16
Diplostephium sp. nov. JUN	76
Diplostephium sp. nov. JUN2	65
Diplostephium sp. nov. JUN3	41
Diplostephium sp. nov. JUN4	61
Diplostephium sp. nov. OXA	55

Table 1.5. (Continued)

Diplostephium spinulosum	16
Diplostephium tachirense	70
Diplostephium tenuifolium	82
Diplostephium venezuelense	71
Diplostephium violaceum	69
Exostigma notobellidiastrum	0
Floscaldasia hypsophila	3
Heterothalamus alienus	4
Hinterhubera ericoides	10
Laennecia sophiifolia	0
Laestadia muscicola	0
Lagenophora cuchumatanica	16
Llerasia caucana	83
Oritrophium peruvianum	121
Parastrephia quadrangularis	19
Soliva sessilis	84

FIGURES

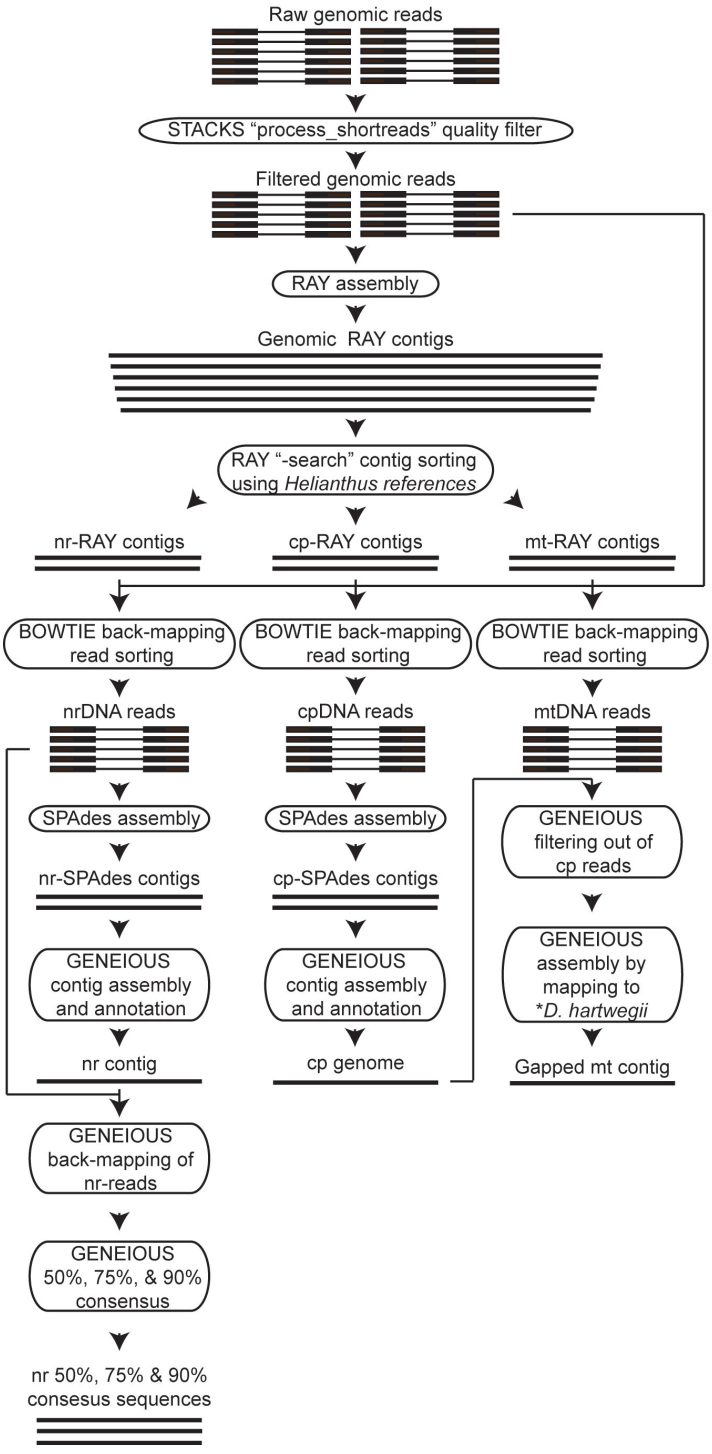

Figure 1.1. Diagram representing the sequence assembly pipeline.

Figure 1.2. Circular representation of the chloroplast genome of *Diplostephium haenkei*.

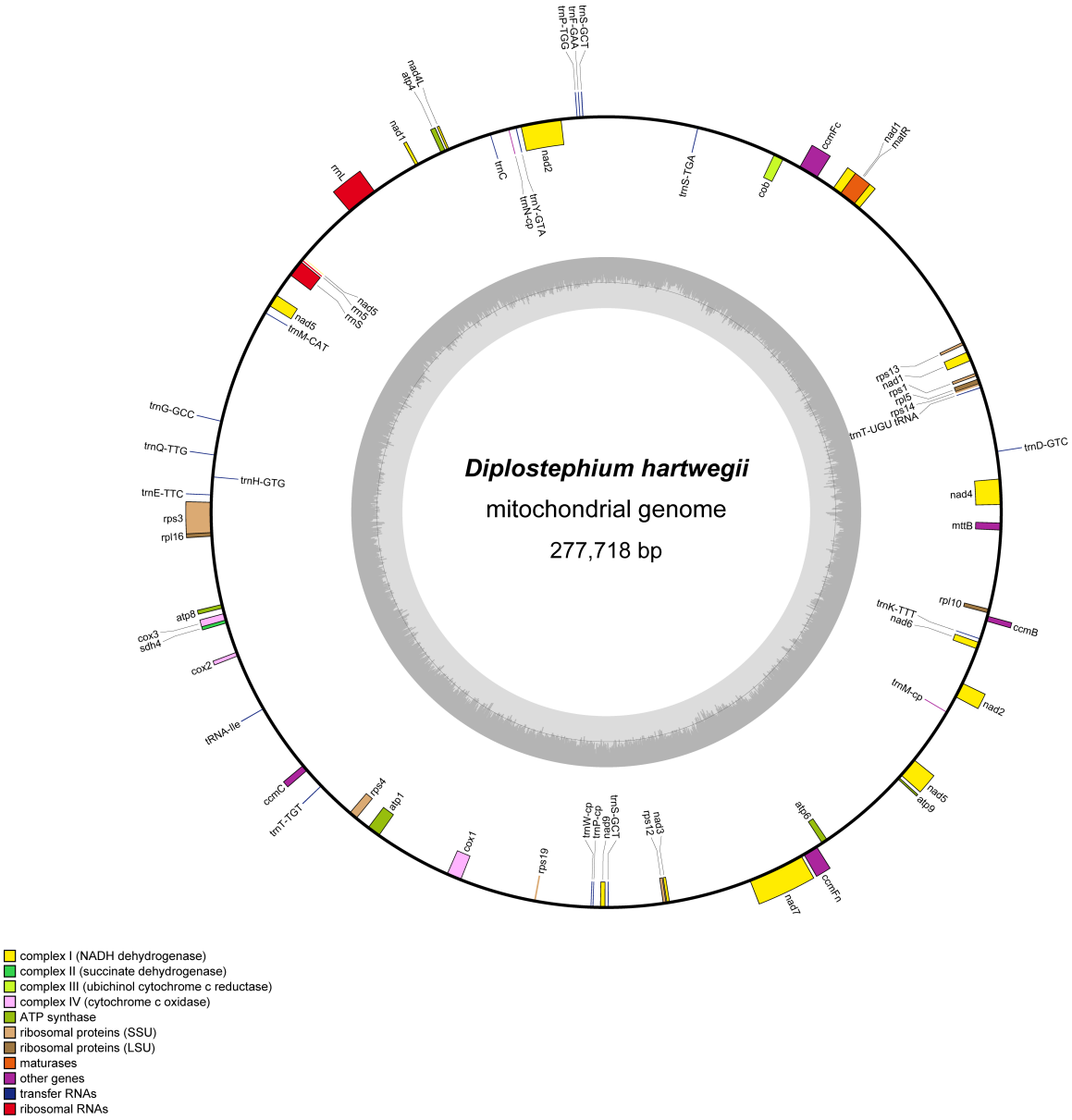

Figure 1.3. Circular representation of the mitochondrial genome of *Diplostephium hartwegii*.

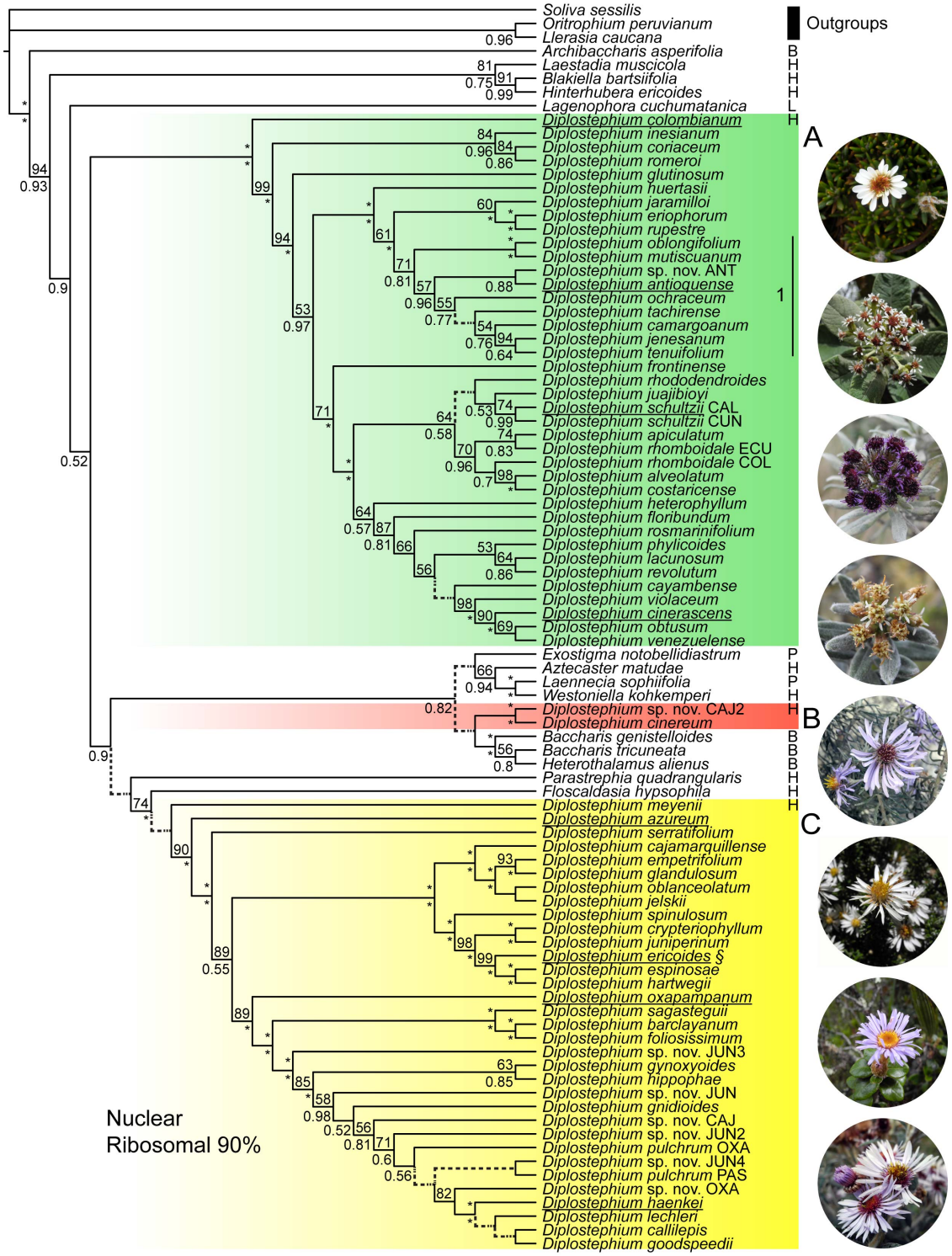
Soliva sessilis
Oritrophium peruvianum
Llerasia caucana
Archibaccharis asperifolia
Laestadia muscicola
Blakiella bartsiifolia
Hinterhubera ericoides
Lagenophora cuchumatanica
Diplostephium colombianum
Diplostephium inesianum
Diplostephium coriaceum
Diplostephium romeroi
Diplostephium glutinosum
Diplostephium huertasii
Diplostephium jaramilloi
Diplostephium eriophorum
Diplostephium rupestre
Diplostephium oblongifolium
Diplostephium mutiscuanum
Diplostephium sp. nov. ANT
Diplostephium antioquense
Diplostephium ochraceum
Diplostephium tachirense
Diplostephium camargoanum
Diplostephium jenesanum
Diplostephium tenuifolium
Diplostephium frontinense
Diplostephium rhododendroides
Diplostephium juajibioyi
Diplostephium schultzii CAL
Diplostephium schultzii CUN
Diplostephium apiculatum
Diplostephium rhomboidale ECU
Diplostephium rhomboidale COL
Diplostephium alveolatum
Diplostephium costaricense
Diplostephium heterophyllum
Diplostephium floribundum
Diplostephium rosmarinifolium
Diplostephium phylicoides
Diplostephium lacunosum
Diplostephium revolutum
Diplostephium cayambense
Diplostephium violaceum
Diplostephium cinerascens
Diplostephium obtusum
Diplostephium venezuelense
Exostigma notobellidiastrum
Aztecaster matudae
Laennecia sophiifolia
Westoniella kohkemperi
Diplostephium sp. nov. CAJ2
Diplostephium cinereum
Baccharis genistelloides
Baccharis tricuneata
Heterothalamus alienus
Parastrephia quadrangularis
Floscaldasia hypsophila
Diplostephium meyenii
Diplostephium azureum
Diplostephium serratifolium
Diplostephium cajamarquillense
Diplostephium empetrifolium
Diplostephium glandulosum
Diplostephium oblanceolatum
Diplostephium jelskii
Diplostephium spinulosum
Diplostephium crypteriophyllum
Diplostephium juniperinum
Diplostephium ericoides §
Diplostephium espinosae
Diplostephium hartwegii
Diplostephium oxapampanum
Diplostephium sagasteguii
Diplostephium barclayanum
Diplostephium foliosissimum
Diplostephium sp. nov. JUN3
Diplostephium gynoxyoides
Diplostephium hippophae
Diplostephium sp. nov. JUN
Diplostephium gnidioides
Diplostephium sp. nov. CAJ
Diplostephium sp. nov. JUN2
Diplostephium pulchrum OXA
Diplostephium sp. nov. JUN4
Diplostephium pulchrum PAS
Diplostephium sp. nov. OXA
Diplostephium haenkei
Diplostephium lechleri
Diplostephium callilepis
Diplostephium goodspeedii
Outgroups
A
B
C
1
Nuclear
Ribosomal 90%

Figure 1.4.

Figure. 1.4. Nuclear ribosomal maximum clade credibility tree obtained by Bayesian inference with the 90% consensus matrix. Numbers above the branches indicate the bootstrap support (BS) obtained by RAxML. Numbers under the branches indicate the Bayesian posterior probability (BPP). Branches with low support (BS<50, BPP<0.5) are dashed and their support is not shown. Asterisks (*) represent a BS of 100 or a BPP of 1 according to their position. The green, red, and yellow boxes delimit clades A, B, and C respectively. The letter next to the species name indicates the subtribe to which the genus belongs: B) Baccharidinae, H) Hinterhuberinae, L) Lagenophorinae, and P) Podocominae. Subtribes for clades A, B, and C are indicated only on the first species at the top. 1) Clade of *Diplostephium* comprised by arborescent species. The section mark (§) indicates the type species of *Diplostephium*. Photos at the right correspond to those species underlined respectively from top to bottom.

Figure 1.5. Nuclear ribosomal maximum credibility tree obtained by Bayesian Inference with the 50% consensus matrix. Numbers below the branches indicate the Bayesian posterior probability (BPP). Branches with low support (BPP<0.5) are dashed and their support is not shown. Color boxes follow the convention of Fig. 1.4.

Figure 1.6. Nuclear ribosomal maximum credibility tree obtained by Bayesian Inference with the 75% consensus matrix. Numbers below the branches indicate the Bayesian posterior probability (BPP). Branches with low support (BPP<0.5) are dashed and their support is not shown. Color boxes follow the convention of Fig. 1.4.

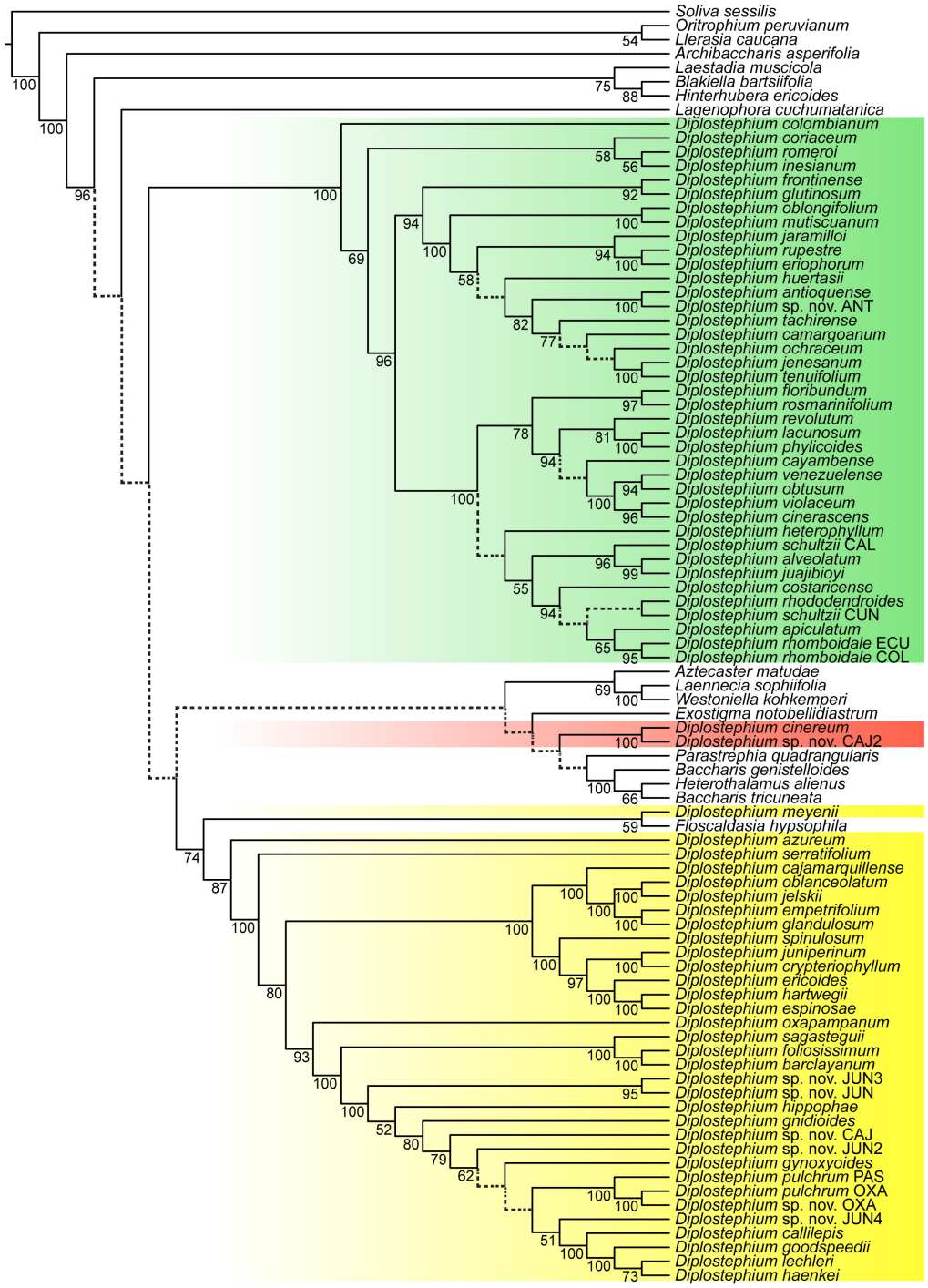

Figure 1.7. Nuclear ribosomal best tree obtained by Maximum Likelihood with the 50% consensus matrix. Numbers below the branches indicate bootstrap support (BS). Branches with low support (BS<50) are dashed and their support is not shown. Color boxes follow the convention of Fig. 1.4.

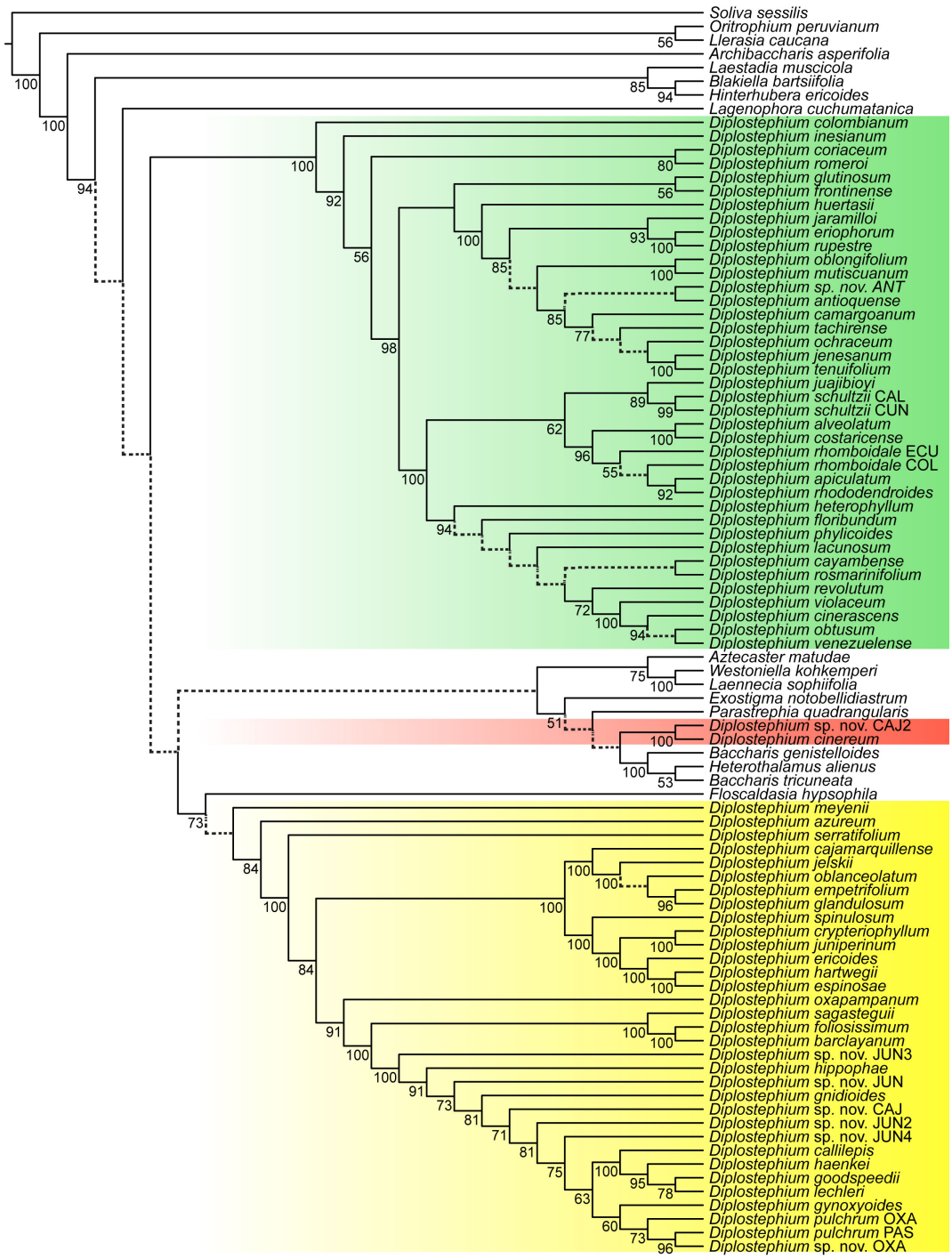

Figure 1.8. Nuclear ribosomal best tree obtained by Maximum Likelihood with the 75% consensus matrix. Numbers below the branches indicate bootstrap support (BS). Branches with low support (BS<50) are dashed and their support is not shown. Color boxes follow the convention of Fig. 1.4.

Figure 1.9. Nuclear ribosomal best tree obtained by Maximum Likelihood with the 90% consensus matrix. Numbers below the branches indicate bootstrap support (BS). Branches with low support (BS<50) are dashed and their support is not shown. Color boxes follow the convention of Fig. 1.4.

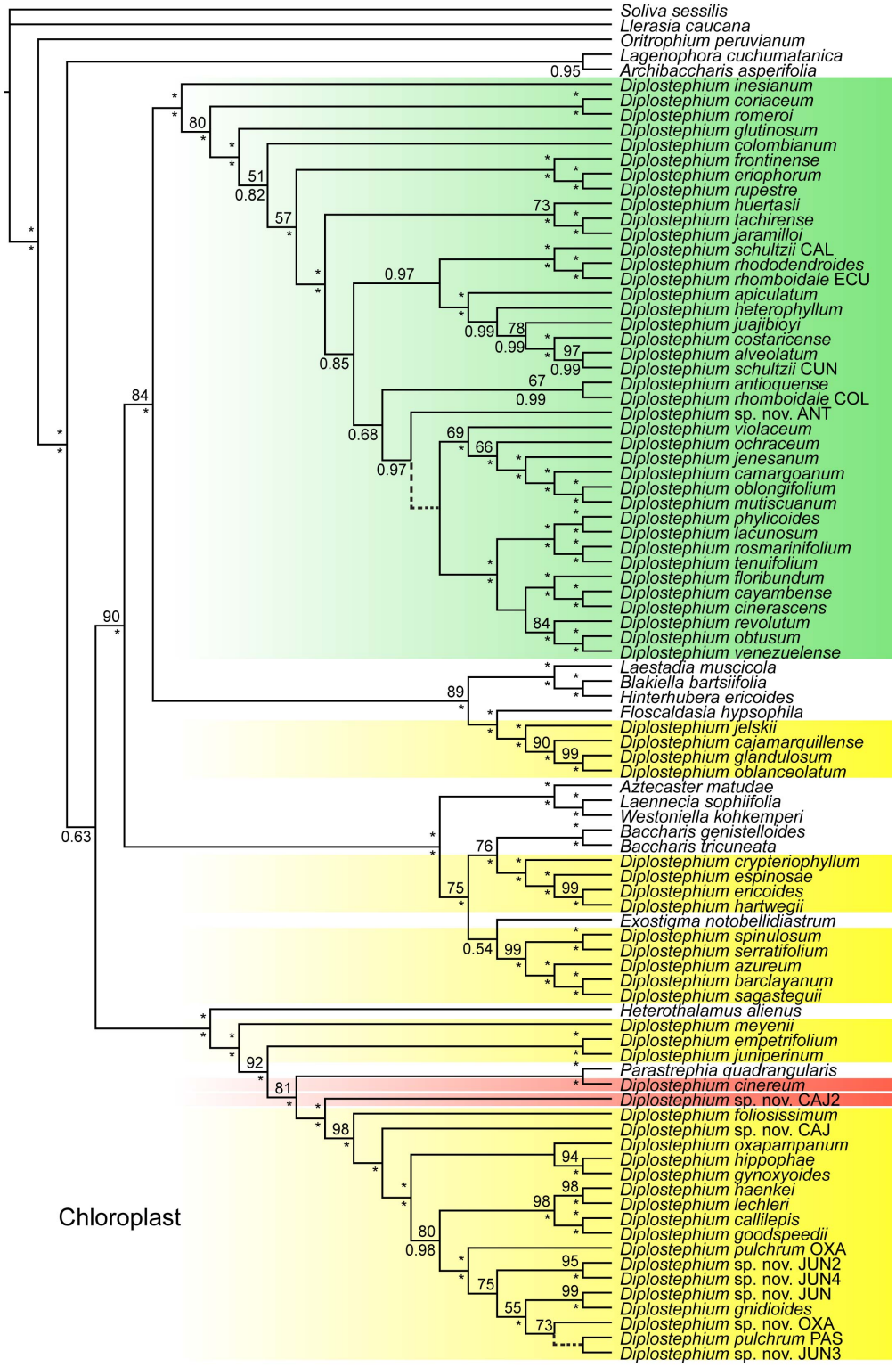
Soliva sessilis
Llerasia caucana
Oritrophium peruvianum
Lagenophora cuchumatanica
Archibaccharis asperifolia
Diplostephium inesianum
Diplostephium coriaceum
Diplostephium romeroi
Diplostephium glutinosum
Diplostephium colombianum
Diplostephium frontinense
Diplostephium eriophorum
Diplostephium rupestre
Diplostephium huertasii
Diplostephium tachirense
Diplostephium jaramilloi
Diplostephium schultzii CAL
Diplostephium rhododendroides
Diplostephium rhomboidale ECU
Diplostephium apiculatum
Diplostephium heterophyllum
Diplostephium juajibioyi
Diplostephium costaricense
Diplostephium alveolatum
Diplostephium schultzii CUN
Diplostephium antioquense
Diplostephium rhomboidale COL
Diplostephium sp. nov. ANT
Diplostephium violaceum
Diplostephium ochraceum
Diplostephium jenesanum
Diplostephium camargoanum
Diplostephium oblongifolium
Diplostephium mutiscuanum
Diplostephium phylicoides
Diplostephium lacunosum
Diplostephium rosmarinifolium
Diplostephium tenuifolium
Diplostephium floribundum
Diplostephium cayambense
Diplostephium cinerascens
Diplostephium revolutum
Diplostephium obtusum
Diplostephium venezuelense
Laestadia muscicola
Blakiella bartsiifolia
Hinterhubera ericoides
Floscaldasia hypsophila
Diplostephium jelskii
Diplostephium cajamarquillense
Diplostephium glandulosum
Diplostephium oblanceolatum
Aztecaster matudae
Laennecia sophiifolia
Westoniella kohkemperi
Baccharis genistelloides
Baccharis tricuneata
Diplostephium crypteriophyllum
Diplostephium espinosae
Diplostephium ericoides
Diplostephium hartwegii
Exostigma notobellidiastrum
Diplostephium spinulosum
Diplostephium serratifolium
Diplostephium azureum
Diplostephium barclayanum
Diplostephium sagasteguii
Heterothalamus alienus
Diplostephium meyenii
Diplostephium empetrifolium
Diplostephium juniperinum
Parastrephia quadrangularis
Diplostephium cinereum
Diplostephium sp. nov. CAJ2
Diplostephium foliosissimum
Diplostephium sp. nov. CAJ
Diplostephium oxapampanum
Diplostephium hippophae
Diplostephium gynoxyoides
Diplostephium haenkei
Diplostephium lechleri
Diplostephium callilepis
Diplostephium goodspeedii
Diplostephium pulchrum OXA
Diplostephium sp. nov. JUN2
Diplostephium sp. nov. JUN4
Diplostephium sp. nov. JUN
Diplostephium gnidioides
Diplostephium sp. nov. OXA
Diplostephium pulchrum PAS
Diplostephium sp. nov. JUN3
Chloroplast

Figure 1.10.

Figure 1.10. Chloroplast maximum credibility tree obtained by Bayesian inference. Numbers above the branches indicate the bootstrap support (BS) obtained by RAxML. Numbers under the branches indicate the Bayesian posterior probability (BPP). Branches with low support (BS<50, BPP<0.5) are dashed and their support is not shown. Asterisks (*) represent a BS of 100 or a BPP of 1 according to their position. Color boxes follow the convention of Fig. 1.4.

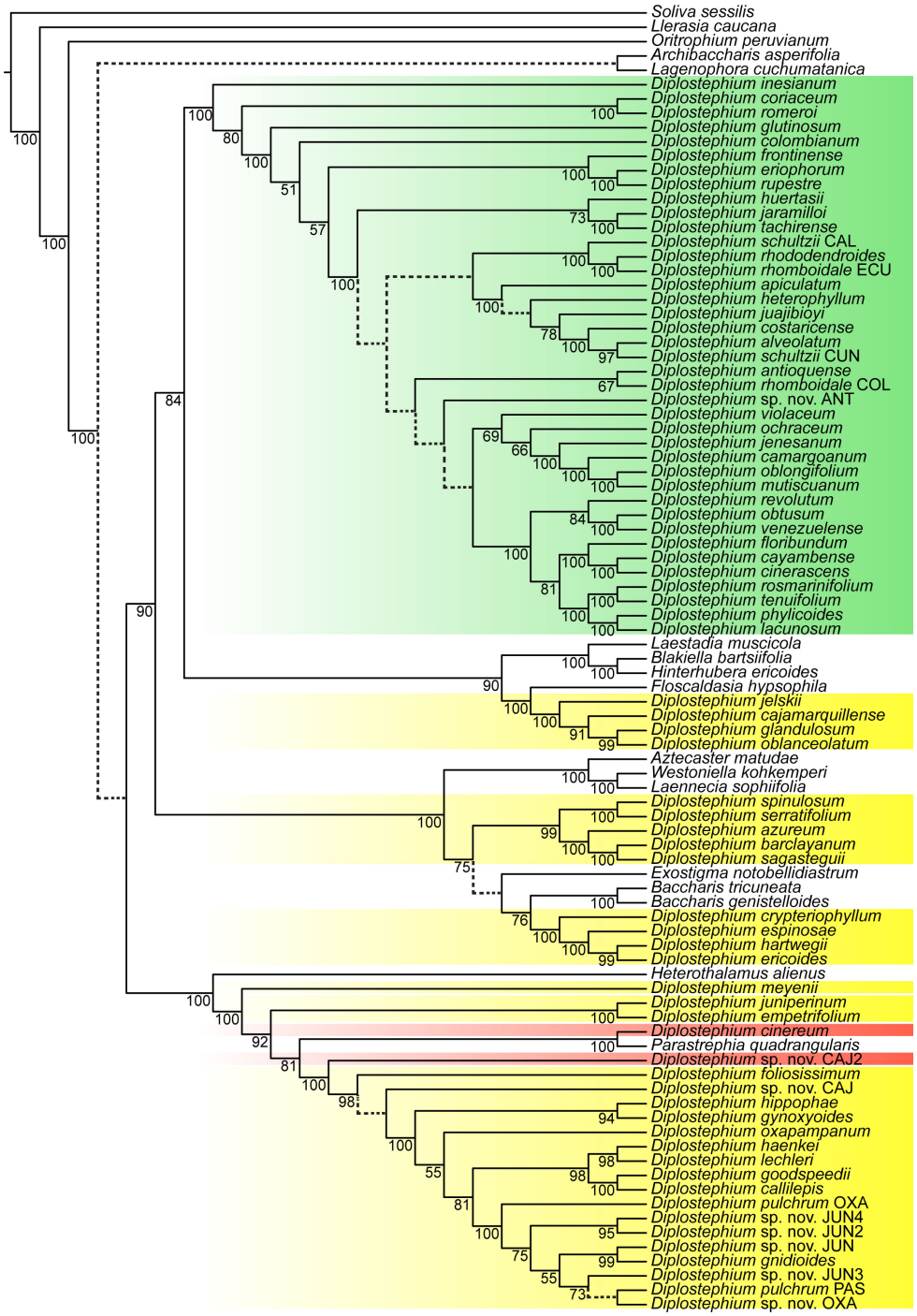

Figure 1.11. Chloroplast best tree obtained by Maximum Likelihood. Numbers below the branches indicate bootstrap support (BS). Branches with low support (BS<50) are dashed and their support is not shown. Color boxes follow the convention of Fig. 1.4.

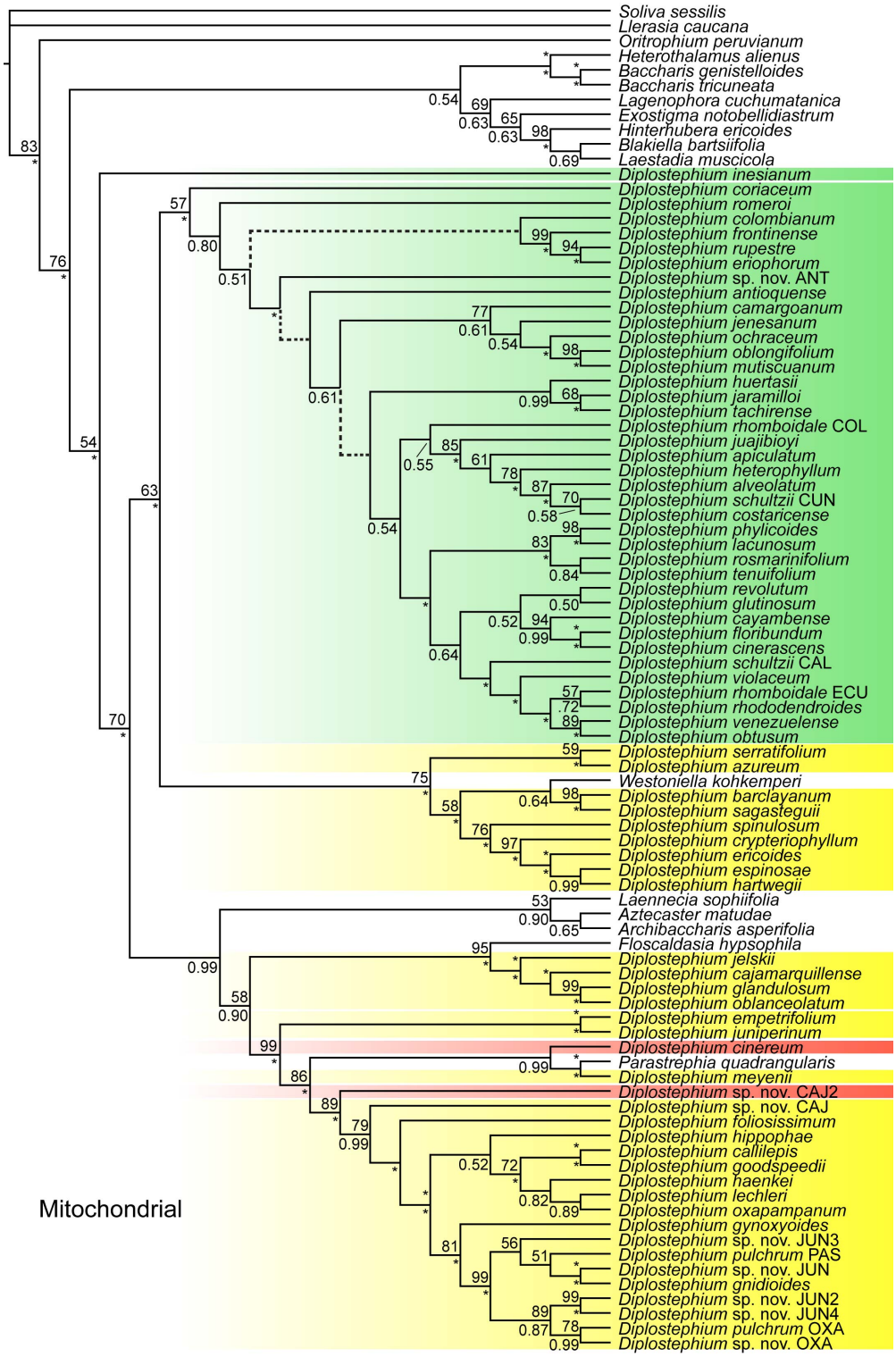
Soliva sessilis
Llerasia caucana
Oritrophium peruvianum
Heterothalamus alienus
Baccharis genistelloides
Baccharis tricuneata
Lagenophora cuchumatanica
Exostigma notobellidiastrum
Hinterhubera ericoides
Blakiella bartsiifolia
Laestadia muscicola
Diplostephium inesianum
Diplostephium coriaceum
Diplostephium romeroi
Diplostephium colombianum
Diplostephium frontinense
Diplostephium rupestre
Diplostephium eriophorum
Diplostephium sp. nov. ANT
Diplostephium antioquense
Diplostephium camargoanum
Diplostephium jenesanum
Diplostephium ochraceum
Diplostephium oblongifolium
Diplostephium mutiscuanum
Diplostephium huertasii
Diplostephium jaramilloi
Diplostephium tachirense
Diplostephium rhomboidale COL
Diplostephium juajibioyi
Diplostephium apiculatum
Diplostephium heterophyllum
Diplostephium alveolatum
Diplostephium schultzii CUN
Diplostephium costaricense
Diplostephium phylicoides
Diplostephium lacunosum
Diplostephium rosmarinifolium
Diplostephium tenuifolium
Diplostephium revolutum
Diplostephium glutinosum
Diplostephium cayambense
Diplostephium floribundum
Diplostephium cinerascens
Diplostephium schultzii CAL
Diplostephium violaceum
Diplostephium rhomboidale ECU
Diplostephium rhododendroides
Diplostephium venezuelense
Diplostephium obtusum
Diplostephium serratifolium
Diplostephium azureum
Westoniella kohkemperi
Diplostephium barclayanum
Diplostephium sagasteguii
Diplostephium spinulosum
Diplostephium crypteriophyllum
Diplostephium ericoides
Diplostephium espinosae
Diplostephium hartwegii
Laennecia sophiifolia
Aztecaster matudae
Archibaccharis asperifolia
Floscaldasia hypsophila
Diplostephium jelskii
Diplostephium cajamarquillense
Diplostephium glandulosum
Diplostephium oblanceolatum
Diplostephium empetrifolium
Diplostephium juniperinum
Diplostephium cinereum
Parastrephia quadrangularis
Diplostephium meyenii
Diplostephium sp. nov. CAJ2
Diplostephium sp. nov. CAJ
Diplostephium foliosissimum
Diplostephium hippophae
Diplostephium callilepis
Diplostephium goodspeedii
Diplostephium haenkei
Diplostephium lechleri
Diplostephium oxapampanum
Diplostephium gynoxyoides
Diplostephium sp. nov. JUN3
Diplostephium pulchrum PAS
Diplostephium sp. nov. JUN
Diplostephium gnidioides
Diplostephium sp. nov. JUN2
Diplostephium sp. nov. JUN4
Diplostephium pulchrum OXA
Diplostephium sp. nov. OXA
Mitochondrial

Figure 1.12.

Figure 1.12. Mitochondrial maximum clade credibility tree obtained by Bayesian inference. Numbers above the branches indicate the bootstrap support (BS) obtained by RAxML. Numbers under the branches indicate the Bayesian posterior probability (BPP). Branches with low support (BS<50, BPP<0.5) are dashed and their support is not shown. Asterisks (*) represent a BS of 100 or a BPP of 1 according to their position. Color boxes follow the convention of Fig. 1.4.

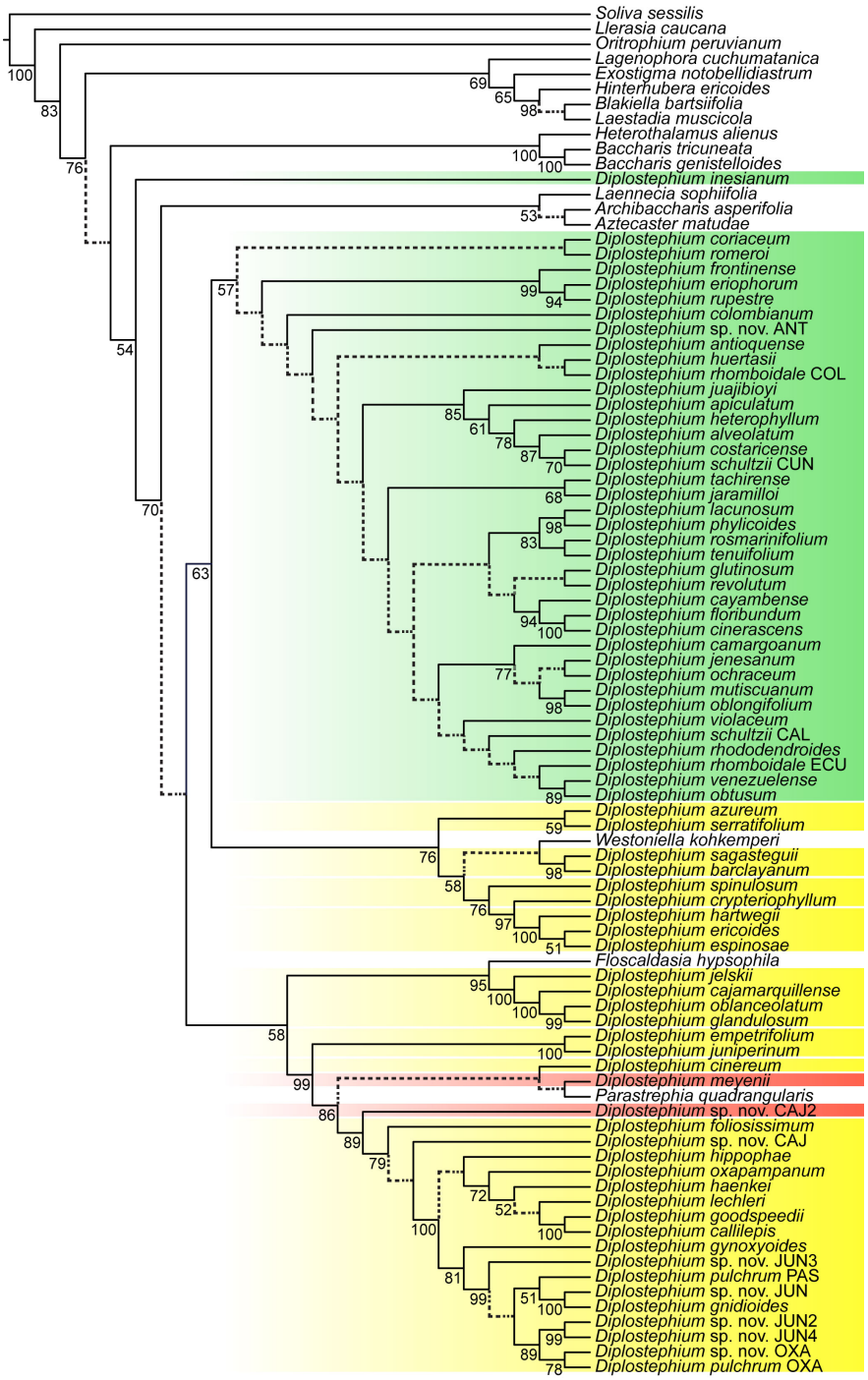

Figure 1.13. Mitochondrial best tree obtained by Maximum Likelihood. Numbers below the branches indicate bootstrap support (BS). Branches with low support (BS<50) are dashed and their support is not shown. Color boxes follow the convention of Fig. 1.4.

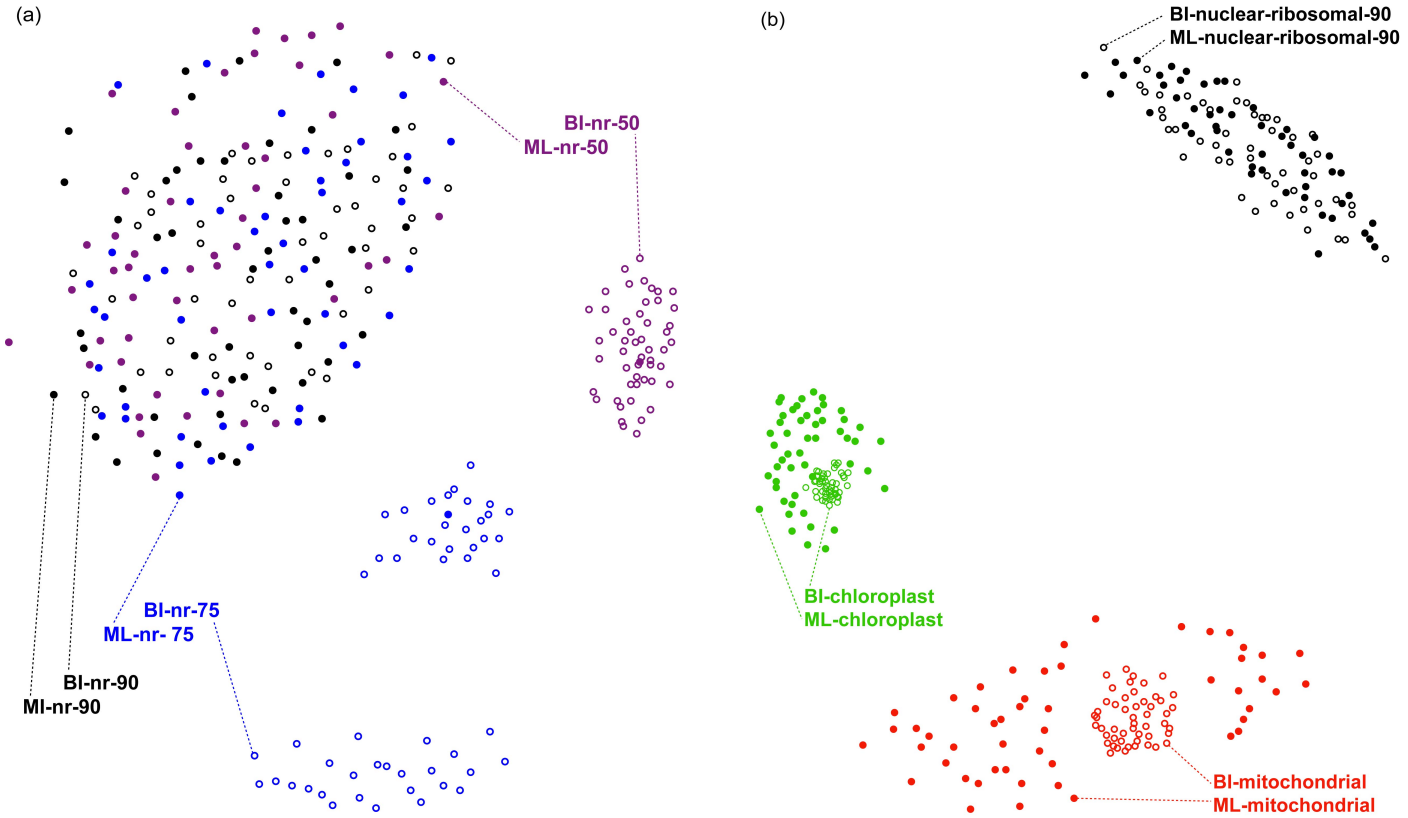

Figure 1.14. Robinson-Foulds tree distances rendered by TreeSetViz. Bayesian inference (BI) tree subsets are composed by the maximum credibility tree and 50 random trees sample from the Markov Chain Monte Carlo runs after a 0.25 burnin. Maximum likelihood (ML) tree subsets are composed by the best tree and 50 random trees sampled from the RAxML bootstrap. Outlined dots represent BI topologies; full dots represent ML topologies. a) Comparison among the nuclear ribosomal 50% (purple), 75% (blue), and 90% (black) consensus datasets. b) Comparison among the mitochondrial (red), chloroplast (green), and nuclear ribosomal 90% (black) datasets.

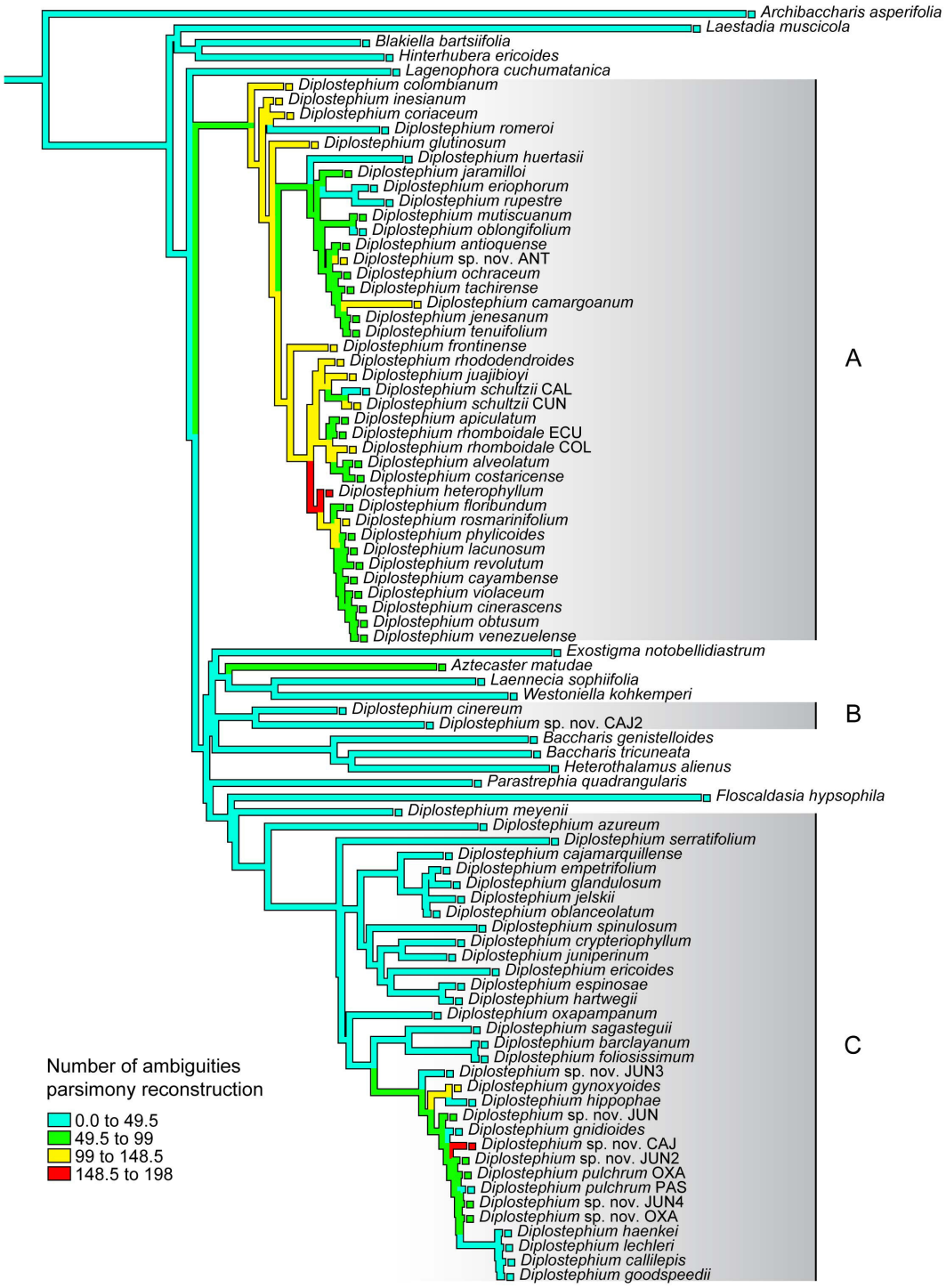

Figure 1.15. Number of intraindividual nuclear ribosomal ambiguities mapped onto the Bayesian nuclear ribosomal 90% phylogram.

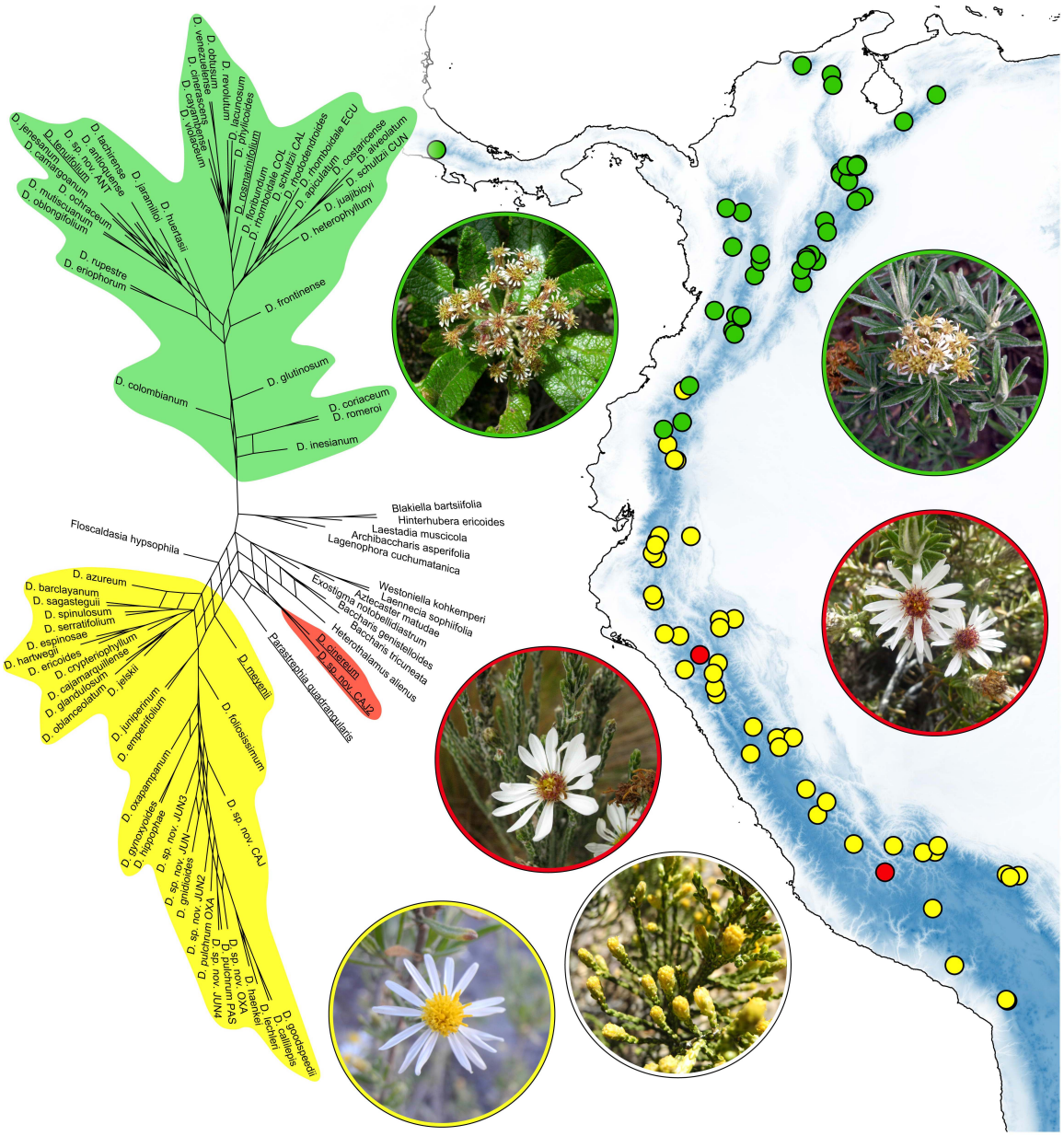

Figure 1.16. Phylogenetic network inferred from the nuclear ribosomal 90% and chloroplast Bayesian trees. Green, red, and yellow areas delimit groups A, B, and C respectively. Photos correspond to the underlined species *Diplostephium tenuifolium*, *D. rosmarinifolium*, *D. cinereum*, *D.* sp. nov. CAJ2, *Parastrephia quadrangularis*, and *D. meyenii* respectively from top to bottom. The map shows the collection localities of types of groups A, B, and C.

SUPPLEMENTARY INFORMATION

Supplementary Information 1.1. MrBayes settings used for the nuclear ribosomal analysis:

```
begin mrbayes;
	charset rRNA = 1-5320;
	charset transcribed_spacers = 5321-7738;
	charset non_transcribed_spacers = 7739-13362;
	partition partition_by_coding = 3: rRNA, transcribed_spacers,
non_transcribed_spacers;
	set partition=partition_by_coding;
	set autoclose=yes nowarn=yes;
	outgroup 19_12Psoli;
	lset applyto= (1,2) nst=6 rates=invgamma;
	lset applyto= (3) nst=6 rates=gamma;
	prset applyto=(1) revmatpr=dirichlet(1,2,2,3,4,5);
	prset applyto=(2) revmatpr=dirichlet(1,2,3,4,5,1);
	prset applyto=(3) revmatpr=dirichlet(1,2,1,1,2,1);
	prset applyto=(all) ratepr=variable;
	unlink revmat=(all) statefreq=(all) shape = (all) pinvar = (all);
	mcmc ngen=10000000 printfreq=1000 samplefreq=1000 relburnin=yes
burninfrac=0.25
	diagnfreq=1000 diagnstat=maxstddev

	nchains=4 savebrlens=yes
	filename=nrDNA_50b_m1_final;
	sump;
	sumt;
end;
```

Supplementary Information 1.2. MrBayes settings used for the chloroplast analysis:

```
begin mrbayes;
        charset non-coding = 1-60522;
        charset coding = 60523-135512;
        partition partition_by_coding = 2: non-coding, coding;
        set partition=partition_by_coding;
        outgroup 19_12Psoli;
        set autoclose=yes nowarn=yes;
        lset applyto=(all) nst=6 rates=invgamma;
        prset applyto=(1) revmatpr=dirichlet(1,2,3,3,4,2);
        prset applyto=(2) revmatpr=dirichlet(1,2,3,1,4,5);
        unlink revmat=(all) statefreq=(all) shape = (all) pinvar = (all);
        prset applyto=(all) ratepr=variable;
        mcmc ngen=10000000 printfreq=1000 samplefreq=1000 relburnin=yes
burninfrac=0.25
        diagnfreq=1000 diagnstat=maxstddev
        nchains=4 savebrlens=yes
        filename=cpdna-bycoding_final;
        sump;
        sumt;

end;
```

Supplementary Information 1.3. MrBayes settings used for the mitochondrial analysis:

```
begin mrbayes;
        charset coding = 1-31074;
        charset non-coding = 31075-209392;
        partition partition_by_coding = 2: coding, non-coding;
        set partition=partition_by_coding;
        outgroup 19_12Psoli;
        set autoclose=yes nowarn=yes;
        lset applyto=(all) nst=6 rates=invgamma;
        prset applyto=(1) revmatpr=dirichlet(1,2,2,2,1,1);
        prset applyto=(2) revmatpr=dirichlet(1,2,3,3,2,1);
        unlink revmat=(all) statefreq=(all) shape=(all) pinvar=(all);
        prset applyto=(all) ratepr=variable;
        mcmc temp=0.5 ngen=10000000 printfreq=1000 samplefreq=1000 relburnin=yes
burninfrac=0.25
        diagnfreq=1000 diagnstat=maxstddev
        nchains=4 savebrlens=yes
        filename=mtDNA_bycoding_final;
        sump;
        sumt;

end;
```

Chapter 2: *Piofontia*, a reinstated genus segregated from *Diplostephium* (Astereae)

INTRODUCTION

Kunth (1820) described the genus *Diplostephium* with a single species *D. lavandulifolium* Kunth (now *D. ericoides* (Lam.) Cabrera) and defined the genus with the following diagnostic characteristics: branched shrubs with dense foliage, alternate linear leaves, solitary capitula, hemispherical involucres with numerous imbricate phyllaries, epaleate foveolate receptacles, radiate heterogamous capitula, tubular hermaphrodite disk florets, peripheral ray florets, and double pappus with a short exterior row of scale-like bristles and an inner row of longer, barbellate bristles. Weddell (1855) redefined the *Diplostephium* adding a geographic component to his concept, defining the genus as Andean shrubs inhabiting montane habitats with alternate often tomentose leaves, terminal solitary capitula on branchlets or in a corymb, foveolate receptacles, and white or purple rays. Weddell's definition expanded the morphological boundaries of *Diplostephium* while restricting its geographical distribution. Additionally, Weddell (1855) described 11 species, transferred five into the genus, and proposed a subgeneric division of two groups: plants with solitary capitula and plants with capitula comprising a corymb. At the turn of the eighteen-century, Hieronymus (1894, 1896, 1900, 1905) added ten taxa to the genus, of which five now are considered synonyms.

In the twentieth-century, Blake (1922, 1928) described 28 new taxa of *Diplostephium* and published two major revisions of the genus. In his first study, Blake (1922) proposed a subgeneric classification of five series based on foliar and floral characters, partially following the division proposed by Weddell (1855). In the second revision, Blake (1928) recognized a total of 43 *Diplostephium* species but he reduced the number of series to three. Subsequently, Cuatrecasas added numerous taxa to

Diplostephium taxa and published two comprehensive studies of the genus (1943a, 1969). In his second revision, Cuatrecasas' (1969) dealt only with the Colombian species and proposed a subgeneric subdivision of 12 series comprising Blake's original five (1922) and seven new series. Cuatrecasas (1969) listed 53 species for Colombia, and estimated a total of 90 species for the genus. After Cuatrecasas' 1969 study, there has not been any major comprehensive revision of *Diplostephium*, although more species were added to the genus. In its broad sense (Cuatrecasas, 1969), *Diplostephium* comprises 111 species distributed in the mountains of Central and South America in Costa Rica, Colombia, Venezuela, Ecuador, Peru, Bolivia, and northern Chile (Vargas, 2006; Vargas, 2011).

A recent phylogenomic study (Vargas & Simpson, in prep.) showed that *Diplostephium sensu* Cuatrecasas (1969) is polyphyletic and suggested that most of the species of the genus should be placed in two clades. The Northern Andean clade, which comprises 63 species, is distributed mainly in the Northern Andes with the exception of two species reported for the Talamanca Cordillera in Central America. The Central Andean clade, which comprise approximately 46 species, is distributed in the Central Andes with some species reaching the southernmost regions of the Northern Andes. The Northern Andes is defined as the Andean mountain range north to the Huancabamba depression, while the Central Andes region is considered the Andean range between the Huancabamba depression and the 27ºS (Weigend, 2004; Luebert and Pliscoff, 2006; Luebert and Weigend, 2014). Vargas & Simpson (in press) hypothesized that a third clade of two species is a hybrid between the Central Andean clade and a putative ancestor of *Parastrephia* Nutt.

Despite the overlapping characteristics shared by the Northern Andean clade and the Central Andean clade (microphyllous leaves, heterogamous capitula, ray florets with a 2–3-lobed limb, rays white to purple, and double pappus) a combination of characters

may differ between the clades. The Northern Andean clade species are characterized by being subshrubs (0.1–0.49 m tall) or shrubs (0.5–3.9 m tall) with leaves 0.3–4 cm long or small trees (4–10 m tall) with leaves 4–23 cm long (Fig. 2.1). Subshrubs mostly have solitary capitula while shrubs and small trees always present multiple heads per capitulescence with small trees having arrangements of 20–100 heads. The branching pattern of the Northern Andean clade species is very consistent. Flowering occurs on terminal branches determining their growth; typically three or four branches develop from axillary buds close the capitulescence continuing the vertical growth of the plant. This architecture gives Northern Andean clade species a characteristic candelabrum pattern of ramification. Species of the Northern Andean clade inhabit the páramo and the upper margin of the cloud forest. The Central Andes clade species are subshrubs or shrubs up to 3 m tall (Fig. 2.2). Subshrubs and medium-size shrubs have leaves 0.2–3 cm long; scandent and large-size shrubs present leaves 4–8 cm long. Most species of the Central Andes clade have solitary capitula, but scandent and large-size shrubs exhibit up to 20 heads per capitulescence. A distinctive feature of the majority of the species in the Central Andean clade with solitary capitula is a architectural pattern in which long-indeterminate branches bear short branchlets topped with solitary capitula. Species of the Central Andean clade inhabit the puna, the humid puna (high yunga), and the páramo of Ecuador and southern Colombia.

Based on this evidence, and taking into account that the type species of *Diplostephium*, *D. ericoides*, is part of the Central Andean clade, I propose to reinstate *Piofontia* Cuatrec. and transfer into it the species comprising the Northern Andean clade. Cuatrecasas (1943b) proposed *Piofontia* as a monotypic genus consisting of *P. colombiana* Cuatrec, but later, he (1953) transferred *P. colombiana* into *Diplostephium* as *D. colombianum* (Cuatrec.) Cuatrec.

Diplostephium s.s now comprises 48 species that inhabit the páramo, the jalca, the humid puna (high yunga) and the puna of the Central Andes and the southernmost region of the Northern Andes. Most of the species are found in the humid puna of Peru on Andean slopes close the Amazon basin. *Diplostephium* remains largely unstudied since the last revision of the genus Blake (1928).

A description of *Piofontia* is proposed along with a list of species for the genus. The list is modified from a previously published nomenclator (Vargas, 2011) in which a complete list of synonyms is available.

TAXONOMIC TREATMENT

Artificial key for the identification of *Diplostephium* and *Piofontia*.

1. Subshrubs, shrubs, and small trees 0.1–10 m tall, always with a candelabrum like branching pattern in which every brach is terminated by a capitulescence. Leaves 0.3–23 cm long. Adaxial leaf surface usually eglandular or sparse-glandulose. Capitulescenses comprised of solitary capitula or with up to 100 heads. Distribution: Costa Rica, Colombia, Venezuela, and Northern Ecuador ..... ***Piofontia***

1. Subshrubs and shrubs 0.2–3.0 m tall with long indeterminate branches bearing short branches topped with solitary capitula or a candelabrum like branching pattern in which every brach is terminated by a capitulescence. Leafs 0.2–8.0 cm long. Adaxial leaf surface usually eglandular or sometimes densely-glandulose. Capitulescenses comprised of solitary capitula or with up to 20 heads. Distribution: southern Colombia, Ecuador, Peru, Bolivia, and northern Chile ..... ***Diplostephium***

Piofontia Cuatrec. Caldasia 2: 5. 1943. Type: *Piofontia colombiana* Cuatrec., Caldasia 2: 5. 1943. [≡ *Diplostephium colombianum* (Cuatrec.) Cuatrec.]

Small trees, shrubs or subshrubs 0.1–10 m tall, woody, branching sympodial by substitution with branches terminated by capitulescences. Branches cylindrical, minutely ribbed, tomentose or glabrous, glandular or eglandular, striate when old; terminal shoots often tomentose. Leaves alternate with phyllotaxis of five , petiolate, pseudopetiolate, or sessile, often mucronate; lamina 5–230 long x 0.5–85 mm wide, linear, lanceolate, ellipsoid, oblong, ovate, or obovate; margin entire, denticulate, or serrate, membranous to coriaceous, usually revolute, sometimes flat, often with adaxial and abaxial surfaces of different color; adaxial surface often lanate when young and glabrous when old, glandular or eglandular, with central vein impressed and canaliculate, secondary venation usually conspicuous in leaves wider than 12 mm, tertiary venation usually conspicuous in leaves wider than 15 mm; abaxial surface often densely lanate, whitish, yellowish, or ocherous, central vein prominent, with secondary and tertiary venation impressed or inconspicuous.

Capitulescence comprised of terminal solitary or multiple heads arranged in corymbs, racemes, or umbels. Capitula heterogamous, radiate, rarely disciform, 5–18 mm long x 5–17 mm in diam.; involucre 6–18 mm long, tubular, cupulate, or campanulate, or subconical, 3–7-seriate; phyllaries numerous, imbricate, unequal, 0.5–12.0 mm long x 0.8–2.6 mm wide, ovate to linear, semicoriaceous or coriaceous, often dorsally lanate and colored towards the apex. Florets 8–200, ray 5–70 and disk 5–140. Ray florets with corolla 2.5–20 mm long, white to purple; tube 1–6 mm long, usually papillose-pilose, rarely with one or two lobes opposite to the limb; limb 0.5–18 mm long x 0.4–4.0 mm wide, linear, oblong-elliptic, oblong-ovate, oblong-obovate, with 3–4 veins, often 3-lobed, rarely 2-lobed or 4-lobed; lobes 0.1–1.0 mm long, triangular and unequal; stigmatic branches 0.3–2 mm long, linear or subulate with papillose margin; ovary 0.6–4 mm long, glabrous or pilose, oblong, ovate, obovate, or oblong-ellipsoid, ribbed,

glandular or eglandular, always ovulated and fertile; pappus biseriate, strawish, reddish, or purplish, outer bristles 0.2–4 mm long, filiform and barbellate, interior bristles 2–7 mm long, barbellate, often with flattened and widened apex. Disk florets often male, corollas actinomorphic, 3–8 mm long, 5-lobed, tubular, tubular-campanulate, or tubular-infundibuliform, whitish, green, yellow, or purple, usually papillose-pilose; tube 0.5–4.5 mm long; lobes triangular 0.4–2 mm long, usually with papillose apex; anthers 1–2.5 mm long, oblong, briefly auriculate at the base, apical appendix membranous, triangular, and obtuse; stigmatic branches 0.3–2.5 mm long, linear or lanceolate, exteriorly papillose; ovary 0.8–7 mm long, linear or oblong, ribbed, glabrous to pilose, glandular or eglandular; pappus biseriate, strawish, reddish, or purplish, outer bristles always filiform, usually barbellate, 0.2–4mm long, interior bristles 3–8 mm long, usually barbellate, often with flattened and widened apex. Receptacle 1–5 mm in diam., alveolate, often muricate.

Piofontia currently consists of 63 species and is a main component of flora of the Northern Andes, the Sierra Nevada of Santa Marta, and the Talamanca Cordillera. Most of the species inhabit the páramo ecosystem, but some species (ca. 16) reside in the cloud forest. Cuatrecasas' series are not recognized here because they do not classify *Piofontia* species into natural groups (Vargas & Simpson, in press).

1. ***Piofontia alveolata*** (Cuatrec.) O.M.Vargas, **comb. nov.** ≡ *Diplostephium alveolatum* Cuatrec.
2. ***Piofontia anactinota*** (Wedd.) O.M.Vargas, **comb. nov.** ≡ *Diplostephium anactinotum* Wedd.
3. ***Piofontia antioquense*** (Cuatrec.) O.M.Vargas, **comb. nov.** ≡ *Diplostephium antioquense* Cuatrec.
4. ***Piofontia apiculata*** (S.F.Blake) O.M.Vargas, **comb. nov.** ≡ *Diplostephium apiculatum* S.F.Blake.

5. ***Piofontia bicolor*** (S.F.Blake) O.M.Vargas, **comb. nov.** ≡ *Diplostephium bicolor* S.F.Blake.

6. ***Piofontia camargoana*** (Cuatrec.) O.M.Vargas, **comb. nov.** ≡ *Diplostephium camargoanum* Cuatrec.

7. ***Piofontia cayambense*** (Cuatrec.) O.M.Vargas, **comb. nov.** ≡ *Diplostephium cayambense* Cuatrec.

8. ***Piofontia chrysotricha*** (S.Díaz & B.L.Restrepo) O.M.Vargas, **comb. nov.** ≡ *Diplostephium chrysotrichum* S.Díaz & B.L.Restrepo.

9. ***Piofontia cinerascens*** (Cuatrec.) O.M.Vargas, **comb. nov.** ≡ *Diplostephium cinerascens* Cuatrec.

9.1. ***Piofontia cinerascens*** subsp. ***puracense*** (Cuatrec.) O.M.Vargas, **comb. nov.** ≡ *Diplostephium violaceum* var. *puracense* Cuatrec.

10. ***Piofontia colombiana*** Cuatrec.

11. ***Piofontia coriacea*** (Cuatrec.) O.M.Vargas, **comb. nov.** ≡ *Diplostephium coriaceum* Cuatrec.

12. ***Piofontia costaricense*** (S.F.Blake) O.M.Vargas, **comb. nov.** ≡ *Diplostephium costaricense* S.F.Blake.

13. ***Piofontia crassifolia*** (Cuatrec.) O.M.Vargas, **comb. nov.** ≡ *Diplostephium crassifolium* Cuatrec.

14. ***Piofontia cyparissias*** (Wedd.) O.M.Vargas, **comb. nov.** ≡ *Diplostephium cyparissias* Wedd.

15. ***Piofontia dentata*** (Cuatrec.) O.M.Vargas, **comb. nov.** ≡ *Diplostephium dentatum* Cuatrec.

16. ***Piofontia elliptica*** (Cuatrec.) O.M.Vargas, **comb. nov.** ≡ *Diplostephium ellipticum* Cuatrec.

17. ***Piofontia eriophora*** (Wedd.) O.M.Vargas, **comb. nov.** ≡ *Diplostephium eriophorum* Wedd.

18. ***Piofontia farallonense*** (Cuatrec.) O.M.Vargas, **comb. nov.** ≡ *Diplostephium floribundum* subsp. *farallonense* Cuatrec., Caldasia 3: 423. 1945. ≡ *Diplostephium farallonense* (Cuatrec.) Cuatrec.

19. ***Piofontia fernandez-alonsoi*** (S.Díaz) O.M.Vargas, **comb. nov.** ≡ *Diplostephium fernandez-alonsoi* S.Díaz.

20. ***Piofontia floribunda*** (Benth.) O.M.Vargas, **comb. nov.** ≡ *Diplostephium floribundum* (Benth.) Wedd.

20.1. ***Piofontia floribunda*** subsp. ***aequatoriense*** (Cuatrec.) O.M.Vargas, **comb. nov.** ≡ *Diplostephium floribundum subsp. aequatoriense* Cuatrec.

20.2. ***Piofontia floribunda*** subsp. ***llanganatense*** (Cuatrec.) O.M.Vargas, **comb. nov.** ≡ *Diplostephium floribundum subsp. llanganatense* Cuatrec.

20.3. ***Piofontia floribunda*** subsp. ***putumayense*** (Cuatrec.) O.M.Vargas, **comb. nov.** ≡ *Diplostephium floribundum* subsp. *putumayense* Cuatrec.

20.4. ***Piofontia floribunda*** subsp***. cundinamarcense*** (Cuatrec.) O.M.Vargas, **comb. nov.** ≡ *Diplostephium floribundum* subsp. *cundinamarcense* Cuatrec.

21. ***Piofontia fosbergii*** (Cuatrec.) O.M.Vargas, **comb. nov.** ≡ *Diplostephium fosbergii* Cuatrec.

22. ***Piofontia frontinense*** (Cuatrec.) O.M.Vargas, **comb. nov.** ≡ *Diplostephium frontinense* Cuatrec.

23. ***Piofontia glutinosa*** (S.F.Blake) O.M.Vargas, **comb. nov.** ≡ *Diplostephium glutinosum* S.F.Blake.

23.1. ***Piofontia glutinosa*** subsp. ***glutinosa*** f. ***microphylla*** (Cuatrec.) O.M.Vargas, **comb. nov.** ≡ *Diplostephium glutinosum* subsp. *glutinosum* f. *microphyllum* Cuatrec.

23.2. ***Piofontia glutinosa*** subsp. ***glutinosa*** f. ***subspathulata*** (Cuatrec.) O.M.Vargas, **comb. nov.** ≡ *Diplostephium subspathulatum* Cuatrec.

23.3. ***Piofontia glutinosa*** subsp. ***cocuyana*** (Cuatrec.) O.M.Vargas, **comb. nov.** ≡ *Diplostephium glutinosum* subsp. *cocuyanum* Cuatrec.

24. ***Piofontia grantii*** (Cuatrec.) O.M.Vargas, **comb. nov.** ≡ *Diplostephium grantii* Cuatrec.

25. ***Piofontia heterophylla*** (Cuatrec.) O.M.Vargas, **comb. nov.** ≡ *Diplostephium heterophyllum* Cuatrec.

26. ***Piofontia huertasii*** (Cuatrec.) O.M.Vargas, **comb. nov.** ≡ *Diplostephium huertasii* Cuatrec.

27. ***Piofontia inesiana*** (Cuatrec.) O.M.Vargas, **comb. nov.** ≡ *Diplostephium inesianum* Cuatrec.

28. ***Piofontia jaramilloi*** (Cuatrec.) O.M.Vargas, **comb. nov.** ≡ *Diplostephium jaramilloi* Cuatrec.

29. ***Piofontia jenesana*** (S.Díaz & M.E.Morales) O.M.Vargas, **comb. nov.** ≡ *Diplostephium jenesanum* S.Díaz & M.E.Morales.

30. ***Piofontia juajibioyi*** (Cuatrec.) O.M.Vargas, **comb. nov.** ≡ *Diplostephium juajibioyi* Cuatrec.

30.1. ***Piofontia juajibioyi*** subsp. ***leucopappa*** (Cuatrec.) O.M.Vargas, **comb. nov.** ≡ *Diplostephium juajibioyi* subsp. *leucopappum* Cuatrec.

31. ***Piofontia juliani*** (Cuatrec.) O.M.Vargas, **comb. nov.** ≡ *Diplostephium juliani* Cuatrec.

32. ***Piofontia lacunosa*** (Cuatrec.) O.M.Vargas, **comb. nov.** ≡ *Diplostephium lacunosum* Cuatrec.

33. ***Piofontia leioclada*** (S.F.Blake) O.M.Vargas, **comb. nov.** ≡ *Diplostephium leiocladum* S.F.Blake.

34. ***Piofontia micradenia*** (S.F.Blake) O.M.Vargas, **comb. nov.** ≡ *Diplostephium micradenium* S.F.Blake.

35. ***Piofontia mutiscuana*** (Cuatrec.) O.M.Vargas, **comb. nov.** ≡ *Diplostephium mutiscuanum* Cuatrec.

36. ***Piofontia nevadense*** (Cuatrec.) O.M.Vargas, **comb. nov.** ≡ *Diplostephium nevadense* Cuatrec.

37. ***Piofontia oblongifolia*** (Cuatrec.) O.M.Vargas, **comb. nov.** ≡ *Diplostephium oblongifolium* Cuatrec.

38. ***Piofontia obtusa*** (S.F.Blake) O.M.Vargas, **comb. nov.** ≡ *Diplostephium obtusum* S.F.Blake.

39. ***Piofontia ocanense*** (Cuatrec.) O.M.Vargas, **comb. nov.** ≡ *Diplostephium ocanense* Cuatrec.

40. ***Piofontia ochracea*** (Kunth) O.M.Vargas, **comb. nov.** ≡ *Diplostephium ochraceum* (Kunth) Nees.

41. ***Piofontia parvifolia*** (S.F.Blake) O.M.Vargas, **comb. nov.** ≡ *Diplostephium microphyllum* Wedd.

42. ***Piofontia perijaense*** (S.Díaz & G.P.Méndez) O.M.Vargas, **comb. nov.** ≡ *Diplostephium perijaense* S.Díaz & G.P.Méndez.

43. ***Piofontia phylicoidea*** (Kunth) O.M.Vargas, **comb. nov.** *Diplostephium phylicoides* (Kunth) Wedd.

44. ***Piofontia pittieri*** (Cuatrec.) O.M.Vargas, **comb. nov.** ≡ *Diplostephium pittieri* Cuatrec.

45. ***Piofontia rangelii*** (Cuatrec.) O.M.Vargas, **comb. nov.** ≡ *Diplostephium rangelii* Cuatrec.

46. ***Piofontia revoluta*** (S.F.Blake) O.M.Vargas, **comb. nov.** ≡ *Diplostephium revolutum* S.F.Blake.

47. ***Piofontia rhododendroides*** (Hieron.) O.M.Vargas, **comb. nov.** ≡ *Diplostephium rhododendroides* Hieron.

48. ***Piofontia rhomboidalis*** (Cuatrec.) O.M.Vargas, **comb. nov.** ≡ *Diplostephium rhomboidale* Cuatrec.

48.1. ***Piofontia rhomboidalis*** var. ***pauciflora*** (Cuatrec.) O.M.Vargas, **comb. nov.** ≡ *Diplostephium rhomboidale* var. *pauciflorum* Cuatrec.

49. ***Piofontia ritterbushii*** (Cuatrec.) O.M.Vargas, **comb. nov.** ≡ *Diplostephium ritterbushii* Cuatrec.

50. ***Piofontia romeroi*** (Cuatrec.) O.M.Vargas, **comb. nov.** ≡ *Diplostephium romeroi* Cuatrec.

51. ***Piofontia rosmarinifolia*** (Benth.) O.M.Vargas, **comb. nov.** ≡ *Diplostephium rosmarinifolium* (Benth.) Wedd.

52. ***Piofontia rupestris*** (Kunth) O.M.Vargas, **comb. nov.** *Diplostephium rupestre* (Kunth) Wedd.

53. ***Piofontia santamartae*** (Cuatrec.) O.M.Vargas, **comb. nov.** ≡ *Diplostephium santamartae* Cuatrec.

54. ***Piofontia saxatile*** (Cuatrec.) O.M.Vargas, **comb. nov.** ≡ *Diplostephium saxatile* Cuatrec.

55. ***Piofontia schultzii*** (Wedd.) O.M.Vargas, **comb. nov.** ≡ *Diplostephium schultzii* Wedd.

55.1. ***Piofontia schultzii*** var. ***lehmanniana*** (Hieron.) O.M.Vargas, **comb. nov.** ≡ *Diplostephium schultzii* var. *lehmannianum* Hieron

55.1.1. ***Piofontia schultzii*** var. ***lehmanniana*** f. ***subincisa*** (Cuatrec.) O.M.Vargas, **comb. nov.** ≡ *Diplostephium schultzii* var. *lehmannianum* f. *subincisum* (Cuatrec.) Cuatrec.

55.2. ***Piofontia schultzii*** var. ***orientale*** (Cuatrec) O.M.Vargas, **comb. nov.** ≡ *Diplostephium pleistogynum* var. *orientale* Cuatrec.

56. ***Piofontia tachirense*** (V.M.Badillo) O.M.Vargas, **comb. nov.** ≡ *Diplostephium tachirense* V.M.Badillo.

57. ***Piofontia tamana*** (Cuatrec) O.M.Vargas, **comb. nov.** ≡ *Diplostephium tamanum* Cuatrec.

58. ***Piofontia tenuifolia*** (Cuatrec) O.M.Vargas, **comb. nov.** ≡ *Diplostephium tenuifolium* Cuatrec.

59. ***Piofontia tergocana*** (Cuatrec) O.M.Vargas, **comb. nov.** ≡ *Diplostephium tergocanum* Cuatrec.

60. ***Piofontia tolimense*** (Cuatrec) O.M.Vargas, **comb. nov.** ≡ *Diplostephium tolimense* Cuatrec.

61. ***Piofontia venezuelense*** (Cuatrec) O.M.Vargas, **comb. nov.** ≡ *Diplostephium venezuelense* Cuatrec.

62. ***Piofontia violacea*** (Cuatrec) O.M.Vargas, **comb. nov.** ≡ *Diplostephium violaceum* Cuatrec.

63. ***Piofontia weddellii*** (Cuatrec) O.M.Vargas, **comb. nov.** ≡ *Diplostephium weddellii* S.F.Blake.

FIGURES

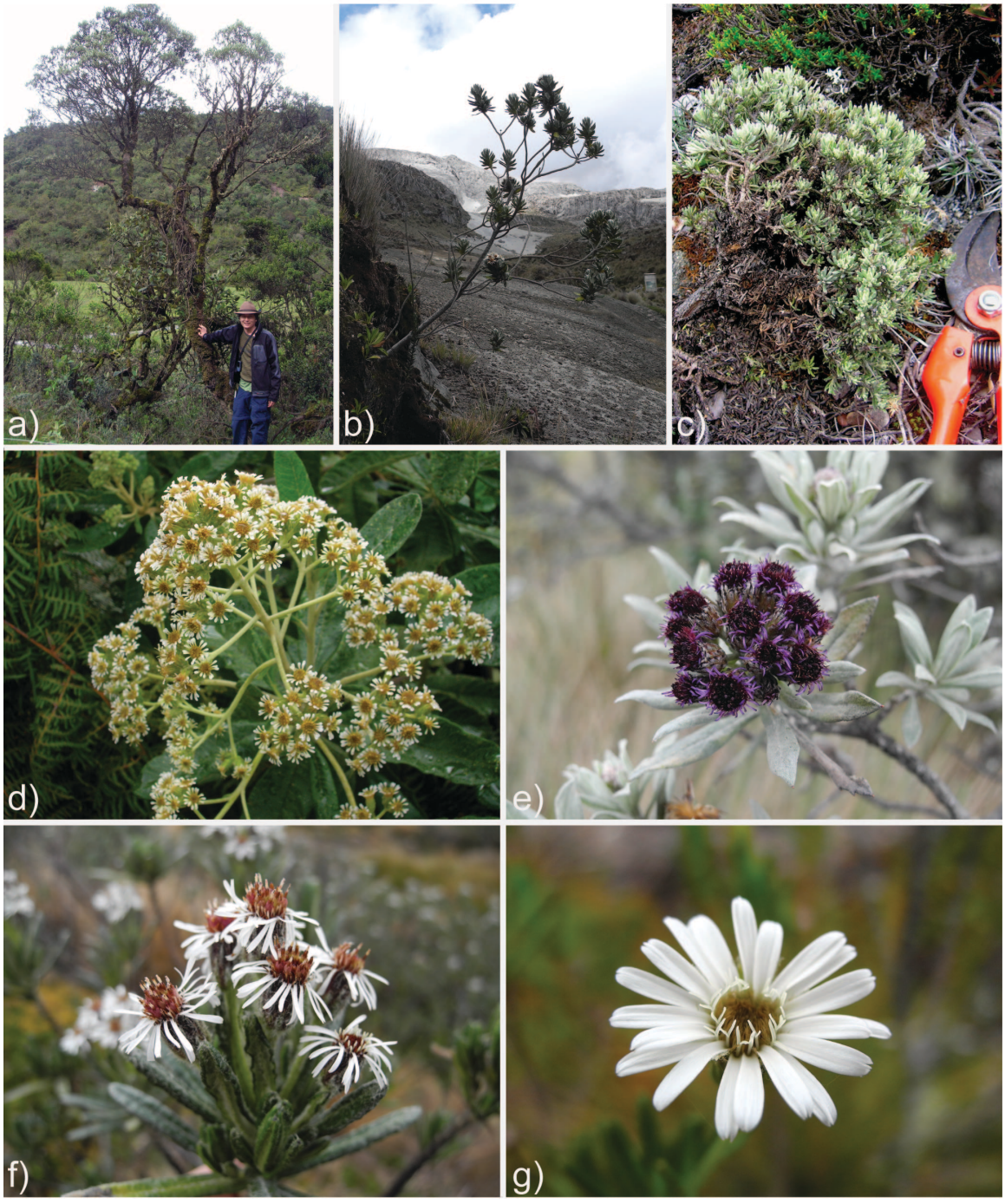

Figure 2.1. a) *Piofontia oblongifolia*, b) *P. eriophora*, c) *P. apiculata*, d) *P. camargoana*, e) *P. schultzii*, f) *P. rupestris*, g) *P. frontinense*.

Figure 2.2. a) *Diplostephium meyenii*, b) *D. haenkei*, c) *D. hartwegii*, d) *D. gnioides*, e) *D. barclayanum*, f) *D. lechleri*, g) *D. oxapampanum*.

Chapter 3: Spatiotemporal patterns of evolution in two parallel high-Andean diversifications (Asteraceae: *Diplostephium* and *Piofontia*)

INTRODUCTION

High indices of phytodiversity often coincide with areas of topographic complexity of humid tropical and subtropical climates (Barthlott *et al*., 1996; Myers *et al*., 2000; Mutke & Barthlott, 2005). The Andes Cordillera is one of such biodiversity centers in which landscape heterogeneity is believed to have fueled speciation by means of isolation and ecological divergence. The tropical Andes, where most biodiversity is concentrated, is generally categorized as two regions, the Northern and the Central Andes. These two regions are characterized based on biogeographic features (Weigend, 2002), geologic history (Gregory-Wodzicki, 2000), and climatic factors (Luebert & Plisscoff, 2006). The Northern Andes comprise the region north of the Amotape-Huancabamba Depression (Weigend, 2002; Luebert & Weigend, 2014) located at the border of Ecuador and Peru. Higher indices of precipitation in the Andes north of the depression make this area more humid than the Central Andes (Sarmiento, 1986; Garreaud, 2009). The high altitudes (>3000 m) of the Northern Andes emerged as a result of rapid uplift during the last 2–4 mya (van der Hammen & Cleef, 1986; Gregory-Wodzicki, 2000). The páramo ecoregion constitutes the zones above the timberline (~3000 m) in the Northern Andes, and with an estimated of ~3,400 species of vascular plants (Luteyn, 1999) it is considered the most species-rich ecosystem of the tropical montane regions (Sklenář *et al*., 2014). Preliminary data suggest that páramo taxa have particularly high rates of speciation (Madriñán *et al*., 2013). The Central Andes, located south of the Amotape-Huancabamba depression, is generally drier (Sarmiento, 1986; Luebert & Plisscoff, 2006; Garreaud, 2009) with the puna dominating high-altitude landscapes. The high elevations of the Central Andes are the result of accelerated uplift

6–10 mya (Gregory-Wodzicki, 2000; Garzione *et al*., 2014). While the páramo is humid and geographically dissected in patches resembling an island system, the puna is mostly dry and continuous (Luteyn, 1999). The first part of this study aims to compare the evolutionary history of two high-altitude genera, *Piofontia* and *Diplostephium*, which centers of diversification are the Northern and the Central Andes, respectively. The second part of this paper focus on understanding the causes of speciation in the páramo.

The fragmented coverage of the páramo and its altitudinal gradient are hypothesized to act as drivers of diversification by promoting allopatric speciation via isolation (van der Hammen & Cleef, 1986) and sympatric (or parapatric) speciation via ecological selection (Hughes & Atchison, 2015). Once a lineage has colonized an island (physical or ecological) it has two options, maintain its ecological niche or adapt into different niches inside the ecosystem. If a lineage maintains its ecological niche in a given island, it will follow an anagenetic pattern of speciation (Takayamya *et al*., 2015) in which the lineage will evolve through mutation and genetic drift. On the other hand, if a lineage radiates into different niches of an island, it can follow a cladogenetic pattern of speciation driven by disruptive adaptation (Simpson, 1953; Givnish, 1997; Schluter, 2000). Hypothetically, if one considers a one-island scenario, an anaganetic event will result in one taxon divergent from the original colonizer via isolation while an ecological radiation event can result in multiple taxa over time. Discriminating isolation and ecological divergence becomes challenging with increasing number of islands because geographic isolation could result in multiple species produced by independent anagenetic processes of evolution. In the páramo islands, assuming no extinction, one would expect that if isolation were driving speciation, recently diverged sister species should be found in allopatry (Fig. 3.1a, 3.1b). In contrast, if the process of adaptive radiation is driving speciation, one would expect, assuming no extinction, most sister taxa to inhabit different

niches in the same island (Fig. 3.1c). Although numerous studies have documented "radiation events" in the Andes, rigorous testing about the role of isolation and ecological divergence on speciation usually does not accompany such claims. As pointed out by Givnish (2015), studies documenting montane plant evolution often employ the word "radiation" to indicate "explosive diversification" without proof of ecological divergence. The distinction is important because "radiation" implies ecological specialization while "explosive diversification" simply means rapid speciation (Givnish, 2015). Therefore, for a pattern to genuinely be called a "radiation," a researcher needs to demonstrate that ecological speciation is the cause of speciation of a given taxa. To quantify the relative contribution of isolation and ecological divergence to speciation we propose a comparative framework that combines phylogenetic, geographical, and ecological information. We employ our novel approach in *Piofontia*, a recently studied genus restricted to the páramo (Cuatrecasas, 1969; Vargas, 2011, Vargas, in prep.).

Piofontia is a genus of 63 species distributed in the mountains of the Talamanca Cordillera, the Sierra Nevada de Santa Marta, and the Northern Andes (Cuatrecasas, 1969; Vargas, in prep.). Most species of the genus inhabit the páramo but some dwell in the upper boundary of the cloud forest thanks to a downslope colonization event (Vargas & Madriñán, 2012). *Piofontia* exhibits a variety of woody habits ranging from decumbent subshrubs only 10 cm tall to small trees 6 m tall. Growth form and leaf shape of *Piofontia* species are related to the habitat they occupy, decumbent shrubs with microphyllous leaves inhabit the open páramo while small trees with broad leaves reside in the upper boundary of the high Andean forest. *Piofontia* was recently segregated from *Diplostephium* (Vargas, in prep.), a genus with similar morphology and ecology.

Diplostephium comprises 51 species is distributed mainly in the puna and humid puna of the Central Andes with some of its species inhabiting the páramo of Ecuador and

southern Colombia. Its species are woody shrubs and subshrubs bearing small and microphyllous leaves, respectively. Like *Piofontia*, the plant height and leaf morphology of *Diplostephium* reflects the habitat it occupies, microphyllous sub-shrubs and shrubs inhabit open grasslands in the puna and the humid puna while tall shrubs with big leaves inhabit the lower boundary of the humid puna on the eastern slopes of the Central Andes.

MATERIALS AND METHODS

Calibration of the Phylogeny

We calibrated a recently published phylogeny of *Diplostephium, Piofontia,* and their allies (Vargas & Simpson, in prep.). Because there is no fossil record for the tribe Astereae, we could not implement a primary calibration directly in our dataset. Therefore, in order to calibrate Vargas & Simpson's (in prep.) nuclear ribosomal phylogeny, we stripped the ITS region (~700 bp) from Vargas & Simpson's (in prep.) matrix and combined it with that of Strijk *et al*. (2012). In addition to Astereae sequences, Strijk *et al*.'s (2012) ITS matrix contains sequences from Heliantheae, Gnaphalieae, and Anthemideae (Appendix S1) providing external nodes for time calibration. We used the same calibration points of Strijk *et al*. (2012): 1) a secondary calibration using a normal distribution with a mean of 32.5 mya and a sigma (standard deviation) of 11 (95% confidence interval [CI]:14.4–50.6), (based on Kim *et al*., 2005) for the root of the tree, which represents the crown clade of the Asteroideae, 2) a mean of 22.3 mya following Bergh & Linder (2009) based on *Ambrosia*-pollen (Becker, 1969; Graham, 1994) with a lognormal distribution and a sigma of 0.3 (95% CI:13.0–34.9) at the split of *Helianthus annuus* L. and *Tagetes patula* L.; 3) a secondary calibration with a mean of 20.0 mya following Bergh and Linder (2009) with a normal distribution and a sigma of 5.0 (95% CI:11.8–28.2) to the stem node of Gnaphalieae, and 4) a mean of 16.98 mya based on the

Artemisia L. fossil record (Sun *et al*., 1981; Graham, 1994; Song *et al*., 1999; Wang, 2004) with a lognormal distribution and a sigma of 0.6 (95% CI:5.29–38.1) to the stem node of *Artemisia*. Species with more than one sample were removed from the Strijk *et al*.'s (2012) dataset. After aligning Vargas & Simpson's (in prep.) and Strijk *et al*.'s (2012) ITS datasets using MAFFT, we calculated the substitution model of the combined matrix with rj-MCMC simulations (Huelsenbeck *et al*., 2004) using MrBayes with 30 million generations, 2 runs, 4 chains per run, and the +Γ and +I parameters. Using the inferred substitution model inferred as a prior, we created a topology with MrBayes with 30 million generations, 2 runs, 4 chains, and a temperature of 0.001. We calculated the chronogram with BEAST using the MrBayes topology (fixed), a lognormal relaxed clock, a Yule model of speciation, 100 million generations, and a sampling frequency of 40 thousand generations. We produced the .xml file using BEAUti v.2.3 (Drummond *et al*., 2012a). The sets of trees from the two runs were combined after a burnin of 0.25 using LogCombiner v.2.3 (Drummond *et al*., 2012a). Finally, we produced a dated maximum clade credibility tree with TreeAnnotator 2.3 (Drummond *et al*., 2012a).

Because the ITS (~700 bp) combined dataset (Vargas & Simpson, in prep. plus Strijk *et al*., 2012) did not provided enough phylogenetic information to produce a robust and resolved topology in the part of the tree corresponding to the "South American lineages" (*Diplostephium*, *Piofontia*, and their allied genera), we calibrated the complete nuclear ribosomal dataset (~13 Kb) of Vargas & Simpson (in prep.) that provides a high-resolution phylogeny of the "South American lineages." We added *Helianthus annuus* (GenBank accession KF767534) to the Vargas & Simpson's (in prep.) dataset and employed the following calibration points: 1) a secondary calibration with a mean of 32.4 mya based on Kim et al. (2005) with a normal distribution and a sigma of 11 (95% CI:14.4–50.6) to the root of the tree that represents the crown clade of the Asteroideae,

and 2) a secondary calibration with a mean of 11.21 mya with a normal distribution and a sigma of 3.1 (95% CI:6.11–16.3) based on the age of the "South American Lineages" (inferred from the ITS combined dataset chronogram calculated in this study) to the node connecting *Archibaccharis* and the rest of the ingroup. We employed BEAST with the same parameters used in the ITS combined dataset to calibrate Vargas & Simpson's (in prep.) dataset.

Biogeographic Analysis of the *"*South American lineages"

We defined our biogeographic areas based on the regionalization of the neotropics proposed by Morrone (2014). We modified the shape file produced by Löwenberg-Neto (2014) of Morrone's categorization (2014) using QGIS 2.8Wien (QGIS Development Team, 2005) to reflect better the altitudinal gradient of South and Central America and make our regions comparable to other studies focused on high Andean biogeography (e.g. Simpson, 1974, 1975; Tovar *et al*., 2013). We edited the areas manually by adding, joining, and extending them using a digital elevation model layer as reference. Areas where sampled taxa were poorly distributed or absent were excluded. The regions used in this study and their correspondences (in quotations) to Morrone's (2014) are:

Northern Central America (M).–Mountainous and lowland areas of northern Central America (an integration of the "Mexican transition zone" and the "Mesoamerican dominion").

Talamanca Cordillera (T).–Highlands of southern Central America. This area represents the páramos of Costa Rica (part of the "Pacific Dominion" and not considered by Morrone (2014) as an independent unit).

Northern Andes (N).–Sierra Nevada de Santa Marta and the Andes of Colombia, Venezuela, and Ecuador (an integration and expansion of the "páramo province"

and the "Cauca Province"). We expanded the combined regions by adding areas above 2,500 m using contour derived from a digital elevation model. The resulting area incorporated the Serrania del Perija, the Sierra Nevada de Santa Marta, and the Venezuelan Andes (none considered by Morrone (2014) as part of the "Páramo Province"). This region comprises the páramos of South America (Cuatrecasas, 1968; Luteyn, 1999) and the upper boundary of the high Andean forest beneath them.

Central Andes (*C*).–Andes of Peru, Bolivia, northern Chile, and northwestern Argentina. This area comprises the puna, humid puna, and the upper boundary of the high Andean forest found at the eastern slope of the Andes (an expansion of the "South American transition zone"). We expanded this area by including regions over 2,500 m in the same way that we did with the Northern Andes.

Dry Lowlands of Western South America (W).–Dry tropical and subtropical areas south to the Amazon rainforest (an integrated area of the "Chacoan and Parana dominions").

The assignment of biogeographic areas to the tips of the phylogeny for *Diplostephium* and *Piofontia* species was based on voucher collections and herbarium material from COL, TEX, and US. Designated regions for non-*Diplostephium* and non-*Piofontia* tips represented the combined distribution of the entire genus (instead of the sole species sampled) inferred from data downloaded from the Global Biodiversity Information Facility portal (http://data.gbif.org) and/or taxonomic revisions (Table 3.1).

We chose BioGeoBEARS (Matzke, 2013) to infer the biogeographic history of the "South American lineages" because it implements different models of ancestral area calculation, DEC (Dispersal-Extinction-Cladogenesis; Ree & Smith, 2008), DIVALIKE (a likelihood version of Dispersal–Vicariance Analysis; Ronquist, 1997), and

BAYAREAALIKE (a likelihood implementation of the BAYAREA model; Landis et al. 2013), and it evaluates the addition of the J parameter (Matzke, 2014) to each model accounting for founder-event speciation (DEC+J, DIVALIKE+J, BAYAREALIKE+J). Matzke (2014) showed that founder-event speciation is a crucial process in the biogeographic dynamics of island clades, and many of the species in the Vargas & Simpson's (in prep.) phylogeny are restricted to mountaintop habitats that can be argued to be ecological islands. We pruned the outgroups from the chronogram to carry out the biogeographic analysis, and we opted not to use a constrained model since the paleoaltitudes of the Northern and Central Andes are still debated (Luebert & Weigend, 2014).

Biogeographic Analysis of *Piofontia*

To understand better the biogeographic dynamics in the Northern Andes, we performed a second biogeographic analysis for the genus *Piofontia*. We defined the biogeographic areas based on the Colombian páramo complexes defined by Londoño et al. (2014) adding three areas to cover completely the distribution of *Piofontia* (and the páramo). Our areas were outlined as follows (areas not included in the Londoño *et al*., 2014 study are indicated with a star):

Northern Páramos (N).– Páramos of the "Sierra Nevada de Santa Marta" and the "Serranía del Perijá."

Talamanca (T)*.– Páramos located in the Talamanca Cordillera of Central America.

Mérida (T)*.– Páramos located in the Mérida Cordillera of Venezuela.

Eastern Cordillera (E).– Páramos located in Eastern Cordillera of Colombia.

Antioquia (A).– Cluster of páramos comprised by areas in the Western and Central Cordilleras of Colombia mostly located in the department of Antioquia, Colombia.

Western Cordillera (W).– Páramos located in the Western Cordillera of Colombia with the exception of those located in the department of Antioquia, Colombia.

Central Cordillera (C).– Páramos located in the Central Cordillera of Colombia with the exception of those located in the department of Antioquia, Colombia.

Southern Páramos (S).– Páramos located in the Colombian Massif and the Ecuadorian Andes.

We assigned the biogeographic areas to species based on a revision of *Piofontia* for Colombia (Vargas in prep.). We pruned the chronogram to include only *Piofontia* species and used BioGeoBEARS infer the biogeographic history of the genus evaluating different models.

Analyses of Speciation Dynamics

We calculated the leaf area of several *Piofontia* specimens as surrogate measure to evaluate the ecological divergence between sister species. When possible we measured the area of 30 leaves from 6 different individuals in each species. We scanned the leaves at 600 dpi from herbarium material belonging to ANDES, TEX, and US. Each leaf was outlined using PHOTOSHOP CS4 (Adobe Systems, San Jose, California). We then used the R package MOMOCS (Bonhomme *et al*., 2014) to calculate the area of each leaf from the images created in the previous step. With a log-transformation of the data, we compared the distribution of the leaf area on the *Piofontia* tree against a Brownian model by calculating Blomberg *et al*.,'s (2003) K and Pagel's (1999) lambda (λ) with the R package PHYTOOLS (Revell, 2012) using 1,000 simulations. Both statistics evaluate if

traits are more similar or more different that expected in relation to a Brownian model of evolution.

To evaluate the potential relative contribution of speciation events produced by isolation and ecological divergence, we compared the distribution and the leaf areas of sister species on the phylogeny of *Piofontia*. We used leaf areas as an ecological indicator (Givnish, 1987). We employed this framework on *Piofontia* because of our comprehensive information about the distribution and taxonomy of its species (Cuatrecasas, 1969; Vargas, 2011; Vargas, in prep.). We performed a Wilcoxon signed-rank tests of the log-transformed leaf areas between sister species using R (R Core Team, 2016). If a pair of sister species were shown to have no statistical difference between their leaf areas we performed a second test between the clade comprising the two species with similar leaf area (considering the two together as one taxonomical unit) and the sister species of that clade. We scored a sister-species pair as allopatric when they inhabited non-overlapping páramo islands and a sister-species pair as sympatric when their distribution overlapped on at least one páramo island.

We interpreted the results in the following fashion: if sister-species are allopatric and there is no significant differences between the their leaf areas, we interpreted this scenario as an event of speciation by isolation in which allopatric speciation has isolated genetically the two species but niche conservatism has conserved the morphology and ecology of sister species (Fig. 3.1a, Wiens, 2004, Pyron *et al*., 2014); if sister-species are allopatric and there is significant difference between their leaf areas, we interpreted this scenario as an event of speciation by isolation (Fig. 3.1b) in which allopatric speciation has isolated genetically the two species with subsequent ecological divergence driven by local adaption (Rundell & Price, 2009; Pyron *et al*., 2015); if sister-species are sympatric and their leaf areas are different, we interpreted this scenario as an event of ecological

speciation in which disruptive selection produced a displacement of morpho-ecological characters (Rundle & Nosil, 2005; Rundell & Price, 2009) (Fig. 3.1c). If sister-species are sympatric and there is no significant difference between their leaf areas, we interpreted this scenario as inconclusive (Fig. 3.1d). The last pattern could be the result different processes: an allopatric speciation event in which the two resultant species came secondarily into sympatry (Rundell & Price 2009, Hopkins, 2013) or a speciation event driven by ecological divergence in which the leaf area is not modified (Snaydon & Davies, 1976; Silvertown *et al*., 2005).

Finally, we employed BAMM v.2.5 (Rabosky, 2014) to calculate net speciation rates of and identify shifts of diversification regimes on the chronogram of the "South American lineages." We employed a sampling correction by indicating the fractions of the genera sampled (Table 3.2). We ran BAMM with four chains and ten million generations. We employed an effective sample size (ESS) >150 and a burnin fraction of 0.1. We used BAMMtools (Rabosky *et al*., 2014) to: calculate a phylorate plot to visualize model-averaged diversification rates and regime shifts over the phylogeny; graph diversification rates through time over the phylogeny; create a macroevolutionary cohort matrix to compare the probability of lineages sharing diversification dynamics; calculate and compare Bayes factors among different scenarios of diversification shifts; and graph the prior and posterior probabilities of the number of regime shifts.

RESULTS

The chronogram obtained by the Bayesian analysis of the combined ITS matrix (Vargas & Simpson, 2015 plus Strijk *et al*., 2012) shows poor support and resolution in nodes positioned in the "South American Lineages" (Fig. 3.2). We expected this result because the combined dataset analysis was performed only with the short ITS region

(~700 bp) that does not appear to contain enough phylogenetic signal to resolve recently diversified groups. Therefore, in addition to a secondary calibration applied to the root of the Asteroideae (Kim *et al*., 2005), we used the node corresponding to the origin of the "South American lineages" from the combined-matrix chronogram (node R, mean age = 11.21 mya 95% CI:6.22–16.36 Fig. 3.2) to calibrate the complete dataset of Vargas & Simpson's (in prep.). The calibration of Vargas & Simpson's (in prep.) phylogeny suggests that the mean age of *Piofontia* is 5.65 mya (95% CI:1.66–10.03) while the mean age of *Diplostephium* is 6.41 mya (95% CI:1.91–10.7) (Fig. 3.3), both supporting the hypothesis of a recent origin (Vargas & Madriñán, 2012, Vargas & Simpson, in prep.).

Among the six models evaluated by BioGeoBEARS on the "South American lineages" phylogeny, DEC+J performed the best with a Ln*L* of -86.46 followed by DEC with a Ln*L* of -87.54 (Table 3.3). Because there is no statistical significance between the likelihoods of DEC vs. DEC+J (p= 0.14) we chose the DEC reconstruction that has only two free parameters (versus 3 on DEC+J) for the discussion of our results. The DEC ancestral reconstruction presents a clear picture of most biogeographic origins for each genus (Fig. 3.4, 3.5) but it fails to reveal a explicit area reconstruction for deep nodes in the "South American lineages." The analysis suggests that *Piofontia* originated in the Northern Andes and *Diplostephium* originated in the Central Andes (Fig. 3.4, 3.5); the most probable area for the node corresponding to the ancestor of the "South American lineages" is an area that combines all the regions with a proportional likelihood of less than 0.33 (Fig 3.4). For *Diplostephium,* which primarily is Central Andean, the analysis also shows that two clades independently colonized the páramo of the Northern Andes (clades 1 and 2, Fig. 3.4, 3.5)

The models with the best likelihood scores of the biogeographic analysis carried on *Piofontia* were DEC-J and DEC with a Ln*L* of -119.8 and -120.9, respectively (Table

3.4). DEC-J and DEC are not statistically different (p= 0.13), so we picked the DEC reconstruction for the discussion of the historical biogeography of *Piofontia* in order to be conservative with the number of parameters included by the model. The DEC reconstruction (Fig. 3.6a, 3.7) shows that the Eastern Cordillera played a major role in the evolution of *Piofontia*. The Eastern Cordillera is the region that contains the most species of *Piofontia,* and the historical reconstruction shows this region as the most probable area for many ancestral *Piofontia* species. The DEC model suggests that *Piofontia* probably originated in a region that combined the Sierra Nevada de Santa Marta and the Eastern Cordillera (Fig. 3.6a, 3.7).

The species with the smallest leaf area is *Piofontia colombiana* with an average of 9.8 mm^2 while the one with the biggest is *P. jaramilloi* with an average of 3377.0 mm^2 (Table 3.5). Blomberg *et al*.,'s (2003) K and Pagel's (1999) lambda (λ) of the log-converted leaf area means calculated on the *Piofontia* phylogeny are 0.63 and 0.95, both departing from a Brownian model evolution with P=0.001 and P<0.001, respectively. The layout of the leaf-log-area boxplots mapped on the phylogeny (Fig. 3.6) allowed us to compare the distribution and ecological morphology of sister *Piofontia* species. The comparison (Fig. 3.6b) shows that in 10 out of the 16 comparisons there are not significant differences between the leaf areas of sister taxa suggesting that in the majority of the cases speciation have not produced ecological divergence between sister-taxa. In terms of distribution, in 9 cases the sister-taxa pairs compared occur in allopatry while in 7 occur in sympatry. When the leaf area and distribution comparison are interpreted by the framework explained in the methods (e.g. *Piofontia mutiscuana* and *P. oblongifolia* are sister species in allopatry with similar leaf areas [P= 0.44] suggesting an event of speciation caused by geographic isolation), our results suggest that isolation drove 56%

of speciation events while ecological divergence drove 19%, the rest, 25%, were driven by unknown processes (Fig. 3.6c).

The average rate of net speciation calculated from the diversification analysis is 0.71 species per Ma (95% CI: 0.55–0.93) for the "South American lineages," 1.12 (95% CI: 0.73–1.69) for *Piofontia*, and 0.74 (95% CI: 0.48–1.12) *Diplostephium*. Simulations carried out with BAMM suggest that there were two shifts of diversification regimes on the phylogeny with a marginal probability of 0.35 (Fig. 3.8a, 3.8f, Table 3.6). One of the shifts happened in *Piofontia* ca. 3.8 mya and the second occurred in *Diplostephium* ca. 4.2 mya. In *Piofontia,* the shift happened close to its root affecting 89% of the species sampled while in *Diplostephium* a shift occurred in a derived node affecting 58% of its species sampled (Fig. 3.8). Only one of the two *Diplostephium* clades that colonized the páramo was involved in the diversification shift (clade 2 Fig. 3.8). The speciation rates plotted trough time reveal that there is a tendency for higher speciation rates after 4 mya (Fig. 3.8b), this acceleration is likely the result of the almost simultaneous shifts in speciation rates in *Piofontia* (Fig. 3.8c) and *Diplostephium* (Fig. 3.8d). Finally, the cohort matrix of diversification regimes shows that the two clades in the phylogeny with the highest speciation rates, one nested in *Piofontia* and the second nested in *Diplostephium,* have different diversification regimes (Fig. 3.8e).

DISCUSSION

Spatiotemporal Patterns of the "South American Lineages"

The calibration of the "South American lineages" phylogeny (Vargas & Simpson, in prep.) shows that most Andean genera in Astereae diverged recently, ca. 8.8–3.8 mya. Taking into account the preference for open and semi-dry areas of New World Astereae (Carlquist, 1960) and that mountains provide a physiologically dry and semidry habitat

for plants (Carlquist, 1994; Leuschner, 2000), our results provide evidence that the rise of the Andes Cordillera during the Miocene and Pliocene (van der Hammen & Cleef, 1986; Gregory-Wodzicki, 2000) made new areas of South America available for Astereae ancestors to colonize and diversify.

Our chronogram shows that *Piofontia* originated in the Northern Andes 5.65 mya predating the estimated origin of the páramo 2–4 mya (van der Hammen & Cleef, 1986; Gregory-Wodzicki, 2000). Despite the fact that *Piofontia*'s inferred age 95% CI (1.66–10.03 mya) can accommodate such incongruence, other genera like *Arcytophyllum, Brunfelsia, Jamesonia+Eriosorus, Lysipomia, Valeriana,* and *Vasconcellea* also show ages older than 4 mya (Luebert & Weigend, 2014). An explanation for this early origin could be that ancestors of these lineages inhabited the summits of middle elevation mountains (<2000 m) extant at that time. Mid-elevation tropical mountains often have open and semi-dry areas at upper elevations, which are somewhat physiologically similar to the páramo. These physiologically dry patches are caused by well-drained soils and strong winds similar to the contemporary *campos de altitude* and *campus rupestres* in Brazil (Safford, 1999; Alves *et al*., 2014). It is possible that middle elevation mountaintops provided an early habitat for *Piofontia* ancestors before higher elevations were available after 4 mya. A second alternative is that páramos were available before 2–4 mya as suggested by Ehlers & Poulsen (2009). A third scenario is that *Piofontia* originated in the Sierra Nevada de Santa Marta (SNSM), a mountain range located in northern Colombia now separated from the main Andes Cordilleras. Unfortunately the SNSM lacks a resolved geological history (Villagómez *et al*., 2011) although it potentially have reached reach high elevations before 4 mya. Our phylogeny provides some evidence for this hypothesis because the SNSM endemics *Piofontia coriacea, P. inesiana,* and *P. romeroi* comprise a clade that diverged 4.71 mya, and the

biogeographical reconstruction of *Piofontia* shows the combined areas of the SNSM and the Eastern Cordillera as the most likely area of origin for the genus (Fig. 3.6a).

Our historical reconstructions suggest that *Diplostephium* originated 6.16 mya at the end of major Central Andean uplift (6–10 mya, Gregory-Wodzicki, 2000; Garzione *et al*., 2014). Although *Diplostephium* is primarily Central Andean, our reconstruction shows that two clades independently colonized the páramo of the Northern Andes (clades 1 and 2, Fig. 3.4) at 3.80 and 1.82 mya. *Diplostephium*-páramo species overlap in distribution with some species of *Piofontia,* and the *Diplostephium*-páramo clade with most species, clade 1 with 11 species, it is not nested in the clade of *Diplostephium* where the shift to higher diversification rates happened (Fig. 3.8). The species of *Diplostephium* that comprise the clade after the diversification shift are mainly distributed in central and southern Peru on the Andean slopes facing the Amazon basin.

According to our results both shifts of diversification regimes happened during the Pliocene around 4 mya coinciding with the rapid uplift of the Northern Andes (van der Hammen & Cleef, 1986; Gregory-Wodzicki, 2000) and a general drier and warmer climate (Haywood *et al*., 2000). Both, mountain building and a warmer-drier climate likely positively affected the speciation rates in *Piofontia* (Fig. 3.8c)*;* whereas for *Diplostephium,* it seems that only the Pleistocene climate had a role increasing *Diplostephium*'s speciation rate, taking into account that the genus originated after the Central Andes have already reached a high elevation 6.16 mya and its speciation rate accelerated at the beginning of the Pleistocene (Fig. 3.8d). Even thought *Piofontia* and *Diplostephium* are similar in terms of morphology and ecology, the evolutionary matrix suggests that their diversification regimes are different. While *Piofontia* is ~5.65 Ma old and has 63 species, *Diplostephium* is ~6.16 Ma and has 51 species, this suggests that rates of speciation in the Northern Andes are slightly higher that those in the Central Andes.

High rates of speciation in the Northern Andes are also evidenced by the high indices of páramo endemism estimated between 60% (Luteyn, 1992) and 100% (Madriñán *et al*., 2013), and the lack of fit of the Eastern-Cordillera-Colombian páramo to abundance models (Simpson & Todzia, 1990). However, it is possible that the lower speciation rate calculated for *Diplostephium* in this study is an artifact of the low degree of exploration in the Central Andes. The first author of this study (OMV) found at least five new taxa of *Diplostephium* while collecting in central and southern Peru, and we suspect that numerous species are going to be discovered with future exploration efforts. Therefore, the humid puna of the central and southern of Peru could potentially have similar diversity indices that those reported for the páramo. The humid puna (also known as high Yunga) comprise a belt of vegetation just above the cloud forest and it is dissected by creeks, valleys, and geological depressions. Endemism and speciation patterns in the humid puna are still unknown, but based on the evidence presented here and studies on Ericaceae (Luteyn & Ortiz, 2008; Pedraza-Peñalosa & Luteyn, 2011) we hypothesize that the diversity of the humid puna could be similar to that of the páramo.

The Relative Role of Isolation and Ecological Divergence

The broad range found in leaf areas of *Piofontia* species demonstrates that the genus has adapted to different niches in the páramo ecosystem. However, when the morphology of sister species is contrasted, the comparisons suggest that most sister taxa (~63%) have a similar leaf area and probably occupy very similar niches. Therefore, phylogenetic niche conservatism has a strong signal in the evolution of *Piofontia* making ecological divergence evident mostly between distantly related species. Using our framework of comparing distribution and leaf area as an ecological indicator, we found that more than a half of the speciation events evaluated were driven by isolation (56%)

while only 19% were driven by ecological divergence. Furthermore, we found a very strong signal of speciation by isolation in the *Denticulata* clade (clade D, Fig. 3.6) that is completely comprised by large-leaved species that inhabit the upper border of the cloud forest. Our comparisons in the *Denticulata* clade found no evidence of ecological divergence between any sister taxa pair and all sister taxa are allopatric. The above statements demonstrate that allopatric speciation via isolation may be responsible for most speciation events in the páramo, a result that aligns with the island-like distribution and endemism pattern of this ecosystem (Simpson, 1974). Nevertheless, there is also a significant fraction of cases (25%) in which speciation events are promoted by factors other than isolation and morpho-ecological divergence; this 25% percent could be explained by ecological divergence that is not reflected in the leaf area or a shift in pollination syndrome. Possible limitations in our approach that could potentially confound the outcome of sister taxa comparisons include the effect of extinction, non-sampled species, and misleading taxonomic information.

Our results agree with previous hypotheses about the evolution of páramo flora that stated that geographical isolation has been a main driver of speciation in the Andes (Simpson, 1974; Cuatrecasas, 1986; van der Hammen & Cleef, 1986). The biogeographic analysis of *Piofontia* shows that dispersion out of the Eastern Cordillera of Colombia was a common process that produced geographical isolation for founder populations. Most species of *Piofontia* are endemic to the Eastern Cordillera, and the biogeographic reconstruction shows that many ancestral species inhabit this cordillera from which there were multiple events of dispersion. The Eastern Cordillera of Colombia has the largest distribution of páramo (Luteyn, 1999; Londoño *et al*., 2014) and is the oldest component of the Northern Andes (although it is possible the Sierra Nevada de Santa Marta could be older since its paleoelevation is unknown). Achenes of *Piofontia* are small and a have a

pappus that allows long-distance dispersion by wind (Cuatrecasas, 1969). Examples of long-distance dispersal are shown by the two species reported for the páramos of Costa Rica. *Piofontia costaricense,* probably a direct descendant of *P. alveolata*, that undoubtedly reached Central America by a long distance dispersal event from the Eastern Cordillera of Colombia (Fig. 3.6a) and the Costa Rican population of *Piofontia floribunda,* which is a species also reported for Colombia and Ecuador, that is likely a descendant from the Central or Eastern Colombian Cordillera populations. The dispersal capability of *Piofontia* allowed the genus to disperse to, and speciate in almost every páramo island of the Andes with the exception of the southern páramo of Ecuador. Two hypotheses can explain this absence. First, it is possible that the genus simply has not yet reached these southern páramos because of the east-to-west wind pattern in South America (Garreaud *et al*., 2009). Second, southern páramos contain *Diplostephium* species with similar morphologies and altitudinal distribution that could have excluded *Piofontia* from these regions by competition.

CONCLUSIONS

Our spatiotemporal inferences about the evolution of *Diplostephium* and *Piofontia* suggest that the tropical Andes provided new habitats for lineages pre-adapted to dry and semi-dry environments. Our novel approach of sister taxa comparisons that incorporates phylogenetics, geographical distributions, and morpho-ecological characters unveiled that dispersal and isolation are the processes driving most of the speciation events in the Northern Andes. The island-like coverage of the páramo is a primary factor of autochthonous speciation via geographic isolation explaining the particular high accumulation of plant species in the páramo (Simpson & Todzia, 1990) and their high speciation rates (Madriñán *et al*., 2013). Nevertheless, ecological divergence and other

factors (Lagomarsino *et al*., 2016) seem to be also contributing to high rates of speciation found by numerous studies in páramo plants (Drummond *et al*., 2012b; Zapata, 2013; Sánchez-Baracaldo & Thomas, 2014; Nürk *et al*., 2015; Uribe-Convers & Tank, 2015). Our findings largely agree with recent claims by Givnish (2015), who indicated that not all rapid diversifications are the product of ecological speciation (radiation) and that researches should be careful when using the terms "diversification" and "radiation." We demonstrate that the main driver of speciation in *Piofontia* is isolation, and that even though ecological divergence is a process acting in the evolution of *Piofontia* its effect on speciation was less influential, or at least comparable to geographic isolation. Moreover, our results indicate that isolation and ecological divergence are synergistic processes acting together positively in the history of the diversification of páramo plants.

TABLES

Table 3.1. References used to infer the distributions of the genera sampled in the analysis. GBIF: Global Biodiversity Information Facility portal http://data.gbif.org.

Genus	Sources
Archibaccharis	GBIF, Jackson, 1975
Aztecaster	GBIF, Nesom, 1993
Baccharis	GBIF
Blakiella	Cuatrecasas, 1969
Exostigma	GBIF, Sancho, 2012
Floscaldasia	Cuatrecasas, 1969
Heterothalamus	GBIF, Nesom & Robinson, 2007
Hinterhubera	Cuatrecasas, 1969
Laennecia	GBIF, Nesom, 1990
Laestadia	Cuatrecasas, 1969
Lagenophora	Cabrera, 1966
Parastrephia	GBIF, Nesom, 1993
Westoniella	GBIF, Cuatrecasas, 1977

Table 3.2. Sampling correction used in BAMM.

Species	Genus	Sampled fraction of the genus
Archibaccharis asperifolia	*Archibaccharis*	0.03
Aztecaster matudae	*Aztecaster*	0.50
Baccharis genistelloides	*Baccharis*	0.01
Baccharis tricuneata	*Baccharis*	0.01
Blakiella bartsiifolia	*Blakiella*	1.00
Diplostephium azureum	*Diplostephium*	0.62
Diplostephium barclayanum	*Diplostephium*	0.62
Diplostephium cajamarquillense	*Diplostephium*	0.62
Diplostephium callilepis	*Diplostephium*	0.62
Diplostephium cinereum	*Hybrid*	1.00
Diplostephium crypteriophyllum	*Diplostephium*	0.62
Diplostephium empetrifolium	*Diplostephium*	0.62
Diplostephium ericoides	*Diplostephium*	0.62
Diplostephium espinosae	*Diplostephium*	0.62
Diplostephium foliosissimum	*Diplostephium*	0.62
Diplostephium glandulosum	*Diplostephium*	0.62
Diplostephium gnidioides	*Diplostephium*	0.62
Diplostephium goodspeedii	*Diplostephium*	0.62
Diplostephium gynoxyoides	*Diplostephium*	0.62
Diplostephium haenkei	*Diplostephium*	0.62
Diplostephium hartwegii	*Diplostephium*	0.62
Diplostephium hippophae	*Diplostephium*	0.62
Diplostephium jelskii	*Diplostephium*	0.62
Diplostephium juniperinum	*Diplostephium*	0.62
Diplostephium lechleri	*Diplostephium*	0.62
Diplostephium meyenii	*Diplostephium*	0.62
Diplostephium oblanceolatum	*Diplostephium*	0.62
Diplostephium oxapampanum	*Diplostephium*	0.62
Diplostephium pulchrum OXA	*Diplostephium*	0.62
Diplostephium pulchrum PAS	*Diplostephium*	0.62
Diplostephium sagasteguii	*Diplostephium*	0.62
Diplostephium serratifolium	*Diplostephium*	0.62
Diplostephium sp. nov. CAJ	*Diplostephium*	0.62
Diplostephium sp. nov. CAJ2	*Hybrid*	1.00
Diplostephium sp. nov. JUN	*Diplostephium*	0.62
Diplostephium sp. nov. JUN2	*Diplostephium*	0.62
Diplostephium sp. nov. JUN3	*Diplostephium*	0.62

Table 3.2. (Continued)

Diplostephium sp. nov. JUN4	*Diplostephium*	0.62
Diplostephium sp. nov. OXA	*Diplostephium*	0.62
Diplostephium spinulosum	*Diplostephium*	0.62
Exostigma notobellidiastrum	*Exostigma*	0.50
Floscaldasia hypsophila	*Floscaldasia*	0.50
Heterothalamus alienus	*Heterothalamus*	0.50
Hinterhubera ericoides	*Hinterhubera*	0.13
Laennecia sophiifolia	*Laennecia*	0.06
Laestadia muscicola	*Laestadia*	0.17
Lagenophora cuchumatanica	*Lagenophora*	0.05
Parastrephia quadrangularis	*Parastrephia*	0.33
Piofontia alveolata	*Piofontia*	0.61
Piofontia antioquense	*Piofontia*	0.61
Piofontia apiculata	*Piofontia*	0.61
Piofontia camargoana	*Piofontia*	0.61
Piofontia cayambense	*Piofontia*	0.61
Piofontia cinerascens	*Piofontia*	0.61
Piofontia colombiana	*Piofontia*	0.61
Piofontia coriacea	*Piofontia*	0.61
Piofontia costaricense	*Piofontia*	0.61
Piofontia eriophora	*Piofontia*	0.61
Piofontia floribunda	*Piofontia*	0.61
Piofontia frontinense	*Piofontia*	0.61
Piofontia glutinosa	*Piofontia*	0.61
Piofontia heterophylla	*Piofontia*	0.61
Piofontia huertasii	*Piofontia*	0.61
Piofontia inesiana	*Piofontia*	0.61
Piofontia jaramilloi	*Piofontia*	0.61
Piofontia jenesana	*Piofontia*	0.61
Piofontia juajibioyi	*Piofontia*	0.61
Piofontia lacunosa	*Piofontia*	0.61
Piofontia mutiscuana	*Piofontia*	0.61
Piofontia oblongifolia	*Piofontia*	0.61
Piofontia obtusa	*Piofontia*	0.61
Piofontia ochracea	*Piofontia*	0.61
Piofontia phylicoidea	*Piofontia*	0.61
Piofontia revoluta	*Piofontia*	0.61
Piofontia rhododendroides	*Piofontia*	0.61
Piofontia rhomboidalis COL	*Piofontia*	0.61

Table 3.2. (Continued)

Piofontia rhomboidalis ECU	*Piofontia*	0.61
Piofontia romeroi	*Piofontia*	0.61
Piofontia rosmarinifolia	*Piofontia*	0.61
Piofontia rupestris	*Piofontia*	0.61
Piofontia schultzii CAL	*Piofontia*	0.61
Piofontia schultzii CUN	*Piofontia*	0.61
Piofontia sp. nov. ANT	*Piofontia*	0.61
Piofontia tachirense	*Piofontia*	0.61
Piofontia tenuifolia	*Piofontia*	0.61
Piofontia venezuelense	*Piofontia*	0.61
Piofontia violacea	*Piofontia*	0.61
Westoniella kohkemperi	*Westoniella*	0.17

Table 3.3. Comparison and chi-squared test among the different models evaluated by BioGeoBEARS in the analysis that included the complete phylogeny of the South American lineages. DF = degrees of freedom.

Alternative model	Null model	*LnL* alt	*LnL* null	DF alt	DF null	P value
DEC+J	DEC	-86.46	-87.54	3	2	0.14
DIVALIKE+J	DIVALIKE	-92.46	-94.06	3	2	0.074
BAYAREALIKE+J	BAYAREALIKE	-92.48	-109	3	2	9.20E-09

Table 3.4. Comparison and chi-squared test among the different models evaluated by BioGeoBEARS in the *Piofontia* analysis. DF = degrees of freedom.

Alternative model	Null model	*LnL* alt	*LnL* null	DF alt	DF null	P value
DEC+J	DEC	-119.8	-120.9	3	2	0.13
DIVALIKE+J	DIVALIKE	-124.3	-124.6	3	2	0.44
BAYAREALIKE+J	BAYAREALIKE	-122.3	-140.5	3	2	1.60E-09

Table 3.5. Average leaf area of sampled species of *Piofontia* included in Vargas & Simpson's (in prep.) study.

Species	Average leaf area (mm^2)
Piofontia alveolata	91.8
Piofontia antioquense	868.4
Piofontia apiculata	9.8
Piofontia camargoana	967.5
Piofontia cayambense	51.2
Piofontia cinerascens	31.6
Piofontia colombiana	7.6
Piofontia coriacea	1560.2
Piofontia costaricense	84.4
Piofontia eriophora	95.3
Piofontia floribunda	264.5
Piofontia frontinense	69.5
Piofontia glutinosa	35.8
Piofontia heterophylla	17.5
Piofontia huertasii	1302.6
Piofontia inesiana	23.9
Piofontia jaramilloi	3377.0
Piofontia jenesana	859.1
Piofontia juajibioyi	189.0
Piofontia lacunosa	23.5
Piofontia mutiscuana	2391.0
Piofontia oblongifolia	1350.0
Piofontia obtusa	191.3
Piofontia ochracea	1380.6
Piofontia phylicoidea	16.6
Piofontia revoluta	19.6
Piofontia rhododendroides	86.6
Piofontia rhomboidalis COL	35.5
Piofontia rhomboidalis ECU	33.6
Piofontia romeroi	570.3
Piofontia rosmarinifolia	33.8
Piofontia rupestris	95.4
Piofontia schultzii CAL	71.4
Piofontia sp. nov.	2636.0
Piofontia tachirense	914.9

Table 3.5. (Continued)

Piofontia tenuifolia	1445.9
Piofontia venezuelense	114.3
Piofontia violacea	53.8

Table 3.6. Bayes factor comparison matrix among different scenarios with different number of shifts. Underlined numbers show that a scenario with two shifts is favored by Bayes factors over a no-shift and a one-shift scenario.

#Shifts	0	1	2	3	4	5	6	7	8
0	1.0	0.2	0.0	0.0	0.0	0.0	0.0	0.0	0.0
1	4.8	1.0	0.1	0.0	0.0	0.0	0.1	0.1	0.2
2	65.9	13.7	1.0	0.6	0.6	0.4	0.8	0.9	2.2
3	112.9	23.4	1.7	1.0	1.0	0.8	1.4	1.5	3.8
4	114.8	23.8	1.7	1.0	1.0	0.8	1.4	1.5	3.8
5	146.8	30.4	2.2	1.3	1.3	1.0	1.8	2.0	4.9
6	82.8	17.2	1.3	0.7	0.7	0.6	1.0	1.1	2.8
7	75.3	15.6	1.1	0.7	0.7	0.5	0.9	1.0	2.5
8	30.1	6.2	0.5	0.3	0.3	0.2	0.4	0.4	1.0

FIGURES

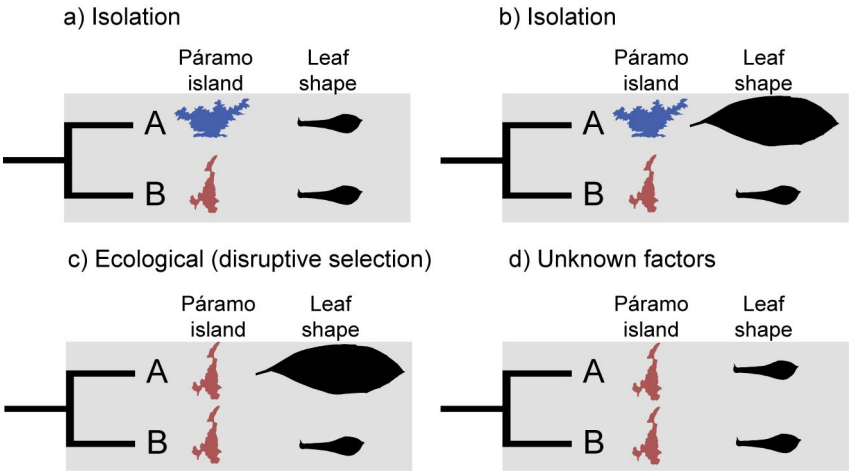

Figure 3.1. Hypothetical scenarios of speciation in sister species. a) An speciation event in which isolation resulted in two species living in separate páramos islands occupying similar niches. b) An speciation event in which isolation resulted in two species living in separate páramos islands that occupy different niches. c) An speciation event in which sister species diverged by ecological selection to different niches in the same páramo island. d) An speciation event produced by factors other than isolation or morpho-ecological divergence in which sister species inhabit the same island and have similar leaf morphologies.

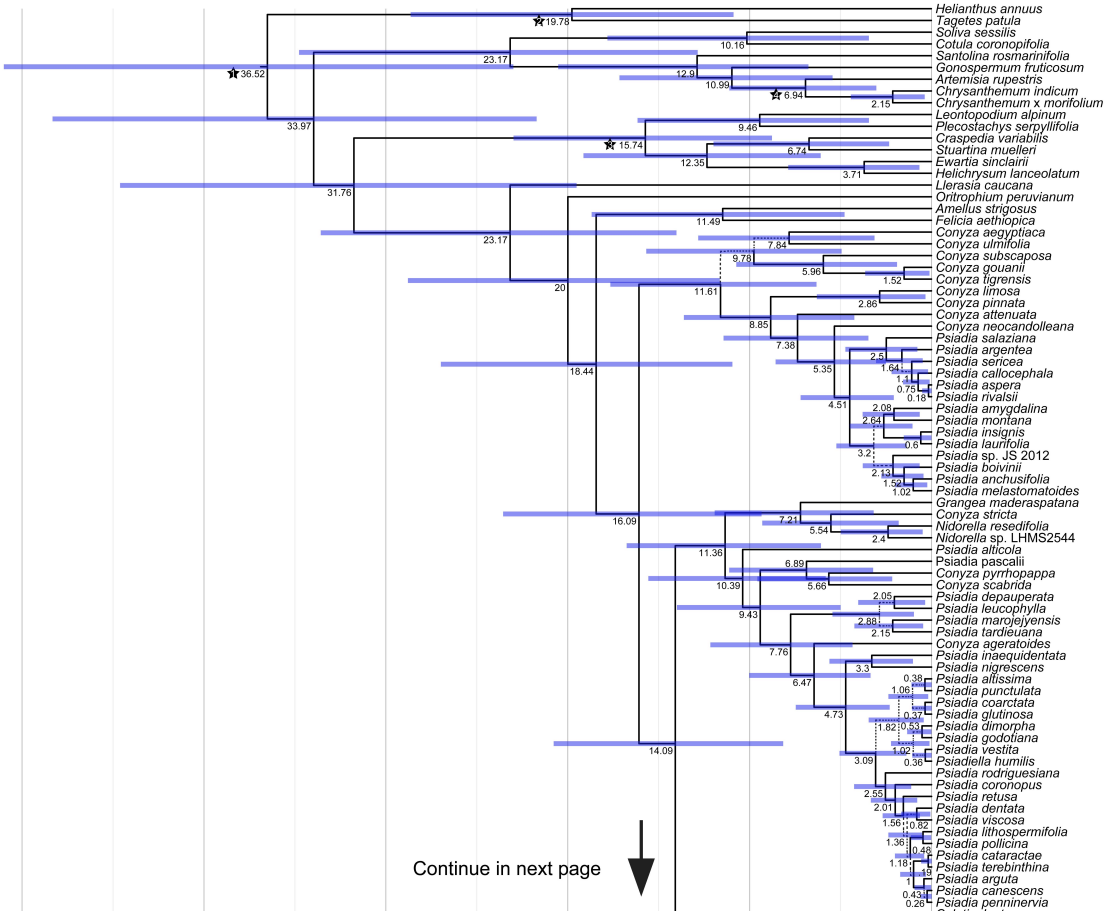

Figure 3.2 (part)

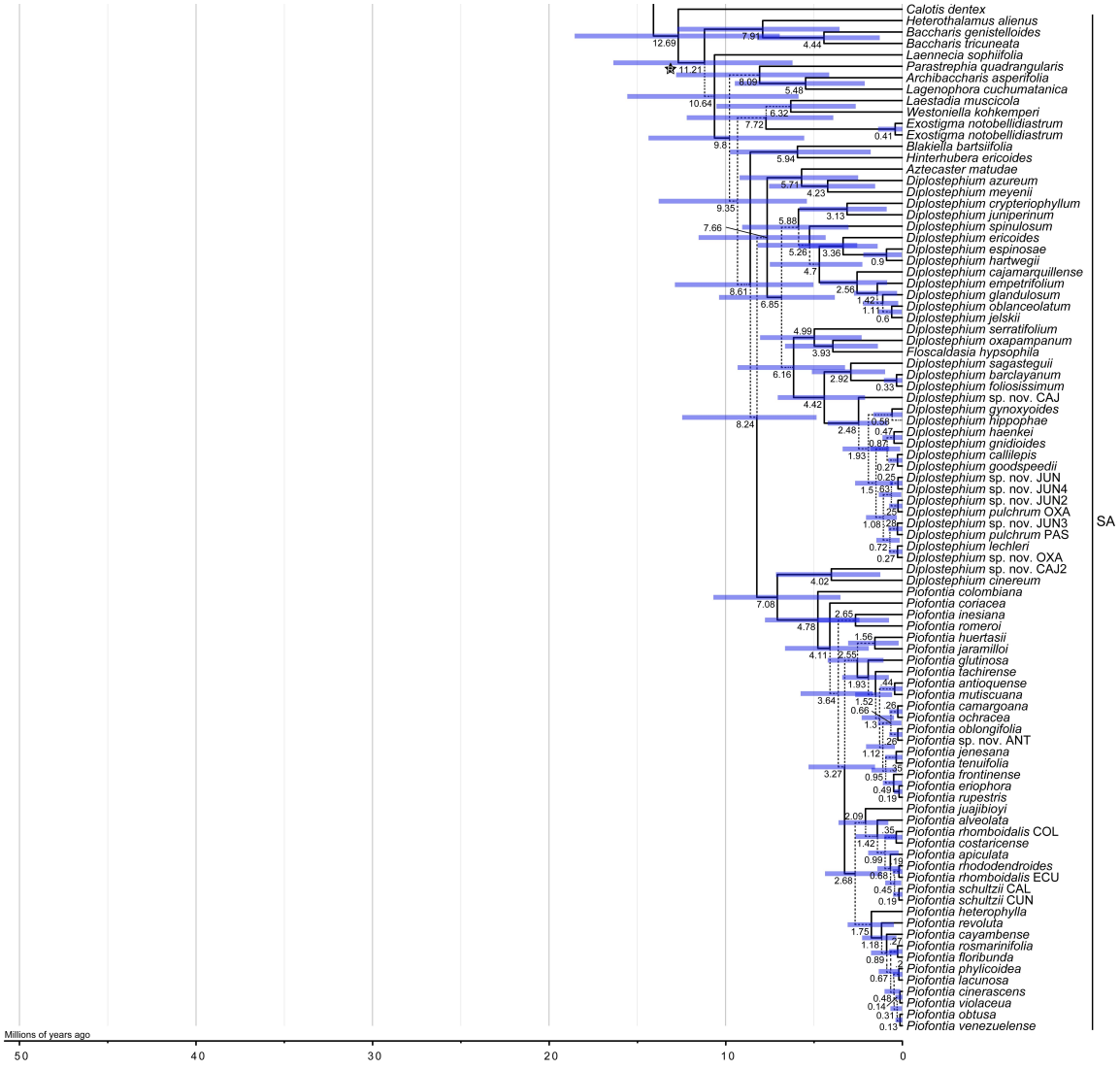

Figure 3.2. Chronogram of the ITS combined dataset. Bars indicate the 95% confidence of node ages. Low supported branches (Bayesian posterior probability <0.50) are indicated by dashed lines. Bars indicate the 95% confidence of node ages. Stars 1–4 indicate calibration points. R star represents the calibration point extracted from this chronogram to calibrate the complete nuclear ribosomal dataset of Vargas & Simpson (in prep.). SA indicates the "South American lineages."

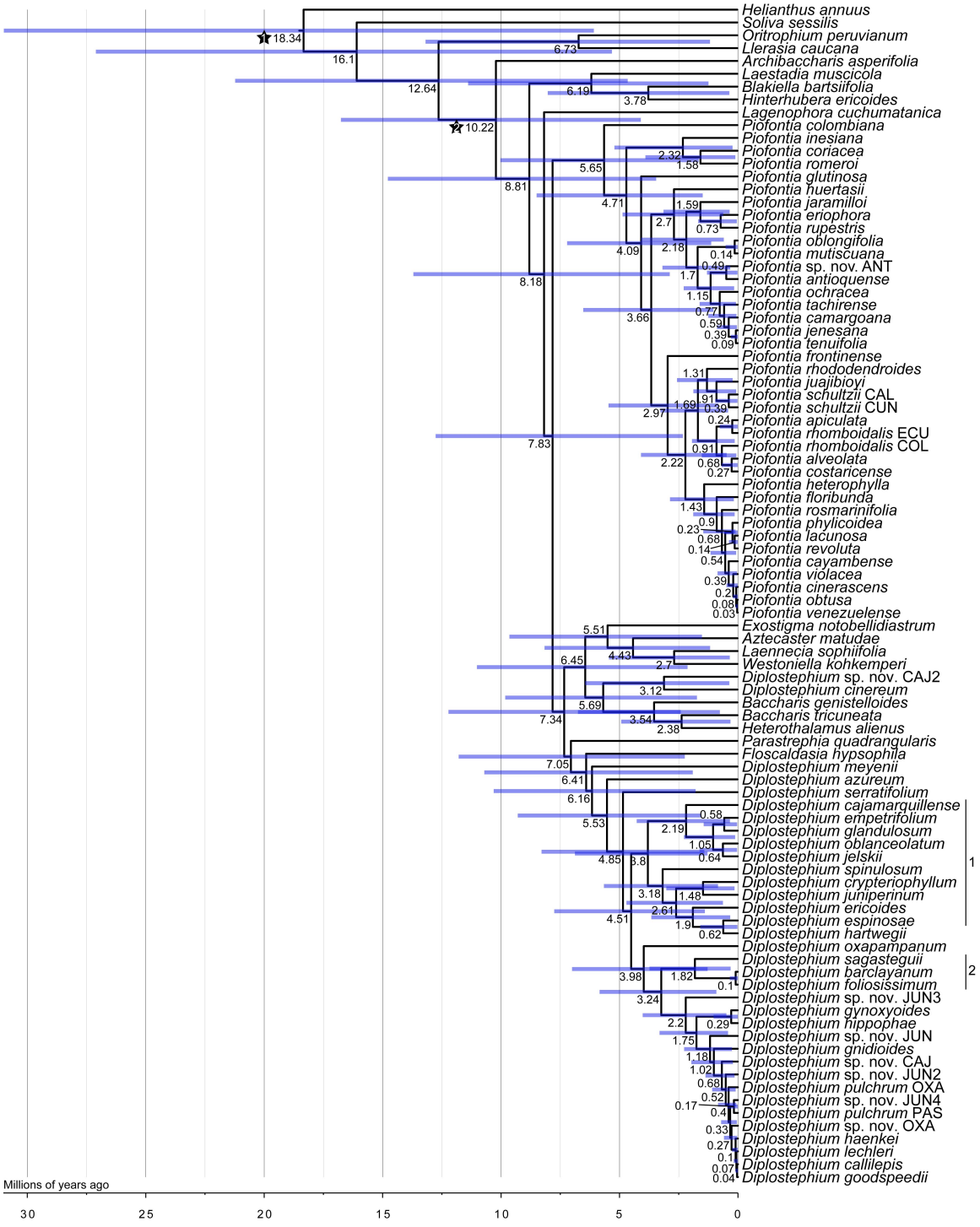
Helianthus annuus
Soliva sessilis
Oritrophium peruvianum
Llerasia caucana
Archibaccharis asperifolia
Laestadia muscicola
Blakiella bartsiifolia
Hinterhubera ericoides
Lagenophora cuchumatanica
Piofontia colombiana
Piofontia inesiana
Piofontia coriacea
Piofontia romeroi
Piofontia glutinosa
Piofontia huertasii
Piofontia jaramilloi
Piofontia eriophora
Piofontia rupestris
Piofontia oblongifolia
Piofontia mutiscuana
Piofontia sp. nov. ANT
Piofontia antioquense
Piofontia ochracea
Piofontia tachirense
Piofontia camargoana
Piofontia jenesana
Piofontia tenuifolia
Piofontia frontinense
Piofontia rhododendroides
Piofontia juajibioyi
Piofontia schultzii CAL
Piofontia schultzii CUN
Piofontia apiculata
Piofontia rhomboidalis ECU
Piofontia rhomboidalis COL
Piofontia alveolata
Piofontia costaricense
Piofontia heterophylla
Piofontia floribunda
Piofontia rosmarinifolia
Piofontia phylicoidea
Piofontia lacunosa
Piofontia revoluta
Piofontia cayambense
Piofontia violacea
Piofontia cinerascens
Piofontia obtusa
Piofontia venezuelense
Exostigma notobellidiastrum
Aztecaster matudae
Laennecia sophiifolia
Westoniella kohkemperi
Diplostephium sp. nov. CAJ2
Diplostephium cinereum
Baccharis genistelloides
Baccharis tricuneata
Heterothalamus alienus
Parastrephia quadrangularis
Floscaldasia hypsophila
Diplostephium meyenii
Diplostephium azureum
Diplostephium serratifolium
Diplostephium cajamarquillense
Diplostephium empetrifolium
Diplostephium glandulosum
Diplostephium oblanceolatum
Diplostephium jelskii
Diplostephium spinulosum
Diplostephium crypteriophyllum
Diplostephium juniperinum
Diplostephium ericoides
Diplostephium espinosae
Diplostephium hartwegii
Diplostephium oxapampanum
Diplostephium sagasteguii
Diplostephium barclayanum
Diplostephium foliosissimum
Diplostephium sp. nov. JUN3
Diplostephium gynoxyoides
Diplostephium hippophae
Diplostephium sp. nov. JUN
Diplostephium gnidioides
Diplostephium sp. nov. CAJ
Diplostephium sp. nov. JUN2
Diplostephium pulchrum OXA
Diplostephium sp. nov. JUN4
Diplostephium pulchrum PAS
Diplostephium sp. nov. OXA
Diplostephium haenkei
Diplostephium lechleri
Diplostephium callilepis
Diplostephium goodspeedii
1
2
Millions of years ago
30
25
20
15
10
5
0

Figure 3.3.

Figure 3.3. Chronogram based on the complete nuclear ribosomal dataset from Vargas & Simpson (in prep.). Bars indicate the 95% confidence of node ages. Stars indicate the calibrations points used. Clades 1 and 2 indicate lineages nested within *Diplostephium* that contain taxa distributed in the Northern Andes.

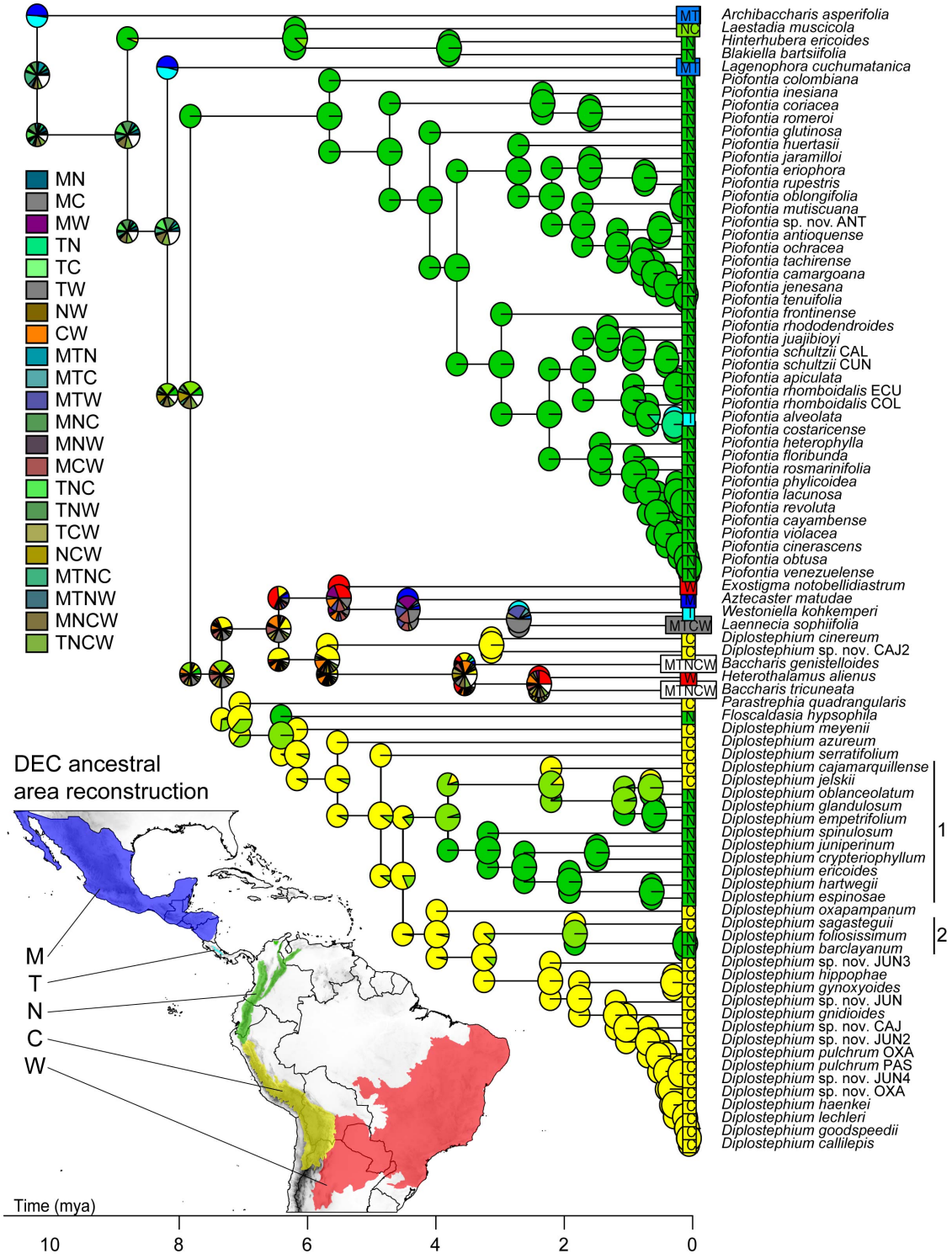
MN
MC
MW
TN
TC
TW
NW
CW
MTN
MTC
MTW
MNC
MNW
MCW
TNC
TNW
TCW
NCW
MTNC
MTNW
MNCW
TNCW
Archibaccharis asperifolia
Laestadia muscicola
Hinterhubera ericoides
Blakiella bartsiifolia
Lagenophora cuchumatanica
Piofontia colombiana
Piofontia inesiana
Piofontia coriacea
Piofontia romeroi
Piofontia glutinosa
Piofontia huertasii
Piofontia jaramilloi
Piofontia eriophora
Piofontia rupestris
Piofontia oblongifolia
Piofontia mutiscuana
Piofontia sp. nov. ANT
Piofontia antioquense
Piofontia ochracea
Piofontia tachirense
Piofontia camargoana
Piofontia jenesana
Piofontia tenuifolia
Piofontia frontinense
Piofontia rhododendroides
Piofontia juajibioyi
Piofontia schultzii CAL
Piofontia schultzii CUN
Piofontia apiculata
Piofontia rhomboidalis ECU
Piofontia rhomboidalis COL
Piofontia alveolata
Piofontia costaricense
Piofontia heterophylla
Piofontia floribunda
Piofontia rosmarinifolia
Piofontia phylicoidea
Piofontia lacunosa
Piofontia revoluta
Piofontia cayambense
Piofontia violacea
Piofontia cinerascens
Piofontia obtusa
Piofontia venezuelense
Exostigma notobellidiastrum
Aztecaster matudae
Westoniella kohkemperi
Laennecia sophiifolia
Diplostephium cinereum
Diplostephium sp. nov. CAJ2
Baccharis genistelloides
Heterothalamus alienus
Baccharis tricuneata
Parastrephia quadrangularis
Floscaldasia hypsophila
Diplostephium meyenii
Diplostephium azureum
Diplostephium serratifolium
Diplostephium cajamarquillense
Diplostephium jelskii
Diplostephium oblanceolatum
Diplostephium glandulosum
Diplostephium empetrifolium
Diplostephium spinulosum
Diplostephium juniperinum
Diplostephium crypteriophyllum
Diplostephium ericoides
Diplostephium hartwegii
Diplostephium espinosae
Diplostephium oxapampanum
Diplostephium sagasteguii
Diplostephium foliosissimum
Diplostephium barclayanum
Diplostephium sp. nov. JUN3
Diplostephium hippophae
Diplostephium gynoxyoides
Diplostephium sp. nov. JUN
Diplostephium gnidioides
Diplostephium sp. nov. CAJ
Diplostephium sp. nov. JUN2
Diplostephium pulchrum OXA
Diplostephium pulchrum PAS
Diplostephium sp. nov. JUN4
Diplostephium sp. nov. OXA
Diplostephium haenkei
Diplostephium lechleri
Diplostephium goodspeedii
Diplostephium callilepis
MTCW
MTNCW
MTNCW
1
2
DEC ancestral
area reconstruction
M
T
N
C
W
Time (mya)
10
8
6
4
2
0

Figure 3.4.

Figure 3.4. BioGeoBEARS DEC ancestral reconstruction based on the nuclear ribosomal phylogeny of the Astereae "South American lineages" based on Vargas & Simpson (in prep.) with proportional likelihoods of the different ancestral areas as pie charts. Node states represent a geographical area before a cladogenesis event, whereas corner states represent a geographic range after a cladogenesis event. Clades 1 and 2 indicate lineages nested within *Diplostephium* that contain taxa distributed in the Northern Andes.

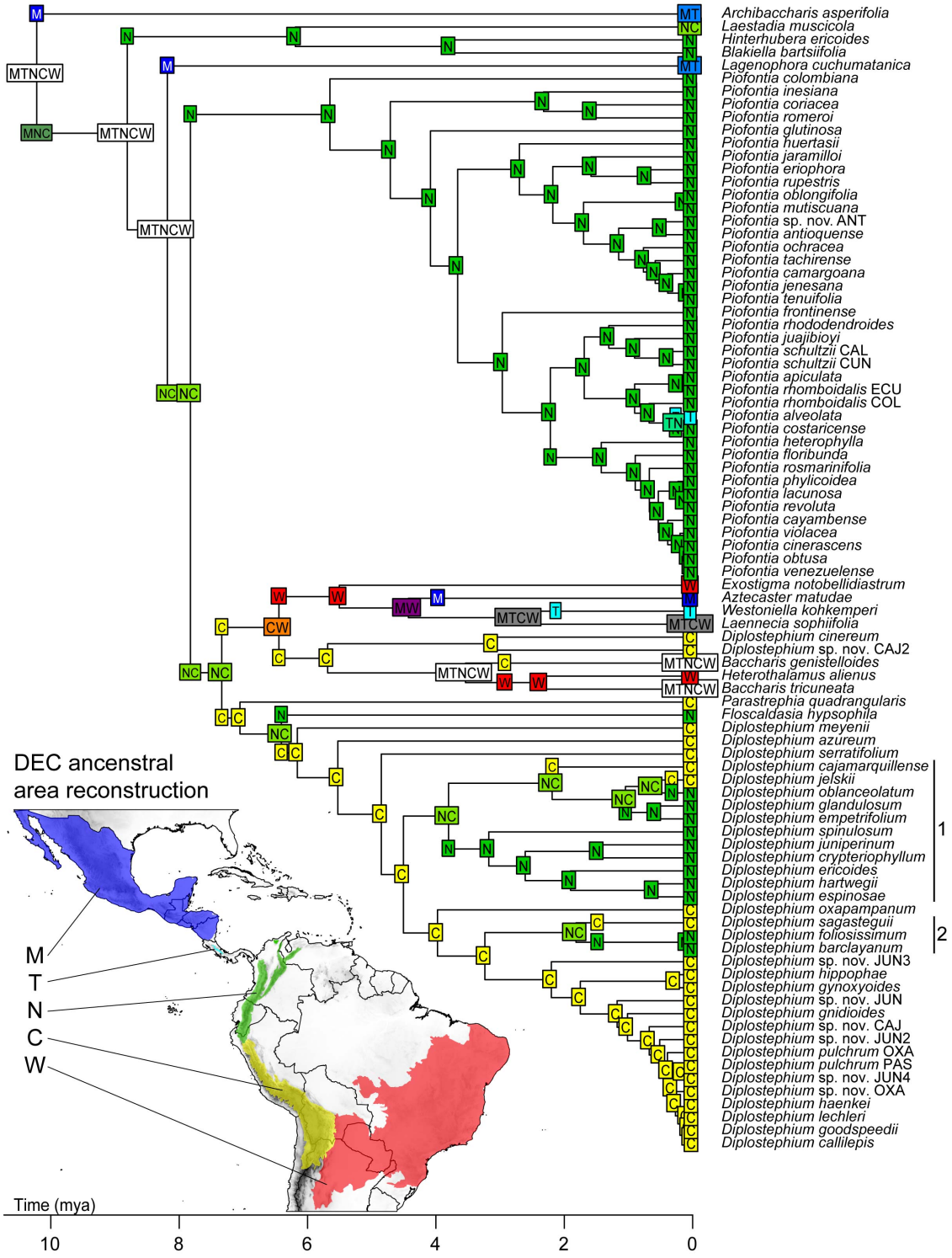
DEC ancenstral
area reconstruction
M
T
N
C
W
Time (mya)
10
8
6
4
2
0
Archibaccharis asperifolia
Laestadia muscicola
Hinterhubera ericoides
Blakiella bartsiifolia
Lagenophora cuchumatanica
Piofontia colombiana
Piofontia inesiana
Piofontia coriacea
Piofontia romeroi
Piofontia glutinosa
Piofontia huertasii
Piofontia jaramilloi
Piofontia eriophora
Piofontia rupestris
Piofontia oblongifolia
Piofontia mutiscuana
Piofontia sp. nov. ANT
Piofontia antioquense
Piofontia ochracea
Piofontia tachirense
Piofontia camargoana
Piofontia jenesana
Piofontia tenuifolia
Piofontia frontinense
Piofontia rhododendroides
Piofontia juajibioyi
Piofontia schultzii CAL
Piofontia schultzii CUN
Piofontia apiculata
Piofontia rhomboidalis ECU
Piofontia rhomboidalis COL
Piofontia alveolata
Piofontia costaricense
Piofontia heterophylla
Piofontia floribunda
Piofontia rosmarinifolia
Piofontia phylicoidea
Piofontia lacunosa
Piofontia revoluta
Piofontia cayambense
Piofontia violacea
Piofontia cinerascens
Piofontia obtusa
Piofontia venezuelense
Exostigma notobellidiastrum
Aztecaster matudae
Westoniella kohkemperi
Laennecia sophiifolia
Diplostephium cinereum
Diplostephium sp. nov. CAJ2
Baccharis genistelloides
Heterothalamus alienus
Baccharis tricuneata
Parastrephia quadrangularis
Floscaldasia hypsophila
Diplostephium meyenii
Diplostephium azureum
Diplostephium serratifolium
Diplostephium cajamarquillense
Diplostephium jelskii
Diplostephium oblanceolatum
Diplostephium glandulosum
Diplostephium empetrifolium
Diplostephium spinulosum
Diplostephium juniperinum
Diplostephium crypteriophyllum
Diplostephium ericoides
Diplostephium hartwegii
Diplostephium espinosae
Diplostephium oxapampanum
Diplostephium sagasteguii
Diplostephium foliosissimum
Diplostephium barclayanum
Diplostephium sp. nov. JUN3
Diplostephium hippophae
Diplostephium gynoxyoides
Diplostephium sp. nov. JUN
Diplostephium gnidioides
Diplostephium sp. nov. CAJ
Diplostephium sp. nov. JUN2
Diplostephium pulchrum OXA
Diplostephium pulchrum PAS
Diplostephium sp. nov. JUN4
Diplostephium sp. nov. OXA
Diplostephium haenkei
Diplostephium lechleri
Diplostephium goodspeedii
Diplostephium callilepis
1
2

Figure 3.5.

Figure 3.5. BioGeoBEARS DEC ancestral reconstruction based on the nuclear ribosomal phylogeny of the Astereae "South American lineages" based on Vargas & Simpson (in prep.) showing the most probable ancestral range. Node states represent the geographical area before cladogenesis, whereas corner states represent the geographic range after a cladogenesis event. Corner states were removed when they were identical to their parental node. Clades 1 and 2 indicate lineages nested within *Diplostephium* that contain taxa distributed in the Northern Andes.

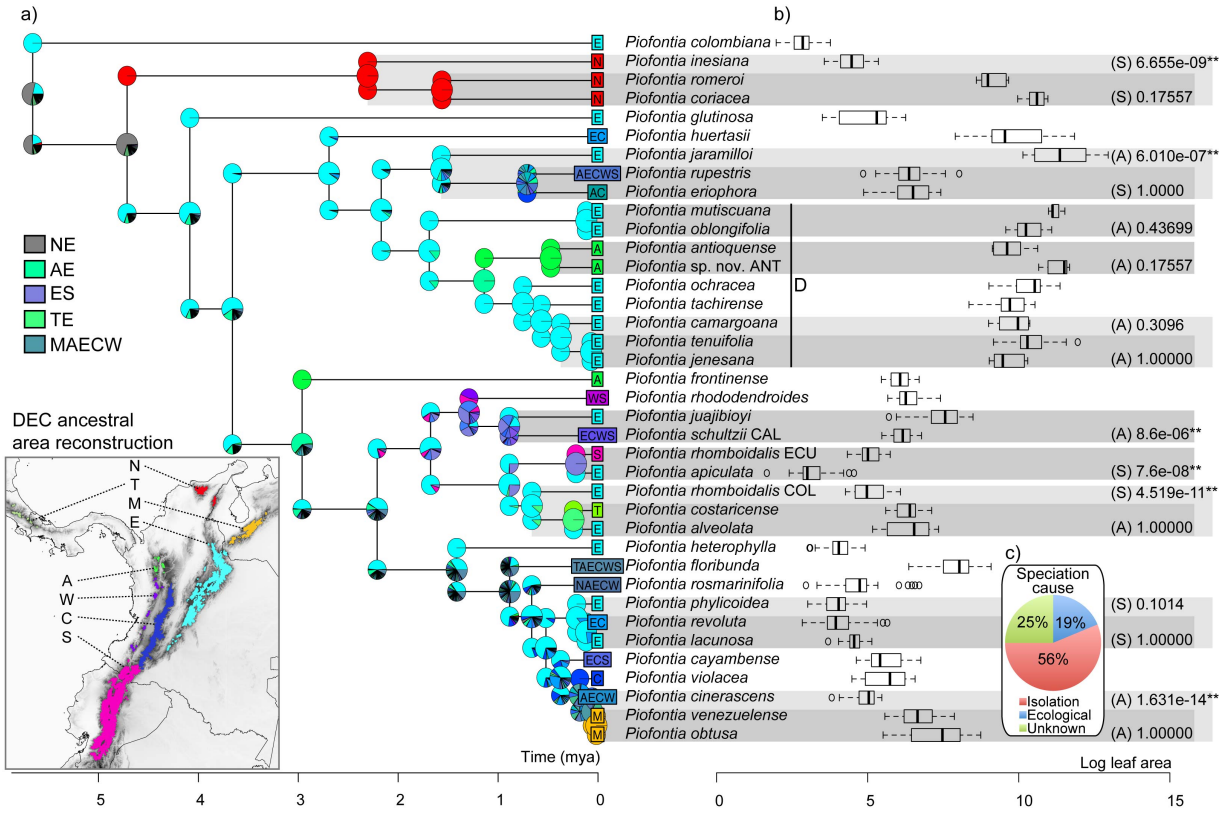

Figure 3.6. a) BioGeoBEARS DEC ancestral reconstruction based on the *Piofontia* nuclear ribosomal phylogeny of Vargas & Simpson (in prep.) with proportional likelihoods of the different ancestral areas as pie charts. Node states represent a geographical area before a cladogenesis event, whereas corner states represent a geographic range after a cladogenesis event. b) Boxplot of the leaf area dataset, shaded boxes indicates the Wilcoxon signed-rank test of sister taxa with its result on the right. Distribution of the sister taxa is indicated by (A) = allopatry or (S) = sympatry. c) Pie chart indicating the inferred cause of speciation after contrasting the Wilcoxon signed-rank test and the distribution of sister taxa.

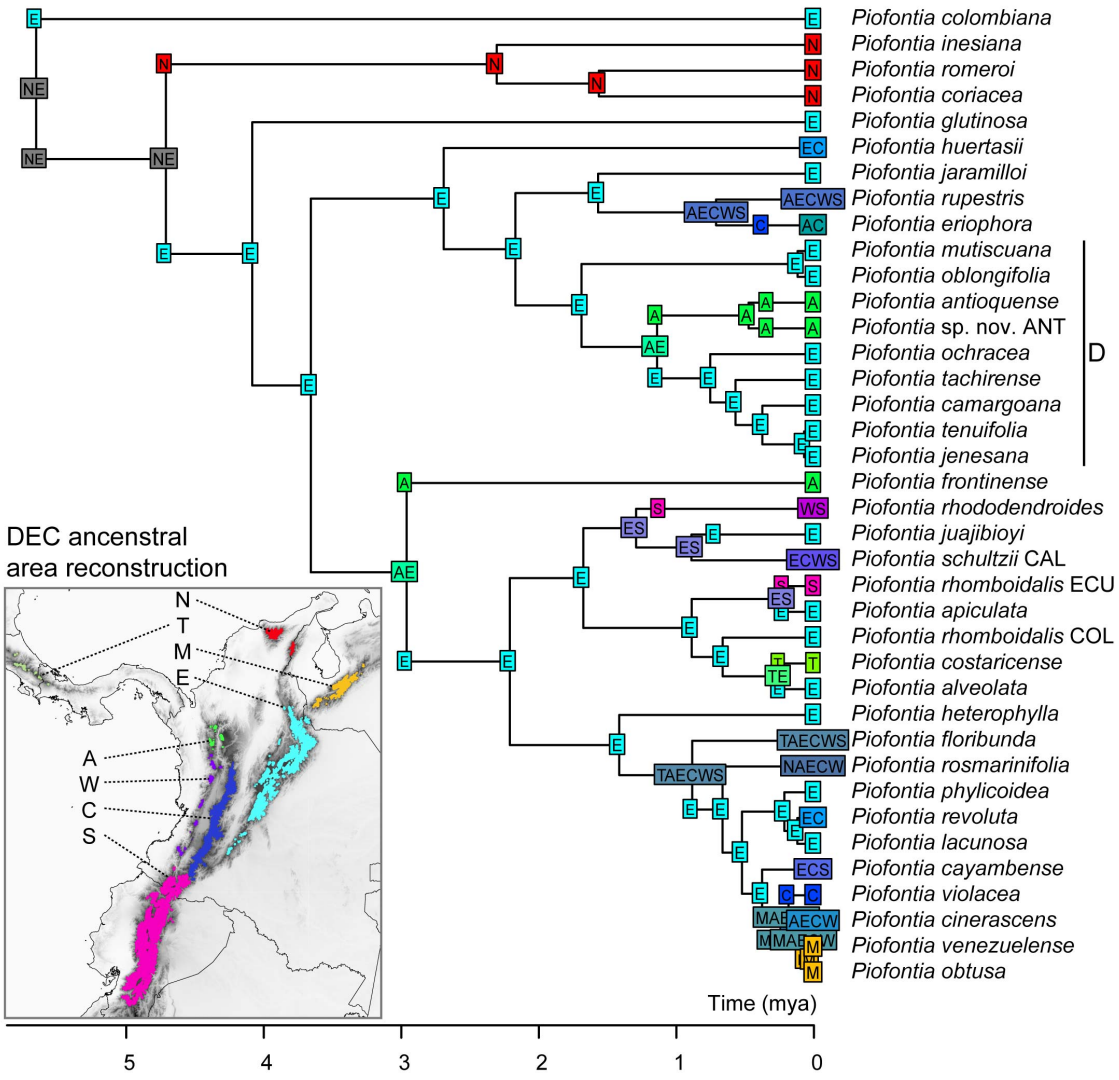

Figure 3.7. BioGeoBEARS DEC biogeographical ancestral reconstruction based on the *Piofontia* nuclear ribosomal tree from Vargas & Simpson (in prep.) showing the most probable ancestral range. Node states represent the geographical area before cladogenesis, whereas corner states represent the geographic range after a cladogenesis event. Corner states were removed when they were identical to their parental node.

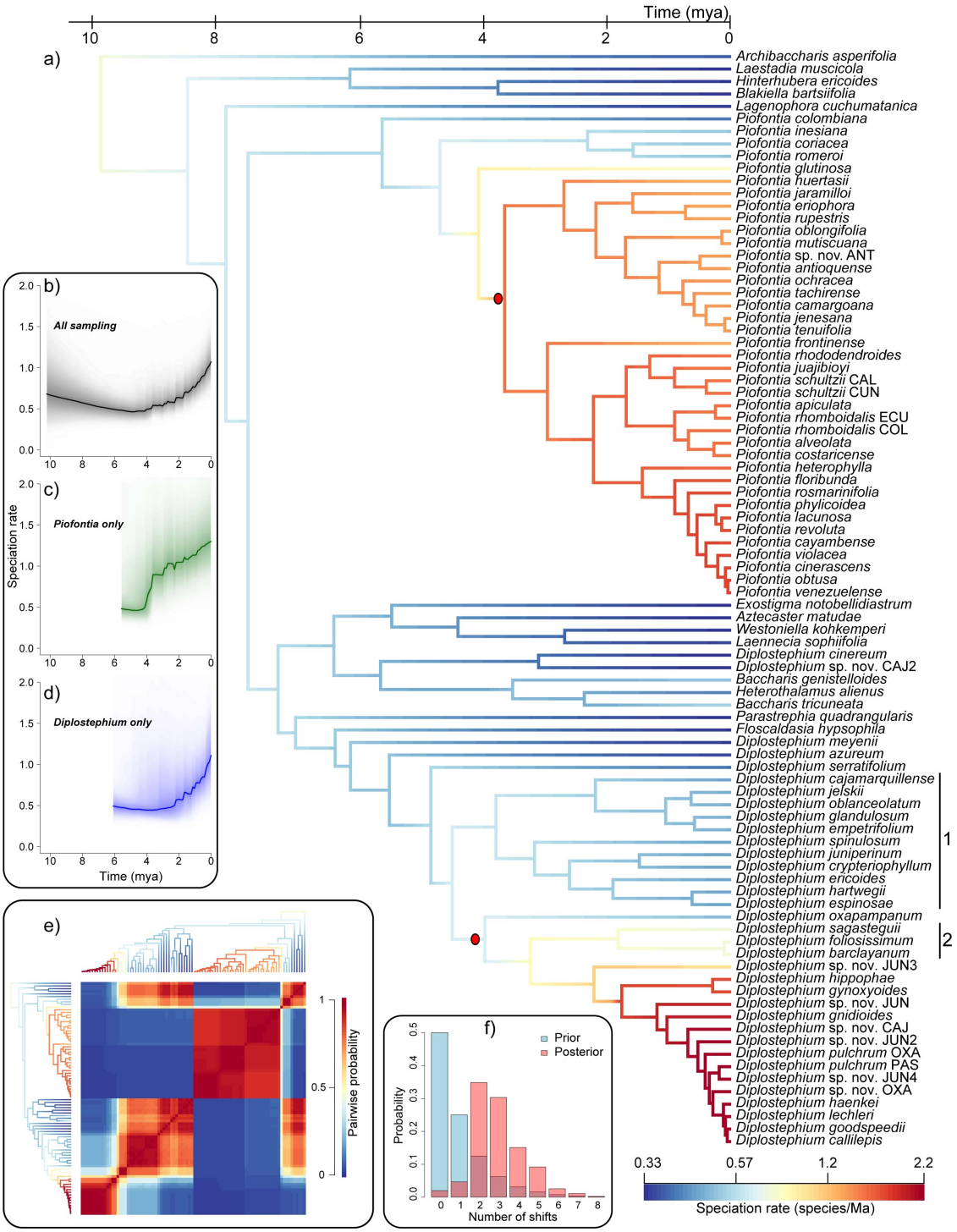
Time (mya)
10
8
6
4
2
0
a)
Archibaccharis asperifolia
Laestadia muscicola
Hinterhubera ericoides
Blakiella bartsiifolia
Lagenophora cuchumatanica
Piofontia colombiana
Piofontia inesiana
Piofontia coriacea
Piofontia romeroi
Piofontia glutinosa
Piofontia huertasii
Piofontia jaramilloi
Piofontia eriophora
Piofontia rupestris
Piofontia oblongifolia
Piofontia mutiscuana
Piofontia sp. nov. ANT
Piofontia antioquense
Piofontia ochracea
Piofontia tachirense
Piofontia camargoana
Piofontia jenesana
Piofontia tenuifolia
Piofontia frontinense
Piofontia rhododendroides
Piofontia juajibioyi
Piofontia schultzii CAL
Piofontia schultzii CUN
Piofontia apiculata
Piofontia rhomboidalis ECU
Piofontia rhomboidalis COL
Piofontia alveolata
Piofontia costaricense
Piofontia heterophylla
Piofontia floribunda
Piofontia rosmarinifolia
Piofontia phylicoidea
Piofontia lacunosa
Piofontia revoluta
Piofontia cayambense
Piofontia violacea
Piofontia cinerascens
Piofontia obtusa
Piofontia venezuelense
Exostigma notobellidiastrum
Aztecaster matudae
Westoniella kohkemperi
Laennecia sophiifolia
Diplostephium cinereum
Diplostephium sp. nov. CAJ2
Baccharis genistelloides
Heterothalamus alienus
Baccharis tricuneata
Parastrephia quadrangularis
Floscaldasia hypsophila
Diplostephium meyenii
Diplostephium azureum
Diplostephium serratifolium
Diplostephium cajamarquillense
Diplostephium jelskii
Diplostephium oblanceolatum
Diplostephium glandulosum
Diplostephium empetrifolium
Diplostephium spinulosum
Diplostephium juniperinum
Diplostephium crypteriophyllum
Diplostephium ericoides
Diplostephium hartwegii
Diplostephium espinosae
Diplostephium oxapampanum
Diplostephium sagasteguii
Diplostephium foliosissimum
Diplostephium barclayanum
Diplostephium sp. nov. JUN3
Diplostephium hippophae
Diplostephium gynoxyoides
Diplostephium sp. nov. JUN
Diplostephium gnidioides
Diplostephium sp. nov. CAJ
Diplostephium sp. nov. JUN2
Diplostephium pulchrum OXA
Diplostephium pulchrum PAS
Diplostephium sp. nov. JUN4
Diplostephium sp. nov. OXA
Diplostephium haenkei
Diplostephium lechleri
Diplostephium goodspeedii
Diplostephium callilepis
1
2
0.33
0.57
1.2
2.2
Speciation rate (species/Ma)
b)
All sampling
c)
Piofontia only
d)
Diplostephium only
Speciation rate
Time (mya)
e)
Pairwise probability
f)
Prior
Posterior
Probability
Number of shifts

Figure 3.8.

Figure 3.8. a) Model-averaged net speciation rates plotted on the phylogeny, red ovals indicate shifts of diversification. b) Speciation rates through time plotted on the phylogeny. c) Speciation rates through time in *Piofontia*. d) Speciation rates through time in *Diplostephium*. e) Macroevolutionary cohort matrix to compare the probability of lineages sharing diversification dynamics. f) Prior and posterior marginal probabilities of the number of shifts. Clades 1 and 2 indicate lineages nested within *Diplostephium* that contain taxa distributed in the Northern Andes.

SUPPLEMENTARY INFORMATION

Supplementary Information 3.1. Biogeographic matrix used for the analysis of the complete phylogeny:

```
88      5 (M T N C W)
Archibaccharis_asperifolia      11000
Aztecaster_matudae      10000
Baccharis_genistelloides        11111
Baccharis_tricuneata    11111
Blakiella_bartsiifolia  00100
Diplostephium_azureum           00010
Diplostephium_barclayanum       00100
Diplostephium_cajamarquillense          00010
Diplostephium_callilepis        00010
Diplostephium_cinereum          00010
Diplostephium_crypteriophyllum          00100
Diplostephium_empetrifolium             00100
Diplostephium_ericoides         00100
Diplostephium_espinosae         00100
Diplostephium_foliosissimum             00100
Diplostephium_glandulosum       00100
Diplostephium_gnidioides        00010
Diplostephium_goodspeedii       00010
Diplostephium_gynoxyoides       00010
Diplostephium_haenkei           00010
Diplostephium_hartwegii         00100
Diplostephium_hippophae         00010
Diplostephium_jelskii   00010
Diplostephium_juniperinum       00100
Diplostephium_lechleri          00010
Diplostephium_meyenii           00010
Diplostephium_oblanceolatum             00100
Diplostephium_oxapampanum               00010
Diplostephium_pulchrum_OXA              00010
Diplostephium_pulchrum_PAS              00010
Diplostephium_sagasteguii       00010
Diplostephium_serratifolium     00010
Diplostephium_sp._nov._CAJ              00010
Diplostephium_sp._nov._CAJ2             00010
Diplostephium_sp._nov._JUN              00010
Diplostephium_sp._nov._JUN2             00010
Diplostephium_sp._nov._JUN3             00010
```

Supplementary Information 3.1. (Continued)

Diplostephium_sp._nov._JUN4	00010
Diplostephium_sp._nov._OXA	00010
Diplostephium_spinulosum	00100
Exostigma_notobellidiastrum	00001
Floscaldasia_hypsophila	00100
Heterothalamus_alienus	00001
Hinterhubera_ericoides	00100
Laennecia_sophiifolia	11011
Laestadia_muscicola	00110
Lagenophora_cuchumatanica	11000
Parastrephia_quadrangularis	00010
Piofontia_alveolata	00100
Piofontia_antioquense	00100
Piofontia_apiculata	00100
Piofontia_camargoana	00100
Piofontia_cayambense	00100
Piofontia_cinerascens	00100
Piofontia_colombiana	00100
Piofontia_coriacea	00100
Piofontia_costaricense	01000
Piofontia_eriophora	00100
Piofontia_floribunda	00100
Piofontia_frontinense	00100
Piofontia_glutinosa	00100
Piofontia_heterophylla	00100
Piofontia_huertasii	00100
Piofontia_inesiana	00100
Piofontia_jaramilloi	00100
Piofontia_jenesana	00100
Piofontia_juajibioyi	00100
Piofontia_lacunosa	00100
Piofontia_mutiscuana	00100
Piofontia_oblongifolia	00100
Piofontia_obtusa	00100
Piofontia_ochracea	00100
Piofontia_phylicoidea	00100
Piofontia_revoluta	00100
Piofontia_rhododendroides	00100
Piofontia_rhomboidalis_COL	00100
Piofontia_rhomboidalis_ECU	00100
Piofontia_romeroi	00100
Piofontia_rosmarinifolia	00100

Supplementary Information 3.1. (Continued)

Piofontia_rupestris	00100
Piofontia_schultzii_CAL	00100
Piofontia_schultzii_CUN	00100
Piofontia_sp._nov._ANT	00100
Piofontia_tachirense	00100
Piofontia_tenuifolia	00100
Piofontia_venezuelense	00100
Piofontia_violacea	00100
Westoniella_kohkemperi	01000

Supplementary Information 3.2. Biogeographic matrix used for the analysis of *Piofontia*:

38 8 (N M T A E C W S)
Piofontia_alveolata 00001000
Piofontia_antioquense 00010000
Piofontia_apiculata 00001000
Piofontia_camargoana 00001000
Piofontia_cayambense 00001101
Piofontia_cinerascens 00011110
Piofontia_colombiana 00001000
Piofontia_coriacea 10000000
Piofontia_costaricense 00100000
Piofontia_eriophora 00010100
Piofontia_floribunda 00111111
Piofontia_frontinense 00010000
Piofontia_glutinosa 00001000
Piofontia_heterophylla 00001000
Piofontia_huertasii 00001100
Piofontia_inesiana 10000000
Piofontia_jaramilloi 00001000
Piofontia_jenesana 00001000
Piofontia_juajibioyi 00001000
Piofontia_lacunosa 00001000
Piofontia_mutiscuana 00001000
Piofontia_oblongifolia 00001000
Piofontia_obtusa 01000000
Piofontia_ochracea 00001000
Piofontia_phylicoidea 00001000
Piofontia_revoluta 00001100
Piofontia_rhododendroides 00000011
Piofontia_rhomboidalis_COL 00001000
Piofontia_rhomboidalis_ECU 00000001
Piofontia_romeroi 10000000
Piofontia_rosmarinifolia 10011110
Piofontia_rupestris 00011111
Piofontia_schultzii_CAL 00001111
Piofontia_sp._nov._ANT 00010000
Piofontia_tachirense 00001000
Piofontia_tenuifolia 00001000
Piofontia_venezuelense 01000000
Piofontia_violacea 00000100

Chapter 4: Ecological anatomy in high Andean woody daisies (Astereae: *Diplostephium*, *Piofontia*)

INTRODUCTION

The Andes Cordillera of South America is a hotspot of plant diversity in which many taxa have diversified during the last 10 Ma (Luebert & Weigend, 2014). Studies documenting plant diversity in the Andes have focused on elucidating the evolutionary history of these taxa by inferring phylogenies and identify key adaptions (or preadaptations) that could potentially enable such diversification events. However, the anatomical characteristics developed by high Andean taxa are still poorly known (Carlquist, 1994). Here we aim to document the stem and leaf anatomy of two genera in the Astereae that inhabit the high altitudes of the tropical Andes.

The Huancabamba depression, located close to the political border between Ecuador and Peru, divides the tropical Andes biogeographically (Weigend, 2002; Luebert & Weigend, 2014) and geologically (Gregory-Wodzicki, 2000). Within both regions there are climatic variations evidenced by the different habitats found at their high altitudes (>3000). While the páramo and the cloud forest dominate in the Northern Andes, the Central Andes are characterized by the puna steppe, the humid puna and cloud forest on the western slopes, and the desertic scrub across the feat altiplano and the eastern slopes. Thanks to the influence of the intertropical convergence of air masses (Sarmiento, 1986; Luteyn, 1999; Garreaud, 2009), most of the Northern Andes (northern Ecuador, Colombia, and Venezuela) are very humid, receiving precipitation throughout most of the year with many areas receiving more than 2,000 mm of rain yearly. Timberline, where cloud forest changes to páramo, varies from 3,000 to 3,500 m depending on slope, temperature, wind, and precipitation (van der Hammen & Cleef, 1986). A mosaic of ecosystems with a high to low east-to-west precipitation gradient

characterizes the Central Andes. The dry winds associated with the Humboldt Current are responsible for the desert landscapes of coastal Peru and the western slopes of the Central Andes, with most places receiving less than 50 mm of rain yearly (Walter *et al*., 1975; Sarmiento, 1986; Luteyn, 1999; Garreaud *et al*., 2009). On the other hand, the moist winds coming from the Amazon basin drop their humidity as they rise when hitting the eastern slopes of the Central Andes (Sarmiento, 1986; Garreaud, 2009) allowing cloud forest and humid puna to dominate with many locations receiving close to 1000 mm of rain yearly. Devoid of this moisture, the wind that blows across the high central plateau lead to the puna and desert scrub ecosystems that dominate the high altitude landscapes of the central Andes and its western slopes, respectively.

Diplostephium and *Piofontia,* both members of the tribe Astereae, are high-altitude genera with centers of diversification in the humid puna in the Central Andes and the páramo in the Northern Andes, respectively. In addition to the humid puna, some *Diplostephium* species inhabit the dry puna and the desert scrub of the Central Andes. *Piofontia*, with species mostly restricted to the páramo, contains a group of taxa that inhabit the cloud forest. Both genera are morphologically similar with their growth forms correlated their habitat. Species of *Diplostephium* and *Piofontia* with broad leaves and a height taller than 2 m inhabit the cloud forest at its upper limit. Contrastingly, shrubs and subshrubs with microphyllous leaves reside in open landscapes like the humid puna and the páramo.

Available anatomical studies on Andean taxa are sparse and focused only on their wood. The only high Andean shrubs for which some anatomical studies have been performed are *Loricaria thuyoides* (Lam.) Sch. Bip. (Carlquist, 1961), *Pentacalia rigidifolia* (V.M.Badillo) Cuatrec, and *Piofontia venezuelense* (Cuatrec.) O.M.Vargas (Rock, 1973). For *Loricaria thuyoides,* which inhabits the páramo, Carlquist (1961)

showed that most of its conducting elements are vasicentric tracheids, which are imperforate tracheary elements located throughout the entire radial section of the secondary xylem of a plant (Carlquist, 1985). Rock (1973) reported vascular tracheids for *Pentacalia rigidifolia* and *Piofontia venezuelese,* both páramo dwelling species. Vascular tracheids are imperforate elements only found at the ends of a growth ring (Carlquist, 1985). Vasicentric and vascular tracheids along with shrubby growth forms and microphyllous leaves are morpho-anatomical characteristics often associated with plants living in dry and semi-dry ecosystems (Carlquist, 1985; Micco & Aronne, 2012). Despite the high precipitation that characterizes the páramo, the presence of imperforate tracheary elements found in the Andean taxa mentioned are explained by the physiological stress induced by low temperature, frozen soil, wind, high radiation, and acid conditions (with high-water osmotic pressure) of the páramo (Carlquist, 1994; Luteyn, 1999; Leuschner, 2000). Because climatic variables fluctuate along the Andean landscape, it is expected that plant anatomical characteristics associated with water transport also change reflecting those climatic gradients.

Our main goal in this study was to document and compare the ecological anatomy of several woody species than inhabit different high Andean ecosystems. Specifically we wanted to identify wood and leaf anatomical adaptations that correlate with the páramo, humid puna, cloud forest, and desertic scrub.

MATERIAL AND METHODS

We collected eleven species of *Diplostephium* and *Piofontia* from four Andean ecosystems: páramo, humid puna, cloud forest, and desertic scrub (Table 4.1). At least two species were sampled from each habitat with the exception of desertic scrub for which only one species was sampled. When possible, and based on the phylogeny of

South American Astereae (Vargas & Simpson, in prep.), we tried to sample species from different lineages in both genera in order to minimize the effects of phylogenetic conservatism. We sampled one or two individuals per species. After collecting plant material in the field, we placed the samples in formalin acid-alcohol (FAA, Ruzin, 1999). We dehydrated our plant material using a standard tertiary butyl alcohol series, then cast the plant material using Paraplast Plus. We sectioned the cast samples in 12–20 μm sections using a rotary microtome. Finally, we stained the sections with a safranin–fast green combination following Mauseth *et al*. (1984). For each individual we produced several cross and longitudinal sections of twigs and leaves. We took several measurements for each species using light microscopy: vessel width (n=30), vessel element length (n=30), thickness of outer epidermis wall (as a range), and cuticle (as a range). We measured the leaf area of the *Diplostephium* species sampled following Vargas & Simpson (in prep.). We employed R to create boxplots of the data.

RESULTS

Pronounced or diffuse growth rings are evident in seven of the eleven species studied, of these, two, *Piofontia oblongifolia* and *P. jenesana,* show growth rings only in one of the individuals studied (Table 4.2). When rings are conspicuous, these are evident by a higher density of libriform fibers in the late wood and wider vessels in the early wood (Fig. 4.1a, 4.1c). Circular and scalariform wall pitting is present in the majority of the samples with the exception of *Diplostephium meyenii* and *P. tachirense* that have only circular wall pitting (Fig. 4.2a–4.2d). Vessels are mostly grouped, and in some cases they have a tendency to cluster radially. Vessel width varies strongly with the habitat of the sample (Table 4.2, Fig. 4.3a), *P. apiculata* presents the narrowest vessels with a mean diameter of 7.8 µm while *P. tachirense* has the widest vessels with an average diameter

30.5 μm. Vessel element length also ranges across species with *P. colombiana* having the shortest vessel elements with an average of 83.5 μm and *P. tachirense* having the longest with an average of 298.5 μm (Table 4.2, Fig, 4.3b). Perforation plates are always simple, and we found no evidence for the presence of vascular or vasicentric tracheids in the species studied. Libriform fibers are present in all the samples and they are arranged mostly in patches (as seen in a cross section). *Piofontia tachirense* and *P. eriophora* have an almost continuous matrix of libriform fibers, as seen in cross section, divided radially by the rays with the vessels scattered in the matrix. Libriform fibers have a thick wall of 2–8 μm with almost no lumen. For the species for which we obtained tangential wood sections, *D. callilepis, D. lechleri, D. meyenii,* and *P. floribunda,* we observed both uniseriate and multiseriate rays in each species (Fig. 4.2d). We identified upright, isodiametric, procumbent cells in the rays of most species (Fig. 4.2c). In most cases the wall of the radial parenchyma is lignified with the exception being *P. colombiana* that has particularly wide rays that are not lignified in the region close the vascular cambium (Fig. 4.1b). Paratracheal parenchyma in all the species studied is scanty and usually one cell thick.

Patches of phloem are divided (seen in cross section) by rays and are always capped or interleaved by patches of phloem fibers (Figs. 4.2e, 4.2f). Resin canals were observed only in the cortex of *P. floribunda*, but it is possible that in many cases they were not conspicuous or difficult to differentiate because in numerous sections the cortex was fragmented.

Leaves of *Piofontia* and *Diplostephium* vary according to habitat and growth form (Figs. 4.3b, 4.4). Species of small trees inhabiting the forest show a typical mesic leaf anatomy with a cuticle 1–4 um thick, a thin-walled epidermis, a palisade parenchyma of two layers of cells, a spongy parenchyma, and an abaxial epidermis with stomata. The

scandent *Piofontia tachirense* has a hypodermis interior to the adaxial epidermis in addition to the characteristics mentioned for forest-tree species (Fig. 4.4f). Species residing in the humid puna and the páramo have similar leaf anatomies with thick cuticles 4–16 μm and in some cases with thick epidermis walls (Figs. 4.3a–4.3c). *Diplostephium meyenii*, the only species sampled from the desert scrub has the thickest epidermis of the species studied with a wall 4–6 μm thick (Fig. 4.4d). We were not able to identify the cuticle for *D. meyenii* (Fig. 4.4d)*;* it is possible that the cuticle of this species is very thin or that the cuticle was dissolved in one of the steps during the sample preparation (although we were able to identify the cuticle for the remaining species). Glands and resin canals are found in leaves of many of the species studied (Table 4.2, Figs. 4.4d, 4.4f). Stomata are always located in the abaxial surface of the leaf and in some cases these are protruded. A layer of indumentum is present in most abaxial surfaces of the leaves completely covering the epidermis.

Our results show that vessel width (Fig. 4.3a), leaf area (Fig. 4.3b), and the thickness of the epidermis and/or the cuticle (Table 4.2) are related with the habitat in which the species studied is distributed.

DISCUSSION

Our stem and leaf anatomical sections show that species of different high elevation habitats of the Northern and Central Andes present different anatomical features. Páramo species (*P. apiculata, P. eriophora,* and *P. colombiana*) have the narrowest vessels of our samples and posses a thick leaf epidermis and/or cuticle. These anatomical characteristics in conjunction with small and revolute leaves are comparable to morpho-anatomical characteristics of low elevation dry and semi-dry ecosystems (Micco & Aronne, 2012; Carlquist, 2013). Narrow vessels mobilize smaller water

volumes and are more resistant to cavitation than wider vessels (Carlquist, 1975), while small leaf areas, thick epidermis walls, and thick cuticles decrease leaf transpiration (Micco & Aronne, 2012). Consequently, the anatomical characteristics of *Piofontia* páramo taxa are an evolutionary response to the physiological dryness of the páramo (Carlquist, 1994; Luteyn, 1999; Leuschner, 2000). Humid puna species (*P. callilepis* and *P. lechleri*) have characteristics similar to those of the páramo. Vessel width and leaf areas are small in humid puna species but they are slightly higher in comparison to páramo taxa. Humid puna species also have thick epidermal walls and cuticles along with revolute or semi-revolute leaves. Our results suggest that the humid puna habitat is similar to the páramo in the physiological challenges that it poses for plants. Continuous precipitation most of the year, and a daily temperature fluctuation of ~0ºC at night to a maximum of 30ºC each day all year characterize both the páramo and humid puna (Walter *et al*., 1975; Luteyn, 1999; Garreaud, 2009) and are responsible for the morpho-anatomical parallelism seen in the plants from these two ecosystems.

Considerable variation in vessel width is found in species from the forest (*P. camargoana, P. jenesana, P. oblongifolia*, and *P. tachirense*) and its upper boundary (*P. floribunda*). Upper montane forest species have wider vessels and larger leaf areas than those species inhabiting the páramo and the humid puna. Forest species also have a mesic leaf morphology with the exception being *P. floribunda,* which also inhabits the lower páramo (considered a "prepáramo species"), and *P. tachirense,* which is a species of the cloud forest understory. *Piofontia floribunda* has a thicker cuticle than the remaining forest species, and *P. tachirense* is the only species in which we found an adaxial leaf hypodermis (Fig. 4.4e). The mesic wood and leaf characteristics found in the forest species show that water stress decreases at lower elevations and that some species of *Piofontia* are adapted to the cloud forest environment. Our results also show that the

transition from páramo to cloud forest is not a strict one, the boxplots of vessel width and leaf area (Figs. 4.3a, 4.3b) vary accordingly with the landscape and there is not a clear gap in the distribution of the measurements between páramo and forest species. *Piofontia floribunda* represents a good example of this kind of variability because it has wood with characteristics similar to the forest species but leaf features similar to those in reported for páramo species (thick cuticle and small leaf area) reflecting its distribution at the transition between the cloud forest and the open páramo.

Diplostephium meyenii, the only desertic species sampled, has an average vessel width similar to the forest species. This similarity was unexpected taking into account that the water stress in the desert is stronger than in the páramo, humid puna, and forest, and thus we expected the wood of *D. meyenii* to be similar to that of the páramo and humid puna species. The vessel pattern of *D. meyenii* could be explained by the precipitation pattern of the desert scrub of the eastern Andean slopes with a strong unimodal patter of precipitation with rain only in January, February, and March (Walter *et al*., 1975). This climatic pattern is different from that of the páramo, the humid puna, and the forest, with a more or less constant precipitation for most of the year with no dry season or a dry season of a couple of months (Walter *et al*., 1975; Luteyn, 1999). *Diplostephium meyenii* is the only species of our sampling that exhibits well-defined growth rings, suggesting that growth in this species happens mostly during the three-month wet season. Consequently, the wide vessels seen in *D. meyenii* correspond to periods of rapid growth when water is available. In contrast to the vessel diameter, the leaves of *D. meyenii* are similar in anatomy to those of páramo and humid puna species: microphyllous, revolute, and linear, with a thick epidermis and thick outer cell walls.

Despite the fact that we only sampled a maximum of two individuals per species, we were able to find infraspecific variation regarding the presence of growth rings. As

mentioned before, the only species with strongly marked growth rings was *D. meyenii*. Some páramo and humid puna species have diffuse rings, and *P. oblongifolia* and *P. jenesana,* both cloud forest species, exhibit tenuous rings only in one of the individuals studied for each species. The presence of rings in those individuals that exhibit them in *P. oblongifolia* and *P. jenesana* can be explained by a well-drained soil (e.g., a sloped terrain) in which the dry season poses a mild water stress thus affecting plant growth. On the other hand, the absence of growth rings in the other two individuals of *P. oblongifolia* and *P. jenesana* can be a consequence of a humid terrain (e.g. a creek or a waterlogged area) that buffers the dry season and provides the plant with a continuous supply of water throughout the year. The variation of growth ring presence/absence in our samples reveals that rings are more common in habitats with long periods of water stress and that at least in the forest species mentioned the presence of rings are likely driven by the local climate fluctuations and soil conditions.

Taking into account that most species of *Diplostephium* and *Piofontia* inhabit the páramo and the humid puna, one can conclude that both genera are semi-xerophytic. This statement agrees with previous studies about the wood anatomy of Astereae (Carlquist, 1960) that suggested that taxa in the tribe have a preference for dry and semi-dry habitats. Carlquist (1960) also proposed that many characteristics of the wood of Astereae have evolved multiple times and therefore parallelism in wood features in the tribe is common. Our results support Carlquist's (1960) ideas because we show that species from different genera in Astereae present similar anatomical characteristics in similar habitats, the páramo and the humid puna. A habitat reconstruction performed for *Piofontia* (Vargas & Madriñán, 2012) suggested that the common ancestor of all *Piofontia* species was likely a bush that inhabited the tops of the northern Andean mountains before their final uplift (i.e. protopáramo *sensu* van der Hammen & Cleef, 1986), and that the cloud forest

species are a monophyletic group derived from a páramo ancestor. The character reconstruction of habitat along with the results found here, consequently suggest that there was one downslope event of colonization, which drove a morphological shift from a shrub (< 1m), with small leaves and narrow vessels, to a small tree (>3 m), with big leaves and wide vessels. This shift produced a clade in *Piofontia* of approximately 16 species than inhabits the upper limit of the cloud forest. *Piofontia floribunda* and *P. rosmarinifolia* (not included in this study), species that do not make part of the 16-species forest clade, dwell in the upper cloud forest and open páramo representing two additional independent cases of partial forest colonization. The evidence presented in this paper suggest that phylogenetic niche conservatism is a strong force in the evolution of anatomical characters in *Piofontia,* agreeing with a previous analysis on leaf shape on the genus (Vargas & Simpson, in prep.), and that ecological divergence happens gradually.

CONCLUSIONS

Our results show that species of the high Andes cordillera that occur in a mosaic of different habitats have anatomical differences that reflect varying physiological demands. Humid puna and páramo taxa exhibit similar stem and leaf characteristics associated with constant physiological semi-dry climate regimes. Forest species exhibit mesic anatomical features facilitated by the lower water stress of lower altitudes. *Diplostephium meyenii*, the only species sampled from the Andean desert, has obvious growth rings that, coupled with climatic data, suggest a seasonal growth period of three months a year. Finally, our correlation analysis reveals that in mountain tropical ecosystems with almost continuous precipitation throughout the year it is possible to predict the leaf area of a shrub or a tree by measuring the width of its vessels. Although this correlation could seem intuitive, our study is to our knowledge, the first to prove

such relation. We demonstrate that the combination of stem and leaf characteristics provides valuable information about the evolutionary tendencies in the anatomy and morphology of vascular plants.

TABLES

Table 4.1. Species studied and their vouchers organized by the habitat were they are found. The first author (OMV) collected all the specimens. ANDES = Herbarium Andes, University of the Andes, Colombia, HUSA = Herbarium Areqvipense, Universidad Nacional de San Agustín de Arequipa, Peru.

Habitat	Taxon	Country	Alt. (m)	Voucher
Páramo	*Piofontia apiculata* (S.F.Blake) O.M.Vargas	Colombia	3814	331, 333, ANDES
	Piofontia colombiana Cuatrec.	Colombia	3900	300, ANDES
	Piofontia eriophora (Wedd.) O.M.Vargas	Colombia	4151, 4376	505, 507, ANDES
Humid puna	*Diplostephium callilepis* S.F.Blake	Peru	3656	375, 376, HUSA
	Diplostephium lechleri (Sch.Bip.) Wedd.	Peru	3670	381, 382, HUSA
(Prepáramo)	*Piofontia floribunda* (Benth.) O.M.Vargas	Colombia	3344, 3692	338, 442, ANDES
Forest	*Piofontia camargoana* (Cuatrec.) O.M.Vargas	Colombia	3476	320, ANDES
	Piofontia oblongifolia (Cuatrec.) O.M.Vargas	Colombia	2668, 3169	344, 345, ANDES
	Piofontia jenesana (Cuatrec.) O.M.Vargas	Colombia	3060, 3230	501, 509, ANDES
	Piofontia tachirense (V.M.Badillo) O.M.Vargas	Colombia	2695	336, 337, ANDES
Desert scrub	*Diplostephium meyenii* Wedd.	Peru	2913, 3489	351, 354, HUSA

Table 4.2. Anatomical characteristics found in the wood and leaf anatomy of the species studied. E = ecosystem. P = páramo. HP = humid puna. PP = prepáramo. F = forest. D= desert scrub. VW = average vessel width (n = 30). VL = average vessel element length (n = 30). FW = libriform fiber wall (n=10). EW = epidermis wall (10 measurements). C = cuticle (10 measurements). All measurements are in μm. Standard deviations (SD) are indicated under averages.

E	Species	Xylem	VW	VL	FW	Leaf	EW	C
P	*Piofontia apiculata*	Growth rings are diffuse. Vessels are arranged in groups of three or more. Irregular growth rings are conspicuous by a higher density of libriform fibers, a lower density if vessels, and narrower vessels in late wood. Wall pitting is circular and scalariform.	7.8 SD= 2.3	124.3 SD= 15.1	2–4	Resin canals located underneath vascular bundles. The spongy parenchyma is tightly packed in when compared to forest species of *Piofontia.* Stomata are somewhat protruded.	<2	14–16
P	*Piofontia colombiana*	No growth rings are evident. Vessels are numerous and with a tendency to group radially. Wall pitting is scalariform and circular.	11.1 SD= 3.5	83.5 SD= 17.0	2–4	Palisade parenchyma is comprised of one to three rows of cells, intercellular space is evident in the palisade parenchyma. The spongy parenchyma has less intercellular space in comparison with the palisade parenchyma. A resin canal is located under the main vascular bundle. Stomata are protruded from the abaxial leaf surface.	16–24	8–10
P	*Piofontia eriophora*	Growth rings are diffuse. Vessels are usually arranged in groups of five or more with a tendency to group radially. Rings are suggested by a higher density of libriform fibers, a lower density of vessels, and narrower vessels in late wood. Wall pitting is circular and scalariform	8.9 SD= 4.4	151.9 SD= 37.3	4–6	Palisade parenchyma is comprised of one or two rows of cells. Resin canals are positioned underneath the vascular bundles.	<2	8–10

Table 4.2. (Continued)

HP	*Diplostephium callilepis*	Growth rings are diffuse. Vessels are arranged in groups of three or more, in some areas vessels form an almost continuous matrix interleaved by rays and patches of libriform fibers. Rings are conspicuous by bigger patches of libriform fibers and a lower density of vessels. Wall pitting is circular and scalariform.	11.5 SD= 2.4	232.9 SD= 39.0	2–8	The palisade parenchyma is comprised of two rows of cells. Stomata protruded. Resin canals located underneath vascular bundles.	~2	8–10
HP	*Diplostephium lechleri*	Diffuse growth rings are present. Vessels are arranged in groups of three or more, sometimes they are found solitary. Rings are conspicuous by a higher density of libriform fibers, a lower number of vessels, and narrower vessels in late wood. Perforations are simple. Wall pitting is circular and scalariform.	16 SD= 4.9	179.3 SD= 50.5	2–4	The palisade parenchyma is comprised mostly of two rows of cells but in some areas of the leaf it comprises three rows. Stomata are protruded. Resin canals located underneath vascular bundles.	~2	4–8
PP	*Piofontia floribunda*	No growth rings are evident. Vessels are arranged in groups of three or more with a tendency to group radially. Wall pitting is scalariform and circular.	19.0 SD= 7.3	139.5 SD= 48.9	2–4	Palisade parenchyma is mostly comprised of two rows of cells but some portions of the leaf present three rows. Resin canals are positioned underneath the vascular bundles.	<2	8–20
F	*Piofontia camargoana*	Growth rings not conspicuous. Vessels are mostly arranged in groups of five or more, sometimes solitary. Wall pitting is circular and scalariform.	18.7 SD= 9.3	223.6 SD= 37.7	6–8	The palisade parenchyma is comprised of two rows of cells. Resin canals located underneath vascular bundles.	< 2	~ 2

Table 4.2. (Continued)

F	*Piofontia jenesana*	Growth rings are evident in one of the two specimens studied. Vessels are arranged in groups of five or more. Rings are conspicuous by narrower vessels in late wood. Wall pitting is circular and scalariform.	26.5 SD= 10.7	196.1 SD= 37.9	2–8	The palisade parenchyma is comprised of two rows of cells. Resin canal present under the main central vein. Stomata are tenuously protruded from the lower epidermis.	<2	2–4
F	*Piofontia oblongifolia*	Growth rings evident in one of two specimens studied. Vessels are arranged in groups of five or more, many aggrupations are radial. Rings are conspicuous by the lower density and width of vessels in late wood. Wall pitting is circular and scalariform.	26.8 SD= 9.57	192.6 SD= 52.0	2–6	The palisade parenchyma is comprised of two rows of cells. Resin canals located underneath vascular bundles.	< 2	< 2
F	*Piofontia tachirense*	No growth rings are evident. Vessels solitary or arranged in radial groups of 3–8 vessels. Wall pitting is circular.	30.5 SD= 30.5	298.5 SD= 298.5	4–6	Hypodermis present. The palisade parenchyma is comprised of two rows of cells. Resin canals located underneath vascular bundles.	< 2	~ 2
D	*Diplostephium meyenii*	Growth rings are evident. Vessels are mostly grouped radially. Rings are conspicuous because by a higher density of libriform fibers, a lower density of vessels, and narrower vessels in late wood. Wall pitting is circular.	20.1 SD= 8.24	142.1 SD= 24.6	2–6	The palisade parenchyma is comprised of one layer of cells. Epidermis wall and cuticle difficult to distinguish. Resin canals located underneath vascular bundles.	4–6	< 2

FIGURES

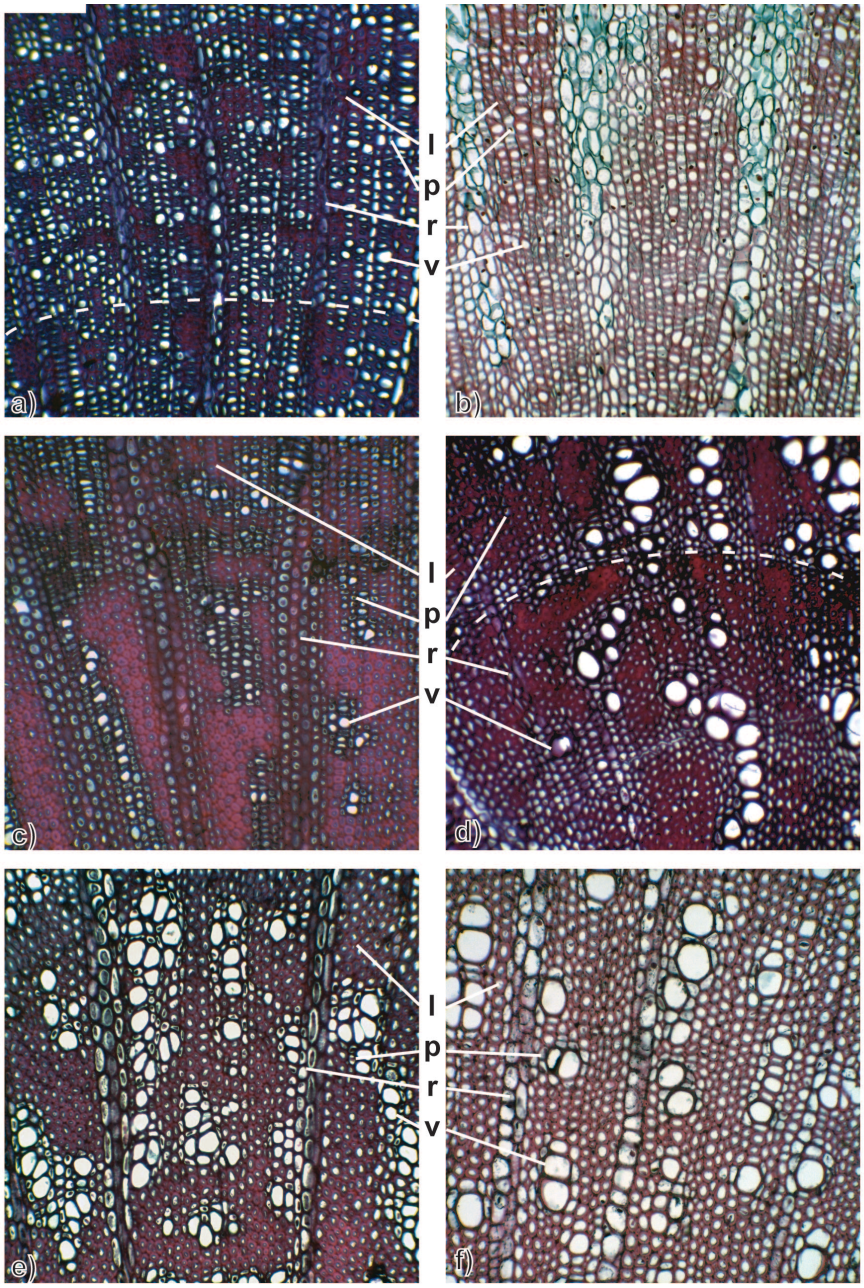

Figure 4.1. Wood cross sections. a) *Piofontia apiculata*. b) *Piofontia colombiana*. c) *Diplostephium callilepis*. d) *Diplostephium meyenii*. e) *Piofontia floribunda*. f) *Piofontia oblongifolia*. All images have the same magnification, scale = 100 um. l = libriform fibers, p = paratracheal parenchyma, r = ray, v = vessel. Dashed lines indicate growth rings.

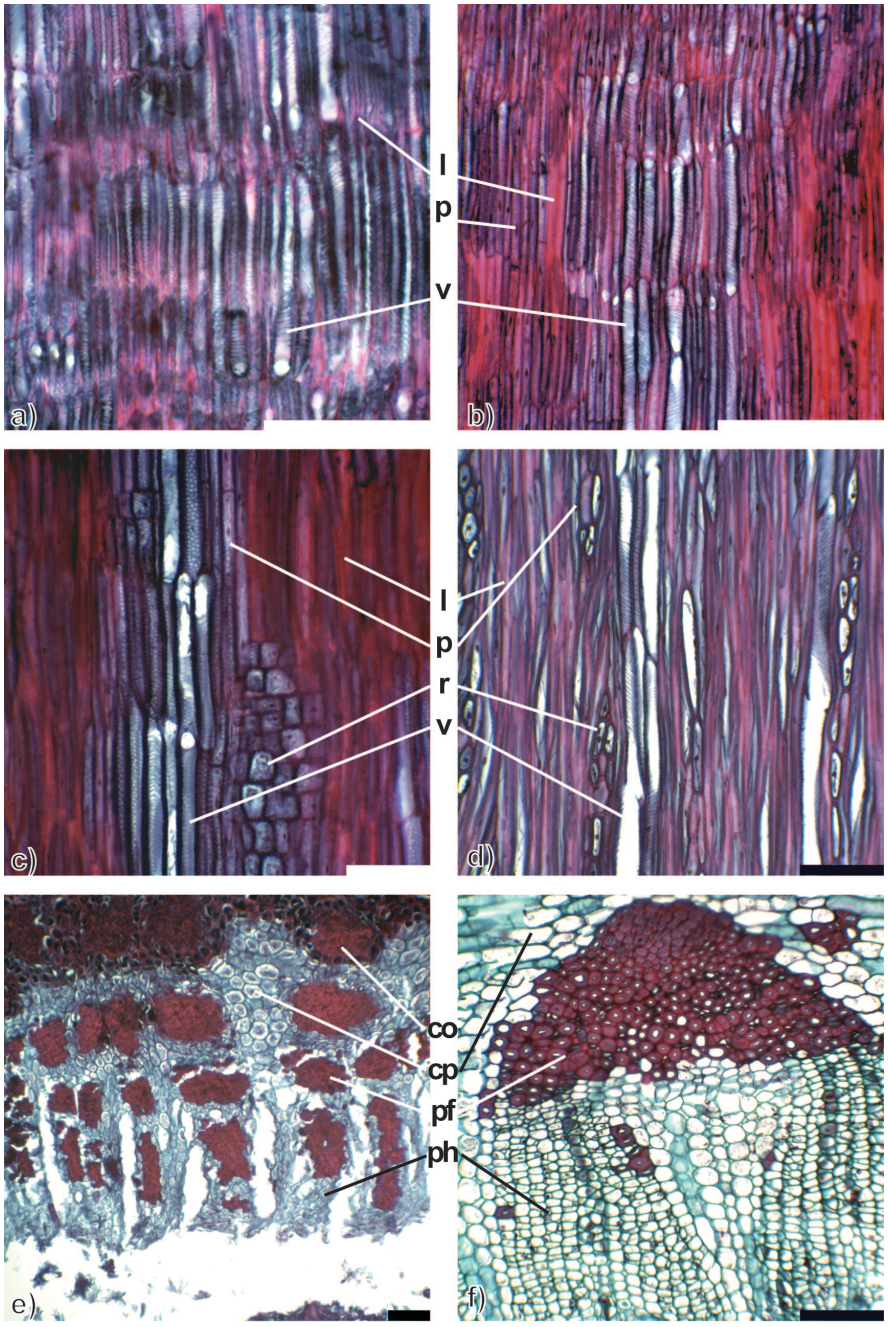

Figure 4.2. Anatomical characteristics of the wood. Radial sections of a) *Piofontia apiculata*, b) *Diplostephium callilepis*, c) *Piofontia oblongifolia*. b) Tangential section of *Diplostephium lechleri*. Phloem and phloem fibers in e) *Piofontia apiculata,* f) Piofontia camargoana. Scale = 100 um. co = cork, cp = cortical parenchyma, l = libriform fibers, p = paratracheal parenchyma, pf = phloem fiber, ph = phloem, r = ray, v = vessel.

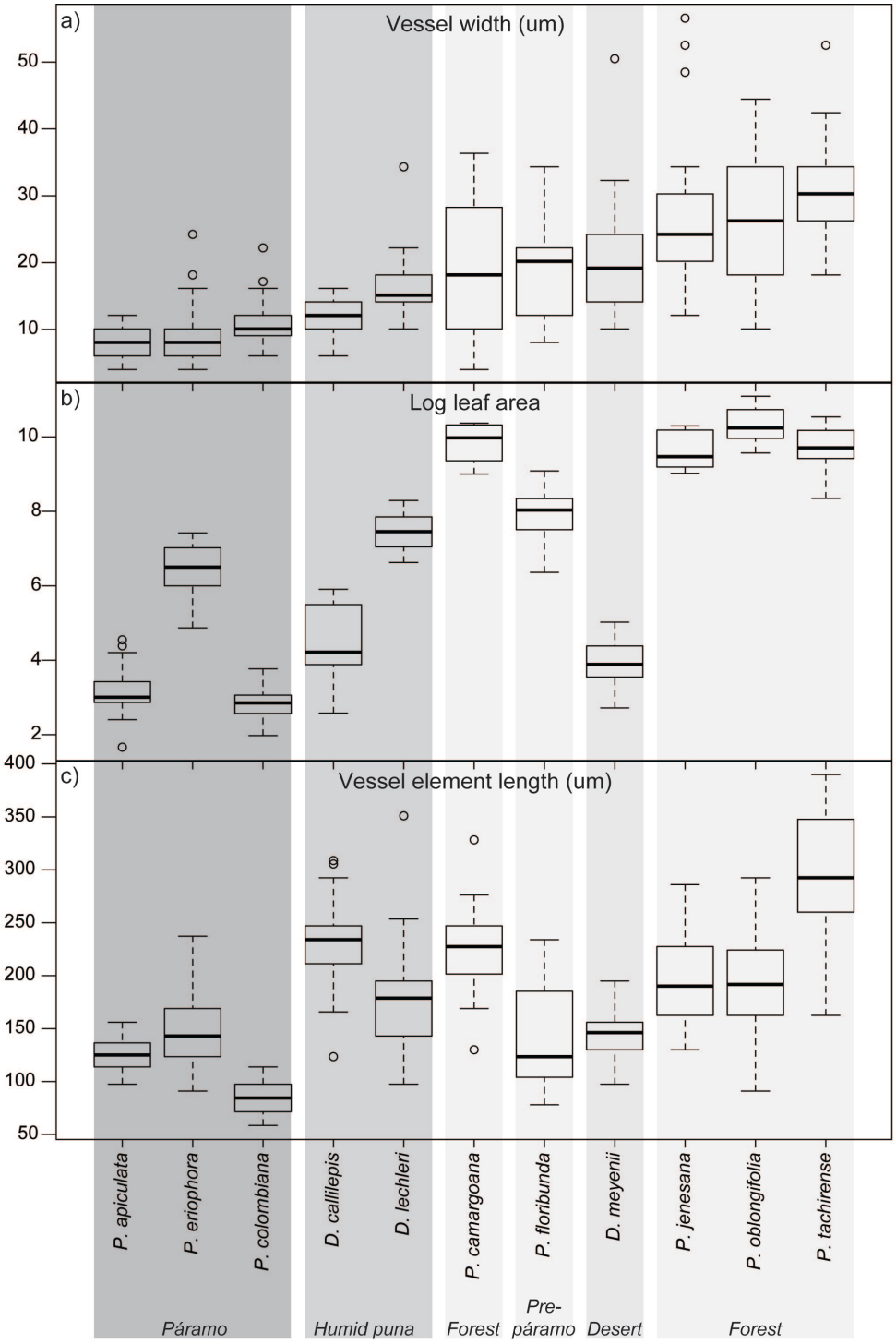

Figure 4.3. Boxplots of a) vessels width, b) log leaf area, and c) vessel element length organized by vessel width.

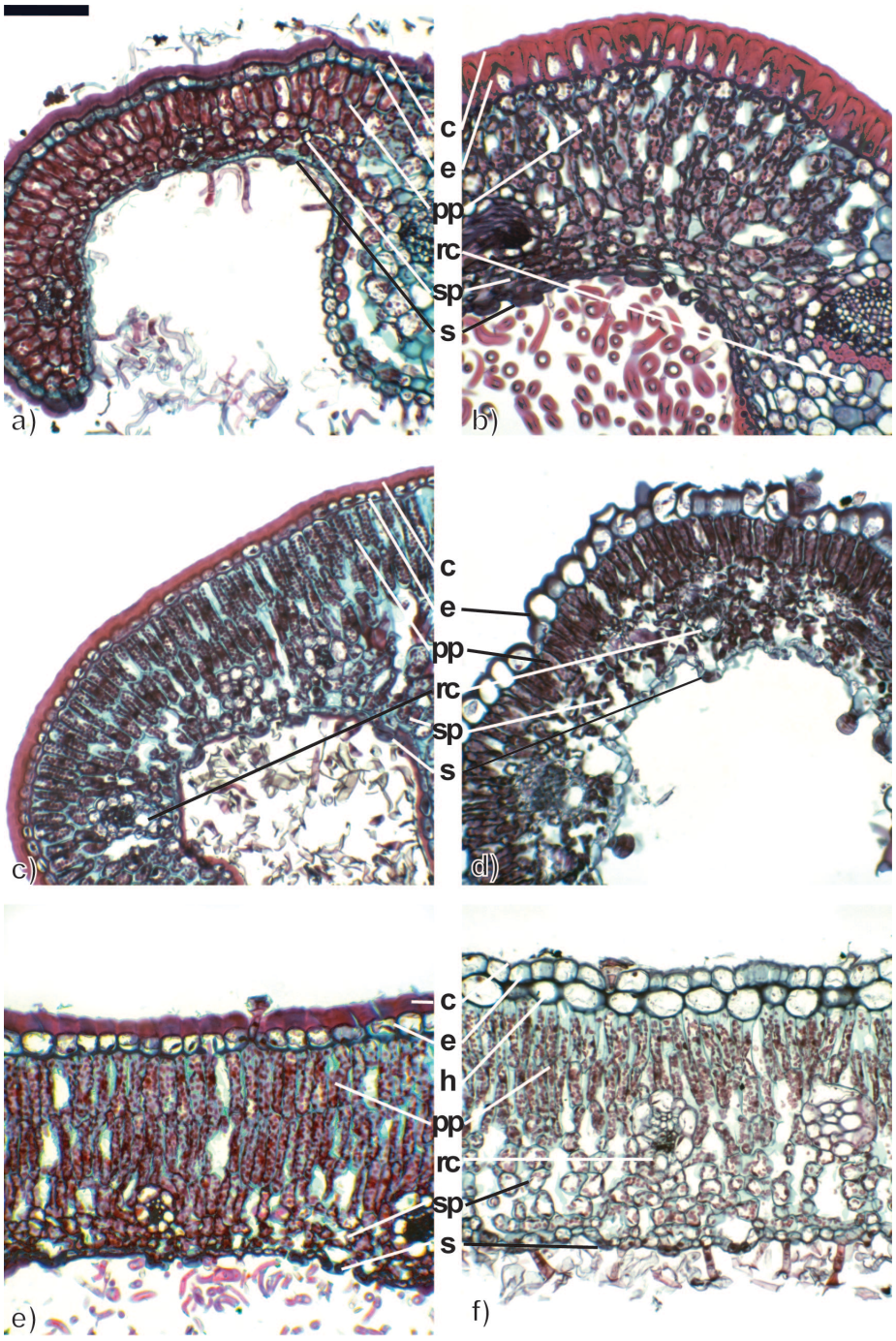

Figure 4.4. Leaf cross sections. a) *Piofontia apiculata*. b) *Piofontia colombiana*. c) *Diplostephium callilepis*. d) *Diplostephium meyenii*. e) *Piofontia floribunda*. f) *Piofontia tachirense*. All images have the same magnification, scale = 100 um. c = cuticle, e = epidermis, h = hypodermis, pp = palisade parenchyma, rc = resin canal, sp = spongy parenchyma, s = stomata.

Bibliography

Albert TJ, Molla MN, Muzny DM, Nazareth L, Wheeler D, Song X, Richmond TA, Middle CM, Rodesch MJ, Packard CJ, Weinstock GM, Gibbs RA. 2007. Direct selection of human genomic loci by microarray hybridization. *Nature Methods* 4: 903–905.

Álvarez I, Wendel JF. 2003. Ribosomal ITS sequences and plant phylogenetic inference. *Molecular Phylogenetics and Evolution* 29: 417–434.

Alverson AJ, Rice DW, Dickinson S, Barry K, Palmer JD. 2011. Origins and recombination of the bacterial-sized multichromosomal mitochondrial genome of cucumber. *The Plant cell* 23: 2499–2513.

Alverson AJ, Wei X, Rice DW, Stern DB, Barry K, Palmer JD. 2010. Insights into the evolution of mitochondrial genome size from complete sequences of *Citrullus lanatus* and *Cucurbita pepo* (Cucurbitaceae). *Molecular Biology and Evolution* 27: 1436–1448.

Alves RJV, Silva NG, Oliveira JA, Medeiros D. 2014. Circumscribing campo rupestre–megadiverse Brazilian rocky montane savanas. *Brazilian Journal of Biology* 74: 355–362.

Ambrose CD, Crease TJ. 2011. Evolution of the nuclear ribosomal DNA intergenic spacer in four species of the *Daphnia pulex* complex. *BMC genetics* 12: 13.

Amenta N, Klingner J. 2002. Case study: visualizing sets of evolutionary trees. *8th IEEE Symposium on Information Visualization* 2002: 71–74.

Andrews S. 2010. *FastQC: A quality control tool for high throughput sequence data*. [WWW document] URL http://www.bioinformatics.babraham.ac.uk/projects/fastqc/.

Bankevich A, Nurk S, Antipov D, Gurevich A a., Dvorkin M, Kulikov AS, Lesin VM, Nikolenko SI, Pham S, Prjibelski AD, *et al*. 2012. SPAdes: A New Genome Assembly Algorithm and Its Applications to Single-Cell Sequencing. *Journal of Computational Biology* 19: 455–477.

Barthlott W, Kauer W, Placke A. 1996. Global distribution of species diversity in vascular plants: towards a world map of phytodiversity. *Erdkunde* 50: 317–327.

Becker HF. 1969. Fossil plants of the Tertiary Beaverhead Basins in Southwestern Montana. *Palaeontographica Abteilung B* 127: 1–142.

Bell CD, Donoghue MJ. 2005. Phylogeny and biogeography of Valerianaceae (Dipsacales) with special reference to the South American valerians. *Organisms Diversity and Evolution* 5: 147–159.

Bergh NG, Linder PH. 2009. Cape diversification and repeated out-of-southern-Africa dispersal in paper daisies (Asteraceae-Gnaphalieae). *Molecular Phylogenetics and Evolution* 51: 5–18.

Biomatters. 2014. *Geneious v.7.1.4*. [WWW document] URL http://www.geneious.com/.

Birky CW. 1995. Uniparental inheritance of mitochondrial and chloroplast genes: mechanisms and evolution. *Proceedings of the National Academy of Sciences of the United States of America, USA* 92: 11331–11338.

Blake SF. 1922. Key to the genus *Diplostephium*, with descriptions of new species. *Contributions from the United States National Herbarium* 24: 65–86.

Blake SF. 1928. Review of the genus *Diplostephium*. *American Journal of Botany* 15: 43–64.

Blomberg SP, Garland T, Ives AR. 2003. Testing for phylogenetic signal in comparative data: behavioral traits are more labile. *Evolution* 57: 717–745.

Bock DG, Kane NC, Ebert DP, Rieseberg LH. 2014. Genome skimming reveals the origin of the Jerusalem Artichoke tuber crop species: Neither from Jerusalem nor an artichoke. *New Phytologist* 201: 1021–1030.

Boisvert S, Raymond F, Godzaridis E, Laviolette F, Corbeil J. 2012. Ray Meta: scalable de novo metagenome assembly and profiling. *Genome Biology* 13: R122.

Bonhomme V, Picq S, Gaucherel C, Claude J. 2014. Momocs: Outline Analysis Using R. *Journal of Statistical Software* 56: 1–24.

Brouillet L, Lowrey TK, Urbatsch LE, Karaman-Castro V, Sancho G, Wagstaff SJ, Semple JC. 2009. Astereae. In: Funk VA, Stuessy T, Bayer R, eds. *Systematics, Evolution and Biogeography of Compositae*. Vienna, Austria: International Association of Plant Taxonomists, 589–629.

Cabrera AL. 1966. The genus *Lagenophora* (Compositae). *Blumea* 14: 3–308.

Carlquist S. 1960. Wood Anatomy of Astereae (Compositae). *Tropical Woods* 113: 54–84.

Carlquist S. 1961. Wood anatomy of Inuleae (Compositae). *Aliso* 5: 21–37.

Carlquist S. 1975. *Ecological strategies of xylem evolution*. Berkley and Los Angeles, California: University of California Press.

Carlquist S. 1985. Vasicentric tracheids as a drought survival mechanism in the woody flora of southern California and similar regions. *Aliso* 11: 37–68.

Carlquist S. 1994. Anatomy of tropical alpine plants. In: Rundel P, Smith A, Meinzer F, eds. *Tropical alpine environments: plant form and function*. Cambridge, UK: Cambridge University Press, 111–128.

Carlquist S. 2013. *Comparative wood anatomy: systematic, ecological, and evolutionary aspects of dicotyledon wood*. Berlin Heidelberg: Springer-Verlag.

Catchen JM, Amores A, Hohenlohe P, Cresko W, Postlethwait JH. 2011. Stacks: building and genotyping loci de novo from short-read sequences. *G3 (Bethesda, Md.)* 1: 171–82.

Chikhi R, Medvedev P. 2014. Informed and automated k-mer size selection for genome assembly. *Bioinformatics (Oxford, England)* 30: 31–7.

Cuatrecasas J. 1943a. Estudios sobre plantas andinas IV. *Caldasia* 2: 5–9

Cuatrecasas J. 1943b. Estudios sobre plantas andinas V. *Caldasia* 2: 209–240.

Cuatrecasas J. 1953. Neue und bemerkenswerte andine Compositen. *Repertorium novarum specierum regni vegetabilis* 55:120–153.

Cuatrecasas J. 1968. Páramo vegetation and its life forms. *Colloquium Geographicum* 9: 163–186.

Cuatrecasas J. 1969. Prima Flora Colombiana. 3. Compositae-Astereae. *Webbia* 24: 1–335.

Cuatrecasas J. 1977. *Westoniella*, a new genus of the Astereae from the Costa Rican páramos. *Phytologia* 35: 471–487.

Cuatrecasas J. 1986. Speciation and radiation of the Speletiinae in the Andes. In: Vuilleumier F, Monasterio M, eds. *High Altitude Tropical Biogeography*. New York, USA: Oxford University Press, 267–303.

Darriba D, Taboada GL, Doallo R, Posada D. 2012. jModelTest 2: more models, new heuristics and parallel computing. *Nature Methods* 9: 772–772.

Davidson R, Vachaspati P, Mirarab S, Warnow T. 2015. Phylogenomic species tree estimation in the presence of incomplete lineage sorting and horizontal gene transfer. *BMC Genomics* 16: S1.

Doolittle WF. 1999. Phylogenetic classification and the universal tree. *Science (New York, N.Y.)* 284: 2124–2129.

Drummond AJ, Suchard MA, Xie D, Rambaut A. 2012a. Bayesian phylogenetics with BEAUti and the BEAST 1.7. *Molecular Biology and Evolution* 29: 1969–1973.

Drummond CS, Eastwood RJ, Miotto STS, Hughes CE. 2012b. Multiple Continental Radiations and Correlates of Diversification in *Lupinus* (Leguminosae): testing for Key Innovation with Incomplete Taxon Sampling. *Systematic Biology* 61: 443–460.

Ehlers TA., Poulsen CJ. 2009. Influence of Andean uplift on climate and paleoaltimetry estimates. *Earth and Planetary Science Letters* 281: 238–248.

Emshwiller E. 2002. Biogeography of the *Oxalis tuberosa* alliance. *The Botanical Review* 68: 128–152.

Fan Y, Wu R, Chen MH, Kuo L, Lewis PO. 2011. Choosing among partition models in Bayesian phylogenetics. *Molecular Biology and Evolution* 28: 523–532.

Garreaud RD, Vuille M, Compagnucci R, Marengo J. 2009. Present-day South American climate. *Palaeogeography, Palaeoclimatology, Palaeoecology* 281: 180–195.

Garreaud RD. 2009. The Andes climate and weather. *Advances in Geosciences* 22: 3–11.

Garzione CN, Auerbach DJ, Jin-Sook Smith J, Rosario JJ, Passey BH, Jordan TE, Eiler JM. 2014. Clumped isotope evidence for diachronous surface cooling of the Altiplano and pulsed surface uplift of the Central Andes. *Earth and Planetary Science Letters* 393: 173–181.

Givnish TJ. 1987. Comparative studies of leaf form: assessing the relative roles of selective pressures and phylogenetic constraints. *New Phytologist* 106: 131–160.

Givnish TJ. 1997. Adaptive radiation and molecular systematics: aims and conceptual issues. In: Givnish TJ, Systma KJ, eds. *Molecular evolution and adaptive radiation*. New York, USA: Cambridge University Press, 1–54.

Givnish TJ. 2015. Adaptive radiation versus 'radiation' and 'explosive diversification': why conceptual distinctions are fundamental to understanding evolution. *New Phytologist* 207: 297–303.

Gnirke A, Melnikov A, Maguire J, Rogov P, LeProust EM, Brockman W, Fennell T, Giannoukos G, Fisher S, Russ C, *et al*. 2009. Solution hybrid selection with ultra-long oligonucleotides for massively parallel targeted sequencing. *Nature biotechnology* 27: 182–9.

Graham A. 1994. A contribution to the geologic history of the Compositae. Compositae: systematics. Proceedings of the international Compositae conference, Kew: 123–140.

Gregory-Wodzicki KM. 2000. Uplift history of the Central and Northern Andes : a review. *Geological Society of America Bulletin*.

Guindon S, Gascuel O. 2003. A simple, fast, and accurate algorithm to estimate large phylogenies by maximum likelihood. *Systematic Biology* 52: 696–704.

Hardig TM, Soltis PS, Soltis DE. 2000. Diversification of the North American shrub genus *Ceanothus* (Rhamnaceae): Conflicting phylogenies from nuclear ribosomal DNA and chloroplast DNA. *American Journal of Botany* 87: 108–123.

Haywood AM, Valdes PJ, Sellwood BW. 2000. Global scale palaeoclimate reconstruction of the middle Pliocene climate using the UKMO GCM: Initial results. *Global and Planetary Change* 25: 239–256.

Heled J, Drummond AJ. 2010. Bayesian inference of species trees from multilocus data. *Molecular Biology and Evolution* 27: 570–580.

Hieronymus G. 1894. Plantae Lehmannianae in Columbia et Ecuador collectae additis quibusdam ab aliis collectoribus ex iisdem regionibus allatis determinatae et descriptae. Compositae. *Botanische Jahrbücher fur Systematik, Pflanzengeschichte und Pflanzengeographie* 19: 43–75.

Hieronymus G. 1896. Plantae Stubelianae novae. *Botanische Jahrbücher fur Systematik, Pflanzengeschichte und Pflanzengeographie* 21: 306–378.

Hieronymus G. 1901 [publ. May 1900]. Aloysius Sodiro, S. J.: Plantae ecuadorenses. II. Compositae. *Botanische Jahrbücher fur Systematik, Pflanzengeschichte und Pflanzengeographie* 29: 1–85.

Hieronymus G. 1905. Plantae peruvianae a claro Constantino de Jelski collectae. Compositae, quas determinavit et descripsit. *Botanische Jahrbücher fur Systematik, Pflanzengeschichte und Pflanzengeographie* 36: 458–513.

Hopkins R. 2013. Reinforcement in plants. *New Phytologist* 197: 1095–1103.

Huelsenbeck JP, Larget B, Alfaro ME. 2004. Bayesian phylogenetic model selection using reversible jump Markov chain Monte Carlo. *Molecular Biology and Evolution* 21: 1123–1133.

Hughes CE, Atchison GW. 2015. The ubiquity of alpine plant radiations: from the Andes to the Hengduan Mountains. *New Phytologist* 207: 275–282.

Hughes CE, Eastwood R. 2006. Island radiation on a continental scale: exceptional rates of plant diversification after uplift of the Andes. *Proceedings of the National Academy of Sciences, USA* 103: 10334–10339.

Hughes KW, Petersen RH. 2001. Apparent recombination or gene conversion in the ribosomal ITS region of a *Flammulina* (Fungi, Agaricales) hybrid. *Molecular Biology and Evolution* 18: 94–96.

Hurvich CM, Tsai C. 1989. Regression and time series model selection in small samples. *Biometrika* 76: 297–307.

Huson DH, Bryant D. 2006. Application of phylogenetic networks in evolutionary studies. *Molecular Biology and Evolution* 23: 254–267.

Jackson JD. 1975. A revision of *Archibaccharis* Heerin. (Compositae - Astereae). *Phytologia* 32: 81–194.

Jansen RK, Ruhlman TA. 2012. Plastid genomes of seed plants. In: Bock R, Knoop V, eds. *Genomics of Chloroplasts and Mitochondria, Advances in Photosynthesis and Respiration*. Dordrecht: Springer Netherlands, 103–126.

Joly S, McLenachan PA, Lockhart PJ. 2009. A statistical approach for distinguishing hybridization and incomplete lineage sorting. *The American Naturalist* 174: E54–E70.

Karaman-Castro V, Urbatsch LE. 2009. Phylogeny of *Hinterhubera* group and related genera (Hinterhuberinae: Astereae) based on the nrDNA ITS and ETS sequences. *Systematic Botany* 34: 805–817.

Katoh K, Misawa K, Kuma K, Miyata T. 2002. MAFFT: a novel method for rapid multiple sequence alignment based on fast Fourier transform. *Nucleic Acids Research* 30: 3059–3066.

Kim KJ, Choi KS, Jansen RK. 2005. Two chloroplast DNA inversions originated simultaneously during the early evolution of the sunflower family (Asteraceae). *Molecular Biology and Evolution* 22: 1783–1792.

Kunth KS. 1820. *Diplostephium*. In: Humboldt A, Bonpland AJ, Kunth KS, eds. *Nova Genera et Species Plantarum* 4. Paris: Lutetiae Parisiorum, 96–97

Lagomarsino LP, Condamine FL, Antonelli A, Mulch A, Davis CC. 2016. The abiotic and biotic drivers of rapid diversification in Andean bellflowers (Campanulaceae). *New Phytologist* 210: 1430–1442.

Landis MJ, Matzke NJ, Moore BR, Huelsenbeck JP. 2013. Bayesian analysis of biogeography when the number of areas is large. *Systematic Biology* 62: 789–804.

Langmead B, Salzberg S. 2012. Fast gapped-read alignment with Bowtie 2. *Nature Methods* 9: 357–359.

Leigh JW, Susko E, Baumgartner M, Roger AJ. 2008. Testing congruence in phylogenomic analysis. *Systematic Biology* 57: 104–115.

Leuschner C. 2000. Are high elevations in tropical mountains arid environments for plants? *Ecology* 81: 1425–1436.

Linder CR, Goertzen LR, Heuvel B V, Francisco-Ortega J, Jansen RK. 2000. The complete external transcribed spacer of 18S-26S rDNA: amplification and phylogenetic utility at low taxonomic levels in Asteraceae and closely allied families. *Molecular Phylogenetics and Evolution* 14: 285–303.

Liu L, Yu L, Edwards SV. 2010. A maximum pseudo-likelihood approach for estimating species trees under the coalescent model. *BMC Evolutionary Biology* 10: 302.

Londoño C, Cleef A, Madriñán S. 2014. Angiosperm flora and biogeography of the páramo region of Colombia, Northern Andes. *Flora - Morphology, Distribution, Functional Ecology of Plants* 209: 81–87.

Löwenberg-Neto P. 2014. Neotropical region: A shapefile of Morrone's (2014) biogeographical regionalisation. *Zootaxa* 3802: 300.

Luebert F, Plisscoff P. 2006. *Sinopsis bioclimática y vegetacional de Chile*. Santiago de Chile: Editorial Universitaria.

Luebert F, Weigend M. 2014. Phylogenetic insights into Andean plant diversification. *Frontiers in Ecology and Evolution* 2: 1–17.

Luteyn JL, Ortiz EM. 2008. Revision of *Siphonandra* (Ericaceae: Vaccinieae), a genus endemic to Peru and Bolivia. *Journal of the Botanical Research Institute of Texas* 2: 249–261.

Luteyn JL. 1992. Páramos: why study them. In: Luteyn JL, In: Baslev H, eds. Paramo: an Andean ecosystem under human influence. London, UK, 1–14.

Luteyn JL. 1999. *Páramos: a checklist of plant diversity, geographical distribution, and botanical literature*. New York, USA: The New York Botanical Garden.

Ma PF, Zhang YX, Zeng CX, Guo ZH, Li DZ. 2014. Chloroplast phylogenomic analyses resolve deep-level relationships of an intractable bamboo tribe Arundinarieae (Poaceae). *Systematic Biology* 63: 933–950.

Maddison WP, Maddison D.R. 2015. *Mesquite: a modular system for evolutionary analysis*. Version 3.04. [WWW document] URL http://mesquiteproject.org.

Madriñán S, Cortés AJ, Richardson JE. 2013. Páramo is the world's fastest evolving and coolest biodiversity hotspot. *Frontiers in genetics* 4: 192.

Matzke NJ. 2013. BioGeoBEARS: Biogeography with Bayesian (and likelihood) evolutionary analysis in R Scripts, CRAN: The Comprehensive R Archive Network, Vienna, Austria. http://cran.r-project.org/package=BioGeoBEARS.

Matzke NJ. 2014. Model selection in historical biogeography reveals that founder-event speciation is a crucial process in island clades. *Systematic Biology* 63: 951–970.

Mauseth J, Montenegro G, Walckowiak A. 1984. Studies of the holoparasite *Tristerix aphyllus* (Loranthaceae) infecting *Trichocereus chilensis* (Cactaceae). *Canadian Journal of Botany* 62: 847–857.

Micco V De, Aronne G. 2012. Plant Responses to Drought Stress. *Plant Responses to Drought Stress*: 37–61.

Miller MA, Feiffer WP, Schwartz T. 2010. Creating the CIPRES science gateway for inference of large phylogenetic trees. *Gateway Computing Environments workshop (GCE)* 2010: 1–8.

Mirarab S, Warnow T. 2015. ASTRAL-II: Coalescent-based species tree estimation with many hundreds of taxa and thousands of genes. *Bioinformatics* 31: i44–i52.

Moore WM. 1995. Inferring phylogenies from mtDNA variation: mitochondrial-gene trees versus nuclear-gene trees. *Evolution* 49: 718–726.

Morrone JJ. 2014. Biogeographical regionalisation of the neotropical region. *Zootaxa* 3782:1–110.

Mort ME, Crawford DJ, Kelly JK, Santos-Guerra A, Menezes de Sequeira M, Moura M, Caujape-Castells J. 2015. Multiplexed-shotgun-genotyping data resolve phylogeny within a very recently derived insular lineage. *American Journal of Botany* 102: 634–641.

Mutke J, Barthlott W. 2005. Patterns of vascular plant diversity at continental to global scales. *Biol. Skr.* 55: 521–537.

Myers N, Mittermeier RA, Mittermeier CG, da Fonseca GA, Kent J. 2000. Biodiversity hotspots for conservation priorities. *Nature* 403: 853–858.

Nesom GL, Robinson H. 2007. Tribe Astereae. In: Kadereit JW, Jeffrey C, eds. *The families and genera of vascular plants vol 8*. Berlin, Germany: Springer, 284–342.

Nesom GL. 1990. Taxonomy of the genus *Laennecia* (Asteraceae: Astereae). *Phytologia* 68: 205–228.

Nesom GL. 1993. *Aztecaster* (Asteraceae: Astereae), a new ditypic genus of dioecious shrubs from Mexico with redefinitions of the subtribes Hinterhuberinae and Baccharidinae. *Phytologia*. 75: 55–73.

Nesom GL. 1993. Synopsis of *Parastrephia* (Asteraceae: Astereae). *Phytologia* 75: 347–357.

Nesom GL. 1994. Subtribal classification of the Astereae (Asteraceae). *Phytologia* 76: 193–274.

Noyes RD, Rieseberg LH. 1999. ITS sequence data support a single origin for North American Astereae (Asteraceae) and reflect deep geographic divisions in *Aster* s.l. *American Journal of Botany* 86: 398–412.

Nürk NM, Scheriau C, Madriñán S. 2013. Explosive radiation in high Andean *Hypericum*–rates of diversification among New World lineages. *Frontiers in Genetics* 4: 175.

Nürk NM, Uribe-Convers S, Gehrke B, Tank DC, Blattner FR. 2015. Oligocene niche shift, Miocene diversification – cold tolerance and accelerated speciation rates in the St. John's Worts (*Hypericum*, Hypericaceae). *BMC Evolutionary Biology* 15: 1–13.

Pagel M. 1999. Inferring the historical patterns of biological evolution. *Nature* 401: 877–884.

Palmer JD, Herbon LA. 1988. Plant mitochondrial DNA evolves rapidly in structure, but slowly in sequence. *Journal of Molecular Evolution* 28: 87–97.

Panero JL, Freire SE, Ariza Espinar L, Crozier BS, Barboza GE, Cantero JJ. 2014. Resolution of deep nodes yields an improved backbone phylogeny and a new basal lineage to study early evolution of Asteraceae. *Molecular Phylogenetics and Evolution* 80: 43–53.

Panero JL, Funk VA. 2008. The value of sampling anomalous taxa in phylogenetic studies: Major clades of the Asteraceae revealed. *Molecular Phylogenetics and Evolution* 47: 757–782.

Pease JB, Hahn MW. 2015. Detection and polarization of introgression in a five-taxon phylogeny. *Systematic Biology* 64: 651–662.

Pedraza-Peñalosa P, Luteyn JL. 2011. Andean *Vaccinium* (Ericaceae: Vaccinieae): seven new species from South America. *Brittonia* 63: 257–275.

Peterson BK, Weber JN, Kay EH, Fisher HS, Hoekstra HE. 2012. Double digest RADseq: an inexpensive method for de novo SNP discovery and genotyping in model and non-model species. *PloS one* 7: e37135.

Phillips RL, Kleese RA, Wang SS. 1971. The nucleolus organizer region of maize (*Zea mays* L.): Chromosomal site of DNA complementary to ribosomal RNA. *Chromosoma* 36: 79–88.

Pyron RA, Costa GC, Patten MA, Burbrink FT. 2015. Phylogenetic niche conservatism and the evolutionary basis of ecological speciation. *Biological Reviews* 90: 1248–1262.

QGIS Development Team. 2005. QGIS Geographic Information System. Open source geospatial foundation project. http://qgis.osgeo.org.

Qiu YL, Li LB, Wang B, Xue JY, Hendry T a, Li RQ, Brown JW, Liu Y, Hudson GT, Chen ZD. 2010. Angiosperm phylogeny inferred from sequences of four mitochondrial genes. *Journal of Systematics and Evolution* 48: 391–425.

R Core Team. 2016. R: A Language and Environment for Statistical Computing. http://www.R-project.org/.

Rabosky DL, Grundler M, Anderson C, Title P, Shi JJ, Brown JW, Huang H, Larson JG. 2014. BAMMtools: An R package for the analysis of evolutionary dynamics on phylogenetic trees. *Methods in Ecology and Evolution* 5: 701–707.

Rabosky DL. 2014. Automatic detection of key innovations, rate shifts, and diversity-dependence on phylogenetic trees. *PLoS ONE* 9: e89543.

Rambaut A, Suchard MA, Xie D, Drummond AJ. 2014. *Tracer v1.6*. [WWW document] URL http://beast.bio.ed.ac.uk/Tracer.

Rambaut A. 2014. *FigTree v1.4.2*. [WWW document] URL http://tree.bio.ed.ac.uk/.

Rauscher JT. 2002. Molecular phylogenetics of the *Espeletia* complex (Asteraceae): Evidence from nrDNA its sequences on the closest relatives of an Andean adaptive radiation. *American Journal of Botany* 89: 1074–1084.

Ree RH, Smith S. 2008. Maximum likelihood inference of geographic range evolution by dispersal, local extinction, and cladogenesis. *Systematic Biology* 57: 4–14.

Revell LJ. 2012. phytools: An R package for phylogenetic comparative biology (and other things). *Methods in Ecology and Evolution* 3: 217–223.

Rice DW, Alverson AJ, Richardson AO, Young GJ, Sanchez-Puerta MV, Munzinger J, Barry K, Boore JL, Zhang Y, DePamphilis CW, *et al*. 2013. Horizontal transfer of entire genomes via mitochondrial fusion in the angiosperm *Amborella*. *Science (New York, N.Y.)* 342: 1468–73.

Rieppel O. 2010. Species monophyly. *Journal of Zoological Systematics and Evolutionary Research* 48: 1–8.

Rieseberg LH, Soltis DE. 1991. Phylogenetic consequences of cytoplasmic gene flow in plants. *Evolutionary Trends in Plants* 5: 64–84.

Rieseberg LH. 1995. The role of hybridization in evolution: old wine in new skins. *American Journal of Botany* 82: 944–953.

Rock BN. 1973. Vegetative anatomy of *Espeletia* (Compositae). PhD thesis, University of Maryland, College Park, MD, USA.

Ronquist F, Huelsenbeck JP, Telensko M. 2011. *MrBayes version 3.2 manual: tutorials and model summaries*. [WWW document] URL http://mrbayes.sourceforge.net/index.php.

Ronquist F, Huelsenbeck JP. 2003. MrBayes 3: Bayesian phylogenetic inference under mixed models. *Bioinformatics* 19: 1572–1574.

Ronquist F. 1997. Dispersal-vicariance analysis: a new approach to the quantification of historical biogeography. *Systematic Biology* 46: 195–203.

Rundell RJ, Price TD. 2009. Adaptive radiation, nonadaptive radiation, ecological speciation and nonecological speciation. *Trends in Ecology and Evolution* 24: 394–399.

Rundle HD, Nosil P. 2005. Ecological speciation. *Ecology Letters* 8: 336–352.

Ruzin SE. 1999. *Plant microtechnique and microscopy*. New York, USA: Oxford University Press.

Safford HD. 1999. Brazilian Páramos II . Macro- and mesoclimate of the *campos de altitude* and affinities with high mountain climates of the tropical Andes and Costa Rica. *Journal of Biogeography* 26: 713–737.

Sánchez-Baracaldo P, Thomas GH. 2014. Adaptation and convergent evolution within the *Jamesonia-Eriosorus* complex in high-elevation biodiverse Andean hotspots. *PLoS ONE* 9: e110618.

Sánchez-Baracaldo P. 2004. Phylogenetics and biogeography of the neotropical fern genera *Jamesonia* and *Eriosorus* (Pteridaceae). *American Journal of Botany* 91: 274–284.

Sancho G, Hind DJN, Pruski JF. 2010. Systematics of *Podocoma* (Asteraceae : Astereae): a generic reassessment. *Botanical Journal of the Linnean Society* 163: 486–513.

Sancho G, Karaman-Castro V. 2008. A Phylogenetic Study in American Podocominae (Asteraceae: Astereae) Based on Morphological and Molecular Data. *Systematic Botany* 33: 762–775.

Sancho G. 2012. *Exostigma*, a new genus of Astereae (Compositae) from southern South America. *Systematic Botany* 37: 516–524.

Sarmiento G. 1986. Ecologically crucial features of climate in high tropical mountains. In: Vuilleumier F, Monasterio M, eds. *High Altitude Tropical Biogeography*. New York, USA: Oxford University Press, 11–45.

Schluter D. 2000. *The Ecology of Adaptive Radiation*. Oxford, UK: Oxford University Press.

Sessa EB, Zimmer EA, Givnish TJ. 2012. Reticulate evolution on a global scale: A nuclear phylogeny for New World *Dryopteris* (Dryopteridaceae). *Molecular Phylogenetics and Evolution* 64: 563–581.

Silvertown J, Servaes C, Biss P, Macleod D. 2005. Reinforcement of reproductive isolation between adjacent populations in the Park Grass Experiment. *Heredity* 95: 198–205.

Simpson BB, Todzia CA. 1990. Patterns and processes in the development of the high Andean flora. *American Journal of Botany* 77: 1419–1432.

Simpson BB. 1974. Glacial migrations of plants: island biogeographical evidence. *Science* 185: 698–700.

Simpson BB. 1975. Pleistocene changes in the flora of the high tropical Andes. *Paleobiology* 1: 273–294.

Simpson GG. 1953. *The Major Features of Evolution*. New York, USA: Columbia University Press.

Sklenář P, Hedberg I, Cleef AM. 2014. Island biogeography of tropical alpine floras (LN Gillman, Ed.). *Journal of Biogeography* 41: 287–297.

Snaydon RW, Davies MS. 1976. Rapid population differentiation in a mosaic environment IV. Populations of *Anthoxanthum odoratum* at sharp boundaries. *Heredity* 37: 9–25.

Sochor M, Vašut RJ, Sharbel TF, Trávníček B. 2015. How just a few makes a lot: speciation via reticulation and apomixis on example of European brambles (*Rubus* subgen. *Rubus*, Rosaceae). *Molecular Phylogenetics and Evolution* 89: 13–27.

Song ZC, Zheng YH, Li MY. 1999. Paleogene palynostratigraphy. In: Song ZC, Zheng YH, Li MY, Zhang YY, Wang WM, Wang DN, Zhao CB, Zhou SF, Zhu ZH, Zhao YN, eds. *Fossil Spores and Pollen of China: The Late Cretaceous and Tertiary Spores and Pollen*. Beijing, China: Science Press, 749–762.

Stamatakis A. 2006. RAxML-VI-HPC: Maximum likelihood-based phylogenetic analyses with thousands of taxa and mixed models. *Bioinformatics* 22: 2688–2690.

Stamatakis A. 2014. RAxML version 8: A tool for phylogenetic analysis and post-analysis of large phylogenies. *Bioinformatics* 30: 1312–1313.

Stamatakis A. 2015. *The RAxML v8.1.X Manual*. [WWW document] URL http://sco.h-its.org/exelixis/web/software/raxml/index.html.

Straub SCK, Parks M, Weitemier K, Fishbein M, Cronn RC, Liston A. 2012. Navigating the tip of the genomic iceberg: Next-generation sequencing for plant systematics. *American Journal of Botany* 99: 349–64.

Strijk JS, Noyes RD, Strasberg D, Cruaud C, Gavory F, Chase MW, Abbott RJ, Thébaud C. 2012. In and out of Madagascar: dispersal to peripheral islands, insular speciation and diversification of Indian ocean daisy trees (*Psiadia*, Asteraceae). *PLoS ONE* 7: e42932.

Sun M, Soltis DE, Soltis PS, Zhu X, Burleigh JG, Chen Z. 2015. Deep phylogenetic incongruence in the angiosperm Rosidae clade. *Molecular Phylogenetics and Evolution* 83: 156–166.

Sun XJ, Li MX, Zhang YY, Lei ZQ, Kong ZC, Li P, Qu Q, Liu QN. 1981. Tertiary palaeontology of North Continental Shelf of South China Sea. *Guangdong Science and Technology Press, Guangzhou*.

Takayama K, López-Sepúlveda P, Greimler J, Crawford DJ, Peñailillo P, Baeza M, Ruiz E, Kohl G, Tremetsberger K, Gatica A, *et al*. 2015. Genetic consequences of cladogenetic vs. anagenetic speciation in endemic plants of oceanic islands. *AoB Plants* 7: plv102.

Tovar C, Arnillas CA, Cuesta F, Buytaert W. 2013. Diverging responses of tropical andean biomes under future climate conditions. *PLoS ONE* 8: e63634.

Uribe-Convers S, Tank DC. 2015. Shifts in diversification rates linked to biogeographic movement into new areas: an example of a recent radiation in the Andes. *American Journal of Botany* 102: 1–16.

van der Hammen T, Cleef AM. 1986. Development of the high Andean páramo flora and vegetation. In: Vuilleumier F, Monasterio M, eds. *High Altitude Tropical Biogeography*. New York, USA: Oxford University Press, 153–201.

Vargas OM, Madriñán S. 2006. Clave para la identificación de las especies del género *Diplostephium* (Asteraceae, Astereae) en Colombia. *Revista de la academia Colombiana de Ciencias Exactas Fisicas y Naturales* 30: 489–494.

Vargas OM, Madriñán S. 2012. Preliminary phylogeny of *Diplostephium* (Asteraceae): speciation rate and character evolution. *Lundellia* 15: 1–15.

Vargas OM. 2011. A nomenclator of *Diplostephium* (Asteraceae: Astereae): a list of species with their synonyms and distribution. *Lundellia* 14: 32–51.

Villagómez D, Spikings R, Mora A, Guzmán G, Ojeda G, Cortés E, van der Lelij R. 2011. Vertical tectonics at a continental crust-oceanic plateau plate boundary zone: fission track thermochronology of the Sierra Nevada de Santa Marta, Colombia. *Tectonics* 30: n/a–n/a.

Volkov RA, Komarova NY, Hemleben V. 2007. Ribosomal DNA in plant hybrids: Inheritance, rearrangement, expression. *Systematics and Biodiversity* 5: 261–276.

Walter H, Harnickell E, Mueller-Dombois D. 1975. *Climate-diagram maps of the individual continents and the ecological climatic regions of the earth*. New York - Heidelberg - Berlin: Springer-Verlag.

Wang WM. 2004. On the origin and development of *Artemisia* (Asteraceae) in the geological past. *Botanical Journal of the Linnean Society* 145: 331–336.

Weddell H. 1855. *Chloris Andina, vol 1*. Paris: Chez P. Bertrand.

Weigend M. 2002. Observations on the biogeography of the Amotape-Huancabamba zone in northern Peru. *The Botanical Review* 68: 38–54.

Weigend M. 2004. Additional observations on the biogeography of the Amotape-Huancabamba zone in Northern Peru: defining the South-Eastern limits. *Revista Peruana de Biología* 11: 127–134.

West C, James SA, Davey RP, Dicks J, Roberts IN. 2014. Ribosomal DNA sequence heterogeneity reflects intraspecies phylogenies and predicts genome structure in two contrasting yeast species. *Systematic Biology* 63: 543–54.

Wiens JJ. 2004. Speciation and ecology revisted: phylogenetic niche conservatism and the origin of species. *Evolution* 58: 193–197.

Wu J, Nyman T, Wang D-C, Argus GW, Yang Y-P, Chen J-H. 2015. Phylogeny of *Salix* subgenus *Salix* s.l. (Salicaceae): delimitation, biogeography, and reticulate evolution. *BMC Evolutionary Biology* 15: 1–13.

Wu Z, Cuthbert JM, Taylor DR, Sloan DB. 2015. The massive mitochondrial genome of the angiosperm *Silene noctiflora* is evolving by gain or loss of entire

chromosomes. *Proceedings of the National Academy of Sciences, USA* 112: 10185–10191.

Wyman SK, Jansen RK, Boore JL. 2004. Automatic annotation of organellar genomes with DOGMA. *Bioinformatics* 20: 3252–3255.

Xie W, Lewis PO, Fan Y, Kuo L, Chen MH. 2011. Improving marginal likelihood estimation for Bayesian phylogenetic model selection. *Systematic Biology* 60: 150–160.

Zapata F. 2013. A multilocus phylogenetic analysis of *Escallonia* (Escalloniaceae): Diversification in montane South America. *American Journal of Botany* 100: 526–545.

Vita

Oscar Mauricio Vargas Hernandez was born in the Andes Cordillera in the city of Bogotá, Colombia. He earned his B.S. in 2005 from the "Universidad de los Andes." Though he began his time at los Andes as an environmental engineering student, he quickly realized his true passion was biology. Fascinated with the plant diversity of his country and the science of systematics, Oscar began working under the mentorship of Santiago Madriñán. Oscar started to work with páramo woody daisies for his undergraduate honor's thesis without realizing he would continue to work with the same group of plants for the next twelve years. As soon as he completed his B.S. in Biology, he entered the M.S. program, also at "Universidad de los Andes." During his time in Washington D.C. in 2006–2007, thanks to the Cuatrecasas award from the Smithsonian Institution, Vicki Funk advised Oscar to enroll in a Ph.D. program in the U.S. and recommended Beryl Simpson. At the 2007 Botany meeting in Chicago, Oscar met Beryl, who suggested that he apply to The University of Texas at Austin (U.T.). Oscar enrolled in the Plant Biology program at U.T. in 2009 under Beryl's supervision. Oscar's Ph.D. dissertation focused on the patterns and processes that drove the evolution of woody daisies in the Andes. He is currently scheduled to start a post-doctoral position at the University of Michigan in the fall of 2016, joining the labs of Christopher Dick and Stephen Smith.

Permanent email: oscarvargash@gmail.com

This dissertation was typed by the author.